Transfer Function and Eigenfunction Analysis (TFEA) Method in Power System Small Signal Stability Analysis

Reza Jalayer

Department of Electrical and Computer Engineering

McGill University

Montreal, Canada

A thesis submitted to McGill University in partial fulfillment of the requirements for the degree of Doctorate of Philosophy in Electrical Engineering

Abstract

This thesis describes the Transfer Function and Eigenfunction Analysis (TFEA) method: an efficient eigenanalysis method for estimating the small signal stability of large interconnected power systems. The method consists of reducing the order of each generator, which is accurately modeled by m state-variables, to only two state-variables, including rotor speed and angle deviations. This efficiency is achieved without loss of dynamic accuracy because the information of the other (m-2) state-variables is compacted into transfer functions in a frequency-dependent state-matrix $[A(\omega)]_{2ng\times 2ng}$. Because the computation count of QR eigenanalysis increases with the cube of system dimension, computation efficiency arises from evaluating the reduced state matrix $[A(\omega)]_{2ng\times 2ng}$, instead of the full state matrix $[A]_{(m\times ng)\times(m\times ng)}$, in a power system consisting of ng generators. The acceptability of the method is based on the engineering knowledge that the electromechanical modes are the least damped modes, and the system stability depends on these eigenvalues' being on the left side of the complex s-plane. In practice, only a small number of low-frequency electromechanical modes determine stability. Consequently, the accuracy of the TFEA method is improved for selected electromechanical modes by applying the eigenvalue sensitivity formula. In the next step, the TFEA method is combined with the well-known Arnoldi method for further improvement of efficiency.

This thesis also develops a method for simultaneous tuning of power system stabilizers (PSSs). The proposed method combines the timesaving TFEA method with the eigenvalue sensitivity concepts and optimization techniques. The key feature of the method is the eigenvalue sensitivity formula, which relates perturbation changes of eigenvalues to perturbation changes of stabilizer parameters. In PSS tuning, the parameters are one amplification gain and the many time constants of each PSS. Tuning consists of formulating an objective function which embeds the desirable improvement in damping of the eigenvalues. To this end, an optimization algorithm (from MATLAB) is applied to satisfy the objective function while meeting the size constraints placed on the parameters.

The accuracy, efficiency and robustness of the TFEA method and the PSS tuning method are compared with the benchmark eigenvalues based on the full state matrix $[A]_{(m\times ng)\times(m\times ng)}$. The numerical tests use a 16-generator and a 69-generator power system. The test results, demonstrate the effective performance of the proposed methods.

Abrégé

Cette thése décrit la Fonction de Transfert et l'Analyse de la méthode de la Fonction propre (TFEA): une méthode efficace d'évaluer stabilité de petits signaux dans les grandes installations électriques connectées. La méthode consiste en réduire l'ordre de chaque générateur qui est précisément modelé par des variables d'état m à seulement variables de deux états incluant la vitesse de rotor et des écarts angulaires. L'efficacité est réalisée sans perte d'exactitude dynamique parce que les informations des autres variables d'état (m-2) sont rendues compactes comme des fonctions de transfert dans l'état de matrice $[A(\omega)]_{2ng\times 2ng}$ que dépend on fréquence. Car le compte de calcul d'analyse QR augment avec le cube de dimension de système, l'efficacité de calcul vient d'évaluer état de matrice $[A(\omega)]_{2ng\times 2ng}$ réduit au lieu de état de matrice $[(A)]_{(m\times ng)\times(m\times ng)}$ plain de générateurs ng. L'acceptabilité de la méthode est basée sur la connaissance d'ingénierie que les modes électromécaniques sont les modes moindres amortis et la stabilité dépend de leurs valeurs propres étant sur le côté gauche du s-plan de complexe. En pratique, seul un petit nombre de modes électromécaniques à basse fréquence déterminet la stabilité. Par conséquent, l'exactitude de la méthode TFEA est améliorée pour ces modes en appliquant la formule de sensibilité de valeur propre. Dans l'étape suivante, la méthode TFEA est combinée avec la méthode bien connue d'Arnoldi pour plus d'amélioration de l'efficacité.

Cette thése développe également une méthode d'ajustassions simultanée des stabilisateurs (PSSs). La méthode proposée combine la méthode d'économie de temps TFEA avec le concept de sensibilité de valeur propre et de techniques d'optimisation. La fonctionnalité clé de cette méthode est la formule de sensibilité qui relie les changements de la perturbation des valeurs propres aux changements de la perturbation de paramètres de système d'alimentation électrique. Dans le réglage de PSS, les paramètres sont une amplification gain et les nombreuses constantes de temps de chaque PSS. Le réglage consiste à formuler une fonction objective qui intègre l'amélioration souhaitable de l'amortissement des valeurs propres. À cette fin, un algorithme d'optimisation (à partir de MATLAB) est appliqué pour satisfaire la fonction d'objectif tout en réalisant contraintes de taille placées sur les paramètres.

L'exactitude, l'efficacité et la robustesse de la méthode TFEA et la méthode réglage de PSS sont comparées avec les valeurs propres d'un référence basé sur l'état complet de matrice $[(A)]_{(m\times ng)\times(m\times ng)}$. Les tests numériques utilisent un 16-générateur et un 69- générateur du système d'alimentation électrique. Les résultats présentés, démontrer l'efficacité des méthodes proposées.

To my parents and to my love, Saba

for their tireless support throughout my life

Acknowledgements

I would like to express my gratitude to my supervisor, Professor Boon-Teck Ooi for his sincere encouragement, guidance, and support during my PhD studies. Completion of my PhD would not have been possible without his ideas and suggestions. He provides me with the promising research opportunities and offers crucial suggestions to lead me in the right direct. I appreciate all his contributions of time and ideas. I acknowledge financial support from NSERC Discovery Grant during my study.

I also express thanks to Professor Geza Joos and Professor Hannah Michalska, my PhD committee members, for their valuable suggestions and help.

I wish to thank all my friends and colleagues who provided me a warm and friendly environment and memorable times during my studies.

My special gratitude goes to my family for their unflagging love and support throughout my life. For my lovely mother whose love, faith, and support are always giving confidence and power to explore, grow, and develop. For my father who motivated me to work hard by his endeavour and ambition, and for my brothers who always encourage me. Last, but by no means least, I would like to thank my wife, Saba, for her understanding, support and encouragement during the past few years.

Table of Contents

List of Figures

List of Tables

List of Acronyms

AESOPS	Analysis of Essentially Spontaneous Oscillations in Power Systems
ARPACK	Arnoldi Package
AVR	Automatic Voltage Regulator
FACTS	Flexible AC Transmission Systems
IITC	Incremental Induced Torque Coefficicents
IRAM	Implicitly Restarted Arnoldi Method
ITC	Induced Torque Coefficicents
LP	Linear Programming
MAM	Modified Arnoldi Method
PEALS	Program for Eigenvalue Analysis of Large Systems
PMU	Phase Measurment Unit
PSS	Power System Stabilizer
pu	per unit
RQI	Rayleigh Quotient Iteration
SARQI	Subspace Accelerated Rayleigh Quotient Iteration
SI	Simultaneous Iteration
SMA	Selective Modal Analysis
SQP	Sequential Quadratic Programming
TFEA	Transfer Function and Eigenfunction Analysis

List of Symbols

$\Delta\delta$	perturbation rotor angle
$\Delta\omega$	perturbation rotor speed
$[A(\omega)]_{2ng\times 2ng}$	reduced state matrix of power system
$[A]_{11ng\times 11ng}$	full state matrix of power system
$[K_S(\omega)]$	matrix of synchronizing torque coefficients
$[K_D(\omega)]$	matrix of damping torque coefficients
$\underline{u}$	eigenvectors of $[A(\omega_K)]_{2ng\times 2ng}$
$\underline{r}$	eigenvectors of $[A(\omega_K)]^T{}_{2ng\times 2ng}$
ω_K	represantative frequency
ω_n	oscillation frequency
s	Laplace transform operator
ng	number of generators in power system
m	number of states per generator
$\lambda(\omega_K=5)$	eigenvalue of $[A(\omega_K)]_{2ng\times 2ng}$ evaluated at $\omega_K=5$
λ_{imp}	improved eigenvalue after applying sensitivity formula
n_{sample}	number of sampling frequencies for curve-fitting interpolation
$[H]_{p\times p}$	upper Hessenberg matrix obtained in Modified Arnoldi Method
K_A	exciter gain
K_{ST}	power system stabilizer gain
T_R	voltage transducer time constant

T_w	washout filter time constant
T_1	power system stabilizer time constant
T_2	power system stabilizer time constant
T_3	power system stabilizer time constant
T_4	power system stabilizer time constant
W_j	weighting function for optimization objective function
$\Delta\lambda_n$	eigenvalue shift for n^{th} mode
$\underline{\Delta pa}$	vector of perturbation PSS parameters
$\Delta\sigma$	damping shift due to power system stabilizer tuning

Chapter One

1. Introduction

1.1 Power System Stability

"Power system stability is the ability of an electric power system, for a given initial operating condition, to regain a state of operating equilibrium after being subjected to a physical disturbance, with most system variables bounded so that practically the entire system remains intact" [1]. According to the nature of the disturbance, the system configuration and the initial operating conditions, different stability issues exist. The definitions and classifications of power system stability are explained in [1, 2, 3, 4].

An important stability problem is rotor angle stability, which involves the study of the electromechanical oscillations inherent in power systems [1]. The analysis of rotor angle stability is classified under: (i) transient stability and (ii) small signal stability. *Transient stability* studies include identifying critical fault clearing time and assessing system stability margin, when subjected to a severe disturbance. The working tool makes use of digital simulation. In *small signal stability*, it is assumed that the power system has reached the steady-state equilibrium. The question is whether it returns to its equilibrium after encountering a small disturbance. Small signal stability problem is usually associated with insufficient damping of oscillations [1]. The working tool is eigenvalue analysis. Small signal stability is assured when all the eigenvalues of the linearized state matrix of the power system lie on the left side of the complex s-plane.

1.2 Problem Definition: Efficient Eigenanalysis of Power System for Small Signal Stability Analysis

As power systems have pooled together to enjoy the benefits of scale of large interconnections, they have been troubled by inter-area oscillations. IEEE and CIGRE have issued special publications to monitor the subject [5, 6, 7, 8, 9]. Viewed as a small signal stability problem, inter-area oscillations have been tackled by eigenfunction analysis applied to the linearized, time-invariant power system state matrix $[A]$ [10, 11]. The full state matrix $[A]$ is very large, unsymmetrical and non-sparse. The well-known QR method, which is robust and has fast convergence, is suitable [12]. However, it cannot be applied directly when the state matrix dimension is large, because it is very time consuming and inefficient [12, 13, 14]. The derivation of the full state matrix is shown in Section 1.3.

Detailed modelling of the entire system is required for accurate power system studies. A system with ng generators, each having an average of m=11 state variables, has system order of $11ng$. Solving all the eigenvalues of an $11ng \times 11ng$ state matrix is overly time-consuming when ng is large. Therefore, there has been research based on reducing the computation time by developing fast and efficient methods [15, 16, 17]. This consists of finding only a selected number of eigenvalues, which from the engineering experience are the dominant electromechanical modes. The methods taken from mathematicians include the Arnoldi method [15, 16] and power iterations [18]. Another method, which integrates the insights of engineers familiar with power networks, is the AESOPS (Analysis of Essentially Spontaneous Oscillations in Power Systems) algorithm [19]. A brief introduction on these methods is provided in Section 1.4.

In power system eigenanalysis, it is the accuracy of the eigenvalues closest to the imaginary axis that determine stability. This fact is implicitly acknowledged by the researchers of [15, 16, 17], because the speed-up efficiency in their algorithms is derived from solving the few dominant eigenvalues clustered together. However, without laboriously solving the eigenvalues of the $11ng \times 11ng$ state matrix, a priori, one does not know where the dominant modes are.

The research of this thesis fills the gap by offering a preview of the eigenvalues of all the electromechanical modes so that a decision can be made regarding which are the dominant modes. In general, all the well-known and accurate eigenanalysis methods, such as Inverse

Iteration [18], Arnoldi method [15, 16] and AESOPS [19], require such previews for efficient performance. This thesis presents the Transfer Function and Eigenfunction Analysis (TFEA) method, which formulates a reduced order frequency-dependent $[A(\omega)]_{2ng\times 2ng}$ matrix that efficiently determines all the eigenvalues of the system. The TFEA method is introduced in Section 1.5.

1.3 Full State Matrix of Power System

The dynamics of a power system is represented by an N-tuple vector $\underline{x}$, governed by a set of first order ordinary differential equations, such as

$$\frac{d\underline{x}}{dt} = \underline{f}(\underline{x}). \tag{1-1}$$

Vector $\underline{x}$ includes the dynamics of the states of the system components, such as the synchronous generators.

In small signal analysis, the state vector is written as $\underline{x}=\underline{X_0}+\underline{\Delta x}$, where the operating state vector $\underline{X_0}$ is solved by a load flow algorithm, and $\underline{\Delta x}$ is the vector of small disturbance. The small signal perturbation is then performed by first order Taylor series expansion,

$$\begin{aligned} &\frac{d(\underline{X}_0 + \Delta\underline{x})}{dt} = \underline{f}(\underline{X}_0 + \Delta\underline{x}) \\ &= \underline{f}(\underline{X}_0) + [\frac{\partial \underline{f}(\underline{x})}{\partial \underline{x}}]_{\underline{X}_0} \Delta\underline{x} + \text{second and higher order terms.} \end{aligned} \tag{1-2}$$

Retaining the first order perturbation state in (1-2), one obtains the linearized equation of

$$\frac{d\underline{\Delta x}}{dt} = [A]_{N\times N}\underline{\Delta x} \tag{1-3}$$

where $[A]_{N\times N}$ is the Jacobian matrix evaluated at $\underline{X}_0$ in (1-2) and is called the full state matrix of the system.

When each synchronous generator of the power system is represented by m-state variables, and the power system has ng generators, then $N=m\times ng$. The m-state variables represent the magnetic fluxes (currents) of the generator, the rotor angle, the rotor speed and additional states from turbine/governor, Automatic Voltage Regulator (AVR), exciter, power system stabilizer (PSS) and other controlling elements.

To derive the full state matrix, all the generator equations are perturbed and arranged in the state space form of (1-3), which results in the non-sparse matrix of $[A]_{(m\times ng)\times(m\times ng)}$,

$$\frac{d}{dt}\begin{bmatrix} st_1g_1 \\ \vdots \\ st_mg_1 \\ \vdots \\ st_1g_j \\ \vdots \\ st_mg_j \\ \vdots \\ st_1g_{ng} \\ \vdots \\ st_mg_{ng} \end{bmatrix}_{(m\times ng)\times 1} = [A]_{(m\times ng)\times(m\times ng)} \begin{bmatrix} st_1g_1 \\ \vdots \\ st_mg_1 \\ \vdots \\ st_1g_j \\ \vdots \\ st_mg_j \\ \vdots \\ st_1g_{ng} \\ \vdots \\ st_mg_{ng} \end{bmatrix}_{(m\times ng)\times 1}. \qquad (1\text{-}4)$$

In (1-4), st_ig_j is the i^{th} state-vector of generator j. In this research, the number of states per generator is m=11.

$[A]_{(m\times ng)\times(m\times ng)}$ is a time-invariant matrix and has ($m\times ng$) eigenvalues. Based on selective modal analysis in [20], [A] has (ng-1) pairs of complex conjugate eigenvalues, which are distinguished from the others by their long time constants. Each pair belongs to one or to a group of generators. From the interpretation of the eigenvectors, these modes are associated with the states representing the rotor angle and speed; thus, they are known as electromechanical modes. The remaining state-variables relate to the electrical quantities and to the dynamics of controlling elements.

1.4 Background on Selective Eigenanalysis

The linearized power system model of (1-4) is easy to derive for QR eigenanalysis [12]. However, this full state matrix is in general not sparse, making QR analysis prohibitively expensive for large power systems. In contrast, sparsity-based methods have been developed, which have the following features:

- Selective eigenanalysis that finds a specific set of eigenvalues efficiently; and
- Good convergence characteristics and numerical stability [16, 21].

Different methods have been proposed to derive sparse system models [17, 22, 23], to be used by the sparsity-based methods. The important sparsity-based eigenvalue methods for general unsymmetrical matrices are [16]:

- Power Iterations and Inverse Iterations [18];
- Lanczos method [18];
- Simultaneous (Subspace) Iterations [24]; and
- Arnoldi method [15, 16].

The most powerful method is the classical method of Power Iterations [18]. This method consists of repeated matrix-vector multiplications, which converges to the eigenvector corresponding to the dominant eigenvalue. The Lanczos method [18], based on the algorithm of Power Iterations, is very successful for the symmetrical eigenvalue problem. A modification of Lanczos method suitable for unsymmetrical matrices is described in [18, 21]. The application of Lanczos method to the eigenanalysis of power systems is mentioned in [17, 23, 25].The Power Iterations method is very robust, but it has slow convergence [26, 27]. The Rayleigh Quotient Iterations method (RQI) of [28] and the Newton method are modifications to Power Iterations to improve convergence speed. The Newton method has quadratic convergence properties, but it is not robust [29, 30, 31].

Simultaneous (Subspace) Iterations (SI), is a generalization of Power Iterations, in which instead of a single vector solution, a subspace solution is obtained. Simultaneous Iterations, although robust, suffer from the same slow convergence as Power Iterations. This method was originally proposed in [24] for the symmetrical eigenvalue problem and then extended to general unsymmetrical matrices [16, 32, 33].

The Arnoldi method is similar to Simultaneous Iterations [15, 16]. The subspace is built as a unitary Krylov subspace to approach the dominant invariant subspace of a matrix [A] [34, 35]. The Arnoldi method is explained and applied to the research of this thesis in Chapter 4. Both Simultaneous Iterations and the Arnoldi method have reliable convergence characteristics. Both are successful in the eigenanalysis of large power systems. The Arnoldi method is the faster of the two.

In addition to the sparsity-based methods, other methods exist for the purpose of selective eigenanalysis, such as the S-Method [17] and Selective Modal Analysis (SMA) [20]. The S-Method is efficient in determining the unstable modes belonging to a group of a few generators.

Selective Modal Analysis (SMA) has been developed to find a group of important eigenvalues of a power system by reducing the system order [20]. The reduced order model is achieved using special techniques to identify variables that are relevant to the selected modes [36, 37].

The iterative method of AESOPS (Analysis of Essentially Spontaneous Oscillations in Power Systems) introduced in [19], is a computer program developed specifically for the study of oscillations in large electric power systems. This method finds one eigenvalue at a time. It calculates the eigenvalues of the electromechanical modes without formulating the entire system state matrix. It uses a frequency response approach to calculate the eigenvalues associated with the rotor angle modes. References [22, 25, 38, 39, 40] describe improved implementations of the AESOPS algorithm.

The initial estimate in such iterative methods is very important to the speed of convergence. According to [25], the intermediate results of the AESOPS method may be used as an initial estimate for Inverse Iterations for more rapid convergence. For example, it can be seen from [25] that, in some case studies, the AESOPS algorithm converged after 45 iterations. However, if the non-converged eigenvalue estimates, obtained from the 10th iteration of the AESOPS algorithm, was used as the initial estimate for the Implicit Inverse Iteration algorithm, convergence was obtained after 6 iterations. This simple example verifies the importance of methods such as TFEA for providing a preview of all electromechanical modes.

1.5 Proposed Method: Transfer Function and Eigenfunction Analysis (TFEA) Method

1.5.1 Stability of Electromechanical Oscillations

Small signal stability is assured when all the eigenvalues of the linearized system state matrix lie on the left side of the complex *s*-plane. As the eigenvalues associated with electrical circuits and control "black boxes" lie on the far left (i.e., heavily damped), this thesis focuses on lightly damped electromechanical modes associated with the rotor angle and speed deviations. Electromechanical oscillations between interconnected synchronous generators are phenomena that are inherent to power systems. The stability of these oscillations is of vital concern, and is a prerequisite for secure system operation [3].

Small signal stability analysis, using the full state [A] matrix of (1-4), is not attractive for the following reasons.

1- The computation time of the QR eigenanalysis method increases with N^3. For $N=m\times ng$, the computation time becomes prohibitive when ng, the number of generators, is large. It is very time consuming for large matrices and is not practical.
2- Small signal stability is determined by electromechanical modes.

Therefore, it is desirable to have the state matrix of electromechanical oscillations only. This matrix is called the Reduced State Matrix.

1.5.2 Reduced State Matrix $[A(\omega)]_{2ng\times 2ng}$

For each generator in the power system, Newton's Law in the rotational frame, governing the speed of the rotor with the moment of inertia of H, consists of

$$p\Delta\omega_r = \frac{1}{2H}(T_m - T_e) \tag{1-5}$$

$$p\delta = \omega_0 \Delta\omega_r \tag{1-6}$$

where T_m is the mechanical input torque, and T_e is the generator electrical torque. Additionally, $\Delta\omega_r$ is the per unit rotor speed deviation, δ is the rotor angle in electrical radians, ω_0 is the base rotor electrical speed in rad/s and p is the differential operator d/dt, with time t in seconds [2].

Perturbing and linearizing (1-5) and (1-6) results in

$$p\Delta\omega_r = \frac{1}{2H}[\Delta T_m - \Delta T_e] \tag{1-7}$$

$$p\Delta\delta = \omega_0 \Delta\omega_r. \tag{1-8}$$

The perturbation electrical torque ΔT_e is resolved into two components: one in phase with the rotor angle deviation and the other in phase with the rotor speed deviation [1]:

$$\Delta T_e = K_S \Delta\delta + K_D \Delta\omega_r. \tag{1-9}$$

Therefore, (1-7) is written as

$$p\Delta\omega_r = \frac{1}{2H}[\Delta T_m - K_S\Delta\delta - K_D\Delta\omega_r] \tag{1-10}$$

where K_S and K_D are called synchronizing and damping torque coefficients, respectively. Insufficient synchronizing torque causes an increase in rotor angle through a non-oscillatory mode, and insufficient damping torque can cause rotor oscillations of increasing amplitude [1].

Combining (1-8) and (1-10) results in the matrix form of

$$\begin{bmatrix} \Delta\dot{\delta} \\ \Delta\dot{\omega}_r \end{bmatrix} = \begin{bmatrix} 0 & \omega_0 \\ -\dfrac{K_S}{2H} & -\dfrac{K_D}{2H} \end{bmatrix} \begin{bmatrix} \Delta\delta \\ \Delta\omega_r \end{bmatrix} + \begin{bmatrix} 0 \\ \dfrac{1}{2H} \end{bmatrix} \Delta T_m. \tag{1-11}$$

Because the rotor angle and speed deviations are the only state variables in (1-11), the state matrix is called the "reduced state matrix". It should be borne in mind that the full state matrix of (1-4) has *m* (i.e., 11) state variables per generator.

When sufficient information is available for K_S and K_D, solving the reduced state matrix of (1-11) yields the eigenfunctions associated with electromechanical modes. The contribution of this research is to provide such information for an interconnected system.

The method adopted in this thesis is an extension of the synchronizing and damping torque coefficients of (1-9), developed for a single generator to *ng* generators. To embed the dynamic properties of (*m*-2) state variables, the power system stabilizer, the exciter and other electrical state variables are represented by transfer functions. Therefore, the synchronizing and damping torque coefficients take the form of transfer functions $[K_S(\omega)]$ and $[K_D(\omega)]$. This method is given the name Transfer Function and Eigenfunction Analysis (TFEA).

1.6 Thesis Contributions

1.6.1 Transfer Function and Eigenfunction Analysis (TFEA) Method

It is the ambition of all researchers to contribute to their national economies and to the knowledge in the field. The main contribution is the Transfer Function and Eigenfunction Analysis (TFEA) method. As computation counts by the QR method are proportional to the cube of the matrix dimension, the cost reduction in reducing from $[A]_{11ng\times 11ng}$ to $[A(\omega)]_{2ng\times 2ng}$ is significant. The TFEA method is fully described in Chapter 2.

The inherent weakness in the TFEA method is that $[A(\omega)]$ is frequency dependent. In a system with *ng* generators, there exist (*ng*-1) electromechanical oscillatory modes, which have modal frequencies ω_n (*n*=1, 2,…, *ng*-1). Because (*ng*-1) eigenvalue evaluations of $[A(\omega_n)]$ (*n*=1, 2,…, *ng*-1), would be expensive, the thesis performs only a few eigenvalue evaluations of $[A(\omega_K)]$ at the so-called representative frequency ω_K.

1.6.2 Accurate Prediction from Eigenvalue Sensitivity Formula

It is shown in Chapter 2 that the eigenvalues predicted by $[A(\omega_K)]$, which have modal frequencies ω_n (n=1, 2,…, ng-1), are accurate only for modes whose frequency ω_n are close to ω_K . Recognizing such weakness, a computationally efficient method, based on the eigenvalue sensitivity formula of [41], has been developed and shown to be efficient and accurate.

In application, the TFEA method enables all the electromechanical modes to be solved from the eigenanalysis of $[A(\omega_K)]$, so that the few dominant ones that determine stability are identified. Improved accuracy for each mode ω_n can be economically obtained by using the eigenvalue sensitivity formula.

1.6.3 Improving Computational Efficiency by Applying Curve Fitting Interpolation to the TFEA Method

Applying the eigenvalue sensitivity formula can be helpful; however, it is costly when all the modes are required to be determined accurately. Such cost, although less than the cost of eigenanalysis, motivates the research to proposing an original method that reduces the computation cost while preserving the accuracy. The method is based on a combination of: (i) the TFEA method, (ii) eigenvalue sensitivity, and (iii) curve fitting interpolation.

1.6.4 Combining TFEA with Modified Arnoldi Method

The TFEA method is combined with the well-known Modified Arnoldi Method (MAM) [16], demonstrating the ability of TFEA to facilitate more accurate methods, thereby improving their efficiency. The efficiency comes from applying MAM to $[A(\omega)]_{2ng\times 2ng}$ instead of $[A]_{11ng\times 11ng}$.

1.6.5 Coordinated Tuning of Power System Stabilizers (PSSs) of Large Power Systems

The TFEA formulation of $[A(\omega)]$ matrix includes Power System Stabilizers (PSSs) as transfer functions. Each PSS has one amplifier gain and several time constants of a “black box”, which compensates for the long delay of the field winding. The amplifier gain and the time constants are treated as parameters to be “tuned” in the eigenvalue sensitivity formula. Because the $[A(\omega)]$

matrix couples *ng* generators together, the eigenvalues can be “tuned” simultaneously, as required in an interconnected power system. The thesis turns to optimization algorithms available in the MATLAB library as mathematical tools to implement the tuning method.

This research has developed a general computation tool for all kinds of tuning strategies such as minimizing the PSSs gains or maximizing the damping of the low frequency modes. The tuning exercises involve a 16-generator and a 69-generators system, in which each PSS have one amplifier gain and four time constants.

1.7 Thesis Overview

In this thesis, the TFEA method is explained in Chapter 2. In Chapter 3, a discussion of the method’s efficiency is provided, and the curve fitting interpolation is introduced to reduce the computation time without losing the accuracy. In addition, the application of TFEA to selective eigenanalysis by the Modified Arnoldi Method is described in Chapter 4. Chapters 5 and 6 show that a combination of TFEA, eigenvalue sensitivity and optimization algorithms constitutes a powerful computational tool for coordinated tuning of PSS in a large interconnected power system.

In each chapter, numerical results from different test systems are presented to demonstrate the efficiency of the proposed method. Finally, the conclusion of the research and future research subjects are provided in Chapter 7.

Chapter Two

2. Transfer Function and Eigenfunction Analysis (TFEA) Method

2.1 Overview

This chapter introduces the reduced state matrix of $[A(\omega)]_{2ng\times 2ng}$, which is formed by the TFEA method. The method combines the equations of synchronous generators and associated controls with the equations of the system network in the format of small signal stability analysis.

It will be shown that for a system with ng generators, $[K_S]$ and $[K_D]$ of (1-9) are expanded as frequency-dependent matrices of $[K_S(\omega)]$ and $[K_D(\omega)]$. Therefore, for ng generators, the torque equation of (1-9) would be reformed as,

$$\begin{bmatrix}\Delta T_{e1}\\ \vdots \\ \Delta T_{ej}\\ \vdots \\ \Delta T_{eng}\end{bmatrix}=\begin{bmatrix}K_{S11}(\omega)..K_{S1j}(\omega)..K_{S1ng}(\omega)\\ ..\\ K_{Sj1}(\omega)..K_{Sjj}(\omega)..K_{Sjng}(\omega)\\ ..\\ K_{Sng1}(\omega)..K_{Sngj}(\omega)..K_{Sngng}(\omega)\end{bmatrix}\begin{bmatrix}\Delta\delta_1\\ \vdots \\ \Delta\delta_j\\ \vdots \\ \Delta\delta_{ng}\end{bmatrix}+\begin{bmatrix}K_{D11}(\omega)..K_{D1j}(\omega)..K_{D1ng}(\omega)\\ ..\\ K_{Dj1}(\omega)..K_{Djj}(\omega)..K_{Djng}(\omega)\\ ..\\ K_{Dng1}(\omega)..K_{Dngj}(\omega)..K_{Dngng}(\omega)\end{bmatrix}\begin{bmatrix}\Delta\omega_{r1}\\ \vdots \\ \Delta\omega_{rj}\\ \vdots \\ \Delta\omega_{rng}\end{bmatrix}. \tag{2-1}$$

One defines

$$[K_S(\omega)]=\left[K_{Sij}(\omega)\right] \quad i,j=1,\ 2,\ldots,\ ng \tag{2-2}$$

$$[K_D(\omega)]=\left[K_{Dij}(\omega)\right] \quad i,j=1,\ 2,\ldots,\ ng. \tag{2-3}$$

Therefore, the reduced state matrix of (1-11) is rearranged for ng generators as,

$$\begin{bmatrix} \Delta\dot{\underline{\delta}} \\ \Delta\dot{\underline{\omega}}_r \end{bmatrix} = [A(\omega)]_{2ng\times 2ng} \begin{bmatrix} \underline{\Delta\delta} \\ \underline{\Delta\omega_r} \end{bmatrix} \quad \text{or} \quad \begin{bmatrix} \Delta\dot{\underline{\delta}} \\ \Delta\dot{\underline{\omega}}_r \end{bmatrix} = \begin{bmatrix} a_{11} & a_{12} \\ a_{21} & a_{22} \end{bmatrix} \begin{bmatrix} \underline{\Delta\delta} \\ \underline{\Delta\omega_r} \end{bmatrix}. \tag{2-4}$$

It should be noted that the mechanical torque is assumed to be constant, so ΔT_m is neglected. The state variables and sub-matrices of (2-4) are:

$$\underline{\Delta\delta} = [\Delta\delta_1, \dots, \Delta\delta_{ng}]^T \tag{2-5}$$

$$\underline{\Delta\omega_r} = [\ \Delta\omega_{r1}, \dots, \Delta\omega_{rng}]^T \tag{2-6}$$

$$[a_{11}] = [0]_{ng\times ng} \tag{2-7}$$

$$[a_{12}] = \omega_0 [I]_{ng\times ng} \tag{2-8}$$

$$[a_{21}(\omega)] = -[H]^{-1}_{ng\times ng}\,[K_S(\omega)]_{ng\times ng} \tag{2-9}$$

$$[a_{22}(\omega)] = -[H]^{-1}_{ng\times ng}\,[K_D(\omega)]_{ng\times ng} \tag{2-10}$$

where $\Delta\delta_i$ (i=1, 2,…, ng) and $\Delta\omega_{ri}$ (i=1, 2,…, ng) are the perturbation rotor angle and speed deviations for the ng generators. $[I]_{ng\times ng}$ is the identity matrix, ω_0 is the system nominal frequency (i.e., 377 rad/s), and $[H]_{ng\times ng}$ is the diagonal matrix of generators inertias, as

$$[H]_{ng\times ng} = diag\,(2H_i) \quad i = 1,\ 2, \dots,\ ng. \tag{2-11}$$

$[A(\omega)]$ is the frequency-dependent reduced state matrix for a system with ng generators. Since each generator is modeled by two state variables, regardless of the system complexity, the order of the matrix $[A(\omega)]$ is always $2ng$. Once this matrix is formed, the QR analysis provides complete information for the electromechanical oscillations. The simple diagram of Figure 2-1 shows the steps performed in TFEA to form $[K_S(\omega)]$ and $[K_D(\omega)]$ matrices. All the steps are described in the following sections.

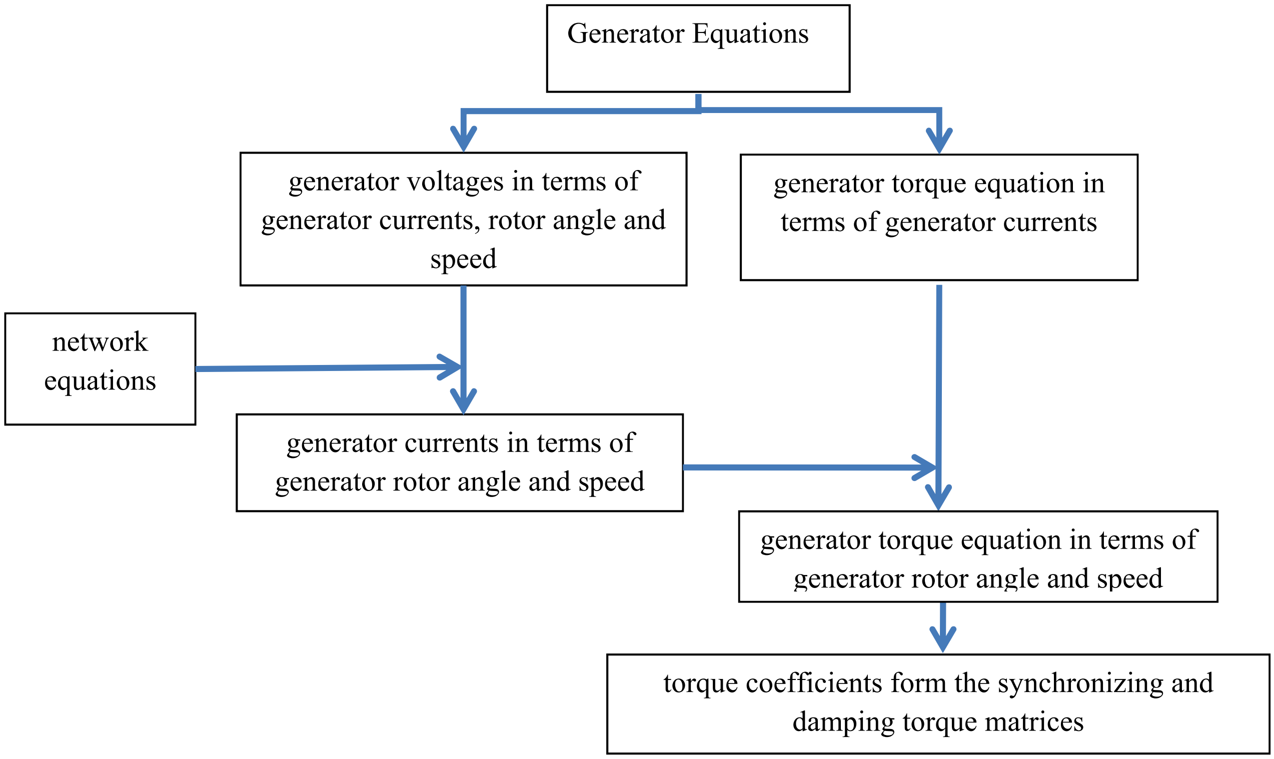

Figure 2-1: TFEA intermediate paths to form the reduced state matrix.

2.2 Complete Set of Electrical Equations of the Synchronous Generator

The generator equations include the mechanical equations of (1-8) and (1-10) as well as the electrical equations shown in this section. The background of this section is taken from Chapter 3 of reference [2]. The generator equations are expressed in $dq0$ frame in per unit with time in seconds. In the following equations, two q-axis damper windings are considered with the subscripts $1q$ and $2q$. Only one d-axis damper winding is considered with the subscript $1d$ [2]. The subscript a and fd are denoted to the stator and field circuits respectively. The L_{ad}-base reciprocal per unit system is chosen which reflects most closely the physical features of the generator [2]. In the L_{ad}-base per unit system, all the mutual inductances between the stator and rotor circuits on each axis (d and q) are equal and are called L_{ad} and L_{aq} respectively. Therefore,

$$L_{afd} = L_{fda} = L_{a1d} = L_{1da} = L_{ad} \qquad (2\text{-}12)$$

$$L_{akq} = L_{kqa} = L_{aq} \qquad for\ k = 1, 2 \qquad (2\text{-}13)$$

$$L_{fd1d} = L_{1dfd}. \tag{2-14}$$

The per unit stator and rotor flux linkage equations in $dq0$ frame, with the inductances in (2-12)-(2-14), are:

$$\Psi_d = -L_d i_d + L_{ad} i_{fd} + L_{ad} i_{1d} \tag{2-15}$$

$$\Psi_q = -L_q i_q + L_{aq} i_{1q} + L_{aq} i_{2q} \tag{2-16}$$

$$\Psi_0 = -L_0 i_0 \tag{2-17}$$

$$\Psi_{fd} = L_{ffd} i_{fd} + L_{fd1d} i_{1d} - L_{ad} i_d \tag{2-18}$$

$$\Psi_{1d} = L_{fd1d} i_{fd} + L_{11d} i_{1d} - L_{ad} i_d \tag{2-19}$$

$$\Psi_{1q} = L_{11q} i_{1q} + L_{aq} i_{2q} - L_{aq} i_q \tag{2-20}$$

$$\Psi_{2q} = L_{aq} i_{1q} + L_{22q} i_{2q} - L_{aq} i_q \tag{2-21}$$

where i_d and i_q are the stator currents in d and q axes respectively. L_d and L_q are the stator self-inductances and L_{ffd}, L_{11d}, L_{11q}, and L_{22q} are the self-inductances of the field and damper winding circuits.

Based on the flux linkages, the per unit stator and rotor voltage equations are as below:

$$e_d = p\Psi_d - \Psi_q \omega_r - R_a i_d \tag{2-22}$$

$$e_q = p\Psi_q + \Psi_d \omega_r - R_a i_q \tag{2-23}$$

$$e_0 = p\Psi_0 - R_a i_0 \tag{2-24}$$

$$e_{fd} = p\Psi_{fd} + R_{fd} i_{fd} \tag{2-25}$$

$$e_{1d} = 0 = p\Psi_{1d} + R_{1d} i_{1d} \tag{2-26}$$

$$e_{1q} = 0 = p\Psi_{1q} + R_{1q} i_{1q} \tag{2-27}$$

$$e_{2q} = 0 = p\Psi_{2q} + R_{2q} i_{2q} \tag{2-28}$$

in which p is the differential operator that can be replaced by (s/ω_0) where ω_0 is the nominal frequency in rad/s and s is the Laplace operator [42]. ω_r is the system frequency in per unit; i and R are the current and resistance of the corresponding circuits respectively.

Finally the per unit air-gap torque is,

$$T_e = \Psi_d i_q - \Psi_q i_d \tag{2-29}$$

which is the most important electrical equation for the use of this research.

2.3 Deriving Electric Currents by Compacting the Generator Equations

2.3.1 Dynamic Model of Generator in *d-q* Frame

As the torque in (2-29) is expressed in terms of currents, the objective of Sections 2.3 and 2.4 is to find a closed form solution for the generator currents.

Combining the flux linkage and voltage equations of (2-15)-(2-28), the generator voltages and currents can be related in the closed form of,

$$\underline{e} = \left(\frac{s}{\omega_0}\right)[L]\underline{i} + \omega_r[P][L]\underline{i} + [R]\underline{i}. \tag{2-30}$$

In addition, the torque equation of (2-29) can be written as,

$$T_e = \underline{i}^T[L]^T[P]^T\underline{i} \tag{2-31}$$

where

$$\underline{e} = [e_d, e_q, e_{fd}, 0, 0, 0]^T \tag{2-32}$$

$$\underline{i} = [i_d, i_q, i_{fd}, i_{1d}, i_{1q}, i_{2q}]^T \tag{2-33}$$

$$[L]_{6\times6} = \begin{bmatrix} -L_d & 0 & L_{ad} & L_{ad} & 0 & 0 \\ 0 & -L_q & 0 & 0 & L_{aq} & L_{aq} \\ -L_{ad} & 0 & L_{ffd} & L_{fd1d} & 0 & 0 \\ -L_{ad} & 0 & L_{fd1d} & L_{11d} & 0 & 0 \\ 0 & -L_{aq} & 0 & 0 & L_{11q} & L_{aq} \\ 0 & -L_{aq} & 0 & 0 & L_{aq} & L_{22q} \end{bmatrix} \tag{2-34}$$

$$[R]_{6\times6} = \begin{bmatrix} -R_a & 0 & 0 & 0 & 0 & 0 \\ 0 & -R_a & 0 & 0 & 0 & 0 \\ 0 & 0 & R_{fd} & 0 & 0 & 0 \\ 0 & 0 & 0 & R_{1d} & 0 & 0 \\ 0 & 0 & 0 & 0 & R_{1q} & 0 \\ 0 & 0 & 0 & 0 & 0 & R_{2q} \end{bmatrix} \tag{2-35}$$

$$[P]_{6\times 6} = \begin{bmatrix} 0 -1\,0\,0\,0\,0 \\ 1\,0\,0\,0\,0\,0 \\ 0\,0\,0\,0\,0\,0 \\ 0\,0\,0\,0\,0\,0 \\ 0\,0\,0\,0\,0\,0 \\ 0\,0\,0\,0\,0\,0 \end{bmatrix}. \tag{2-36}$$

Linearizing (2-30) about the steady-state operating point ($\underline{i}_0$, ω_{r0}) and dropping the steady state terms, results in the following equation:

$$\underline{\Delta e} = \left(\frac{s}{\omega_0}[L] + \omega_{r0}[P][L] + [R] \right) \underline{\Delta i} + \Delta\omega_r [P][L]\underline{i_0} \tag{2-37}$$

in which ω_{r0}=1 pu and

$$\underline{\Delta e} = [\Delta e_d, \Delta e_q, \Delta e_{fd}, 0, 0, 0]^T \tag{2-38}$$

$$\underline{\Delta i} = [\Delta i_d, \Delta i_q, \Delta i_{fd}, \Delta i_{1d}, \Delta i_{1q}, \Delta i_{2q}]^T \tag{2-39}$$

$$\underline{i}_0 = [i_{0d}, i_{0q}, i_{0fd}, i_{01d}, i_{01q}, i_{02q}]^T. \tag{2-40}$$

From (2-31), the perturbation electrical torque is

$$\Delta T_e = \underline{\Delta i}^T [L]^T [P]^T \underline{i}_0 + \underline{i}_0^T [L]^T [P]^T \underline{\Delta i}. \tag{2-41}$$

For simplicity in calculations, it is desirable to derive equations involving d and q axes quantities only, from the equations involving six-tuple vector.

The voltage equations of (2-37) can be shown as,

$$\begin{bmatrix} \underline{\Delta e}_{dq} \\ \Delta e_{fd} \\ \underline{\Delta e}_{kdq} \end{bmatrix} = \begin{bmatrix} g_{11}^{(1)} & g_{12}^{(1)} & g_{13}^{(1)} \\ g_{21}^{(1)} & g_{22}^{(1)} & g_{23}^{(1)} \\ g_{31}^{(1)} & g_{32}^{(1)} & g_{33}^{(1)} \end{bmatrix} \begin{bmatrix} \underline{\Delta i}_{dq} \\ \Delta i_{fd} \\ \underline{\Delta i}_{kdq} \end{bmatrix} + \Delta\omega_r [P][L]\underline{i}_0 \tag{2-42}$$

where

$$\underline{\Delta e}_{dq} = [\Delta e_d, \Delta e_q]^T \tag{2-43}$$

$$\underline{\Delta i}_{dq} = [\Delta i_d, \Delta i_q]^T \tag{2-44}$$

$$\underline{\Delta e}_{kdq} = [\Delta e_{1d}, \Delta e_{1q}, \Delta e_{2q}]^T = [0, 0, 0]^T \tag{2-45}$$

$$\underline{\Delta i}_{kdq} = [\Delta i_{1d}, \Delta i_{1q}, \Delta i_{2q}]^T \tag{2-46}$$

$$\begin{bmatrix} g_{11}^{(1)} & g_{12}^{(1)} & g_{13}^{(1)} \\ g_{21}^{(1)} & g_{22}^{(1)} & g_{23}^{(1)} \\ g_{31}^{(1)} & g_{32}^{(1)} & g_{33}^{(1)} \end{bmatrix}_{6\times 6} = \left(\frac{s}{\omega_0}[L] + \omega_{r0}[P][L] + [R] \right). \tag{2-47}$$

The sub matrices in (2-47) are:

$$[g_{11}^{(1)}]_{2\times 2} = \begin{bmatrix} -R_a - {sL_d}/{\omega_0} & L_q\omega_{r0} \\ -L_d\omega_{r0} & -R_a - {sL_q}/{\omega_0} \end{bmatrix} \tag{2-48}$$

$$[g_{12}^{(1)}]_{2\times 1} = \begin{bmatrix} {sL_{ad}}/{\omega_0} \\ L_{ad}\omega_{r0} \end{bmatrix} \tag{2-49}$$

$$[g_{13}^{(1)}]_{2\times 3} = \begin{bmatrix} {sL_{ad}}/{\omega_0} & -L_{aq}\omega_{r0} & -L_{aq}\omega_{r0} \\ L_{ad}\omega_{r0} & {sL_{aq}}/{\omega_0} & {sL_{aq}}/{\omega_0} \end{bmatrix} \tag{2-50}$$

$$[g_{21}^{(1)}]_{1\times 2} = \begin{bmatrix} -{sL_{ad}}/{\omega_0} & 0 \end{bmatrix} \tag{2-51}$$

$$[g_{22}^{(1)}]_{1\times 1} = \begin{bmatrix} R_{fd} + {sL_{ffd}}/{\omega_0} \end{bmatrix} \tag{2-52}$$

$$[g_{23}^{(1)}]_{1\times 3} = \begin{bmatrix} {sL_{fd1d}}/{\omega_0} & 0 & 0 \end{bmatrix} \tag{2-53}$$

$$[g_{31}^{(1)}]_{3\times 2} = \begin{bmatrix} -{sL_{ad}}/{\omega_0} & 0 \\ 0 & -{sL_{aq}}/{\omega_0} \\ 0 & -{sL_{aq}}/{\omega_0} \end{bmatrix} \tag{2-54}$$

$$[g_{32}^{(1)}]_{3\times 1} = \begin{bmatrix} {sL_{fd1d}}/{\omega_0} \\ 0 \\ 0 \end{bmatrix} \tag{2-55}$$

$$[g_{33}^{(1)}]_{3\times 3} = \begin{bmatrix} R_{1d} + {sL_{11d}}/{\omega_0} & 0 & 0 \\ 0 & R_{1q} + {sL_{11q}}/{\omega_0} & {sL_{aq}}/{\omega_0} \\ 0 & {sL_{aq}}/{\omega_0} & R_{2d} + {sL_{22d}}/{\omega_0} \end{bmatrix}. \tag{2-56}$$

Since the voltages across the damper windings are zero, as given by (2-45), the effects of $\underline{\Delta} i_{kdq}$ can be embedded in the perturbation currents of Δi_d, Δi_q and Δi_{fd}. Mathematically, this consists of eliminating $\underline{\Delta} i_{kdq}$ using the third row of (2-42). Therefore,

$$\begin{bmatrix} \underline{\Delta e}_{dq} \\ \Delta e_{fd} \end{bmatrix} = \begin{bmatrix} g_{11}^{(2)} & g_{12}^{(2)} \\ g_{21}^{(2)} & g_{22}^{(2)} \end{bmatrix} \begin{bmatrix} \underline{\Delta i}_{dq} \\ \Delta i_{fd} \end{bmatrix} + \Delta\omega_r \begin{bmatrix} L_1 \\ 0 \end{bmatrix} \underline{i}_{0dqf} \tag{2-57}$$

where

$$\underline{i}_{0dqf} = [i_{0d}, i_{0q}, i_{0fd}]^T \tag{2-58}$$

$$[L_1]_{2\times3} = \begin{bmatrix} 0 & L_q & 0 \\ -L_d & 0 & L_{ad} \end{bmatrix} \tag{2-59}$$

$$[g_{11}^{(2)}]_{2\times2} = [g_{11}^{(1)}] - [g_{13}^{(1)}][g_{33}^{(1)}]^{-1}[g_{31}^{(1)}] \tag{2-60}$$

$$[g_{12}^{(2)}]_{2\times1} = [g_{12}^{(1)}] - [g_{13}^{(1)}][g_{33}^{(1)}]^{-1}[g_{32}^{(1)}] \tag{2-61}$$

$$[g_{21}^{(2)}]_{1\times2} = [g_{21}^{(1)}] - [g_{23}^{(1)}][g_{33}^{(1)}]^{-1}[g_{31}^{(1)}] \tag{2-62}$$

$$[g_{22}^{(2)}]_{1\times1} = [g_{22}^{(1)}] - [g_{23}^{(1)}][g_{33}^{(1)}]^{-1}[g_{32}^{(1)}]. \tag{2-63}$$

Consequently eliminating Δi_{fd} in (2-57), we have,

$$\underline{\Delta e}_{dq} = [g_{11}^{(3)}]\underline{\Delta i}_{dq} + [g_{12}^{(3)}]\,\Delta e_{fd} + \Delta\omega_r\,[L_1]\,\underline{i}_{0dqf} \tag{2-64}$$

where

$$[g_{11}^{(3)}]_{2\times2} = [g_{11}^{(2)}] - [g_{12}^{(2)}][g_{22}^{(2)}]^{-1}[g_{21}^{(2)}] \tag{2-65}$$

$$[g_{12}^{(3)}]_{2\times1} = [g_{12}^{(2)}][g_{22}^{(2)}]^{-1}. \tag{2-66}$$

2.3.2 Modeling Excitation System and Power System Stabilizer

In (2-64), the field voltage Δe_{fd} is the point of entry for feedback from excitation control and power system stabilizer (PSS), as shown in Figure 2-2 [2].

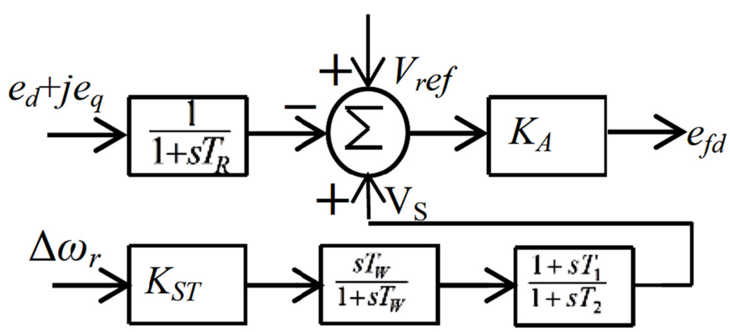

Figure 2-2: Exciter and PSS model [2] .

Based on the transfer functions of the exciter and PSS in Figure 2-2, Δe_{fd} can be written in the following form:

$$\Delta e_{fd} = G_{exc}(s)\,\underline{\Delta e}_{dq} + G_{pss}(s)\,\Delta\omega_r \tag{2-67}$$

where

$$G_{exc}(s)=\left(\frac{-K_A}{1+sT_R}\right)\left(\frac{1}{e_{t0}}\right)\left[e_{d0}\ e_{q0}\right] \tag{2-68}$$

$$G_{pss}(s)=K_A K_{ST}\frac{sT_W}{1+sT_W}\frac{1+sT_1}{1+sT_2} \tag{2-69}$$

in which K_A and K_{ST} are the exciter and stabilizer gains, and T_w, T_1 and T_2 are the stabilizer time constants; e_{d0} and e_{q0} are the steady state terminal voltages, and T_R is the voltage transducer time constant.

Substituting (2-67) for Δe_{fd} in (2-64) gives

$$\left([I]_{2\times2}-[g_{12}^{(3)}]\,G_{exc}(s)\right)\underline{\Delta e}_{dq}=[g_{11}^{(3)}]\underline{\Delta i}_{dq}+\left([L_1]\,\underline{i}_{0dqf}+[g_{12}^{(3)}]\ G_{pss}(s)\right)\Delta\omega_r \tag{2-70}$$

where $[I]_{2\times2}$ is a 2×2 identity matrix.

Now the currents can be extracted from (2-70) as,

$$\underline{\Delta i}_{dq}=[A(s)]\underline{\Delta e}_{dq}+[B(s)]\,\Delta\omega_r \tag{2-71}$$

where

$$[A(s)]_{2\times2}=[g_{11}^{(3)}]^{-1}\left([I_{2\times2}]-[g_{12}^{(3)}]G_{exc}(s)\right) \tag{2-72}$$

$$[B(s)]_{2\times1}=-[g_{11}^{(3)}]^{-1}\left([L_1]\underline{i}_{0dqf}+[g_{12}^{(3)}]G_{pss}(s)\right) \tag{2-73}$$

2.3.3 Transformation from *d-q* Frame to *R-I* Frame

In a network with *ng* generators, there exists *ng* sets of equations (2-12)-(2-73), while the final useable form for this research is (2-71). Each equation set is valid in the *d-q* frame of the individual generator. The standard technique is to unite all the generators by transforming the individual *d-q* frames to the common Real-Imaginary (*R-I*) frame of the system grid. Figure 2-3 illustrates the relationship between the *d-q* frame of an individual generator and the *R-I* frame of the system. According to this figure, the rotor angular orientation δ is the angle by which the *q*-axis leads the reference *R* [2]. As the result of load flow, the rotor angle δ_n and the steady state *d-q* currents $\underline{i}_{0dqn}$, and voltages $\underline{e}_{0dqn}$ of all the *ng* generators (i.e., *n*= 1, 2,…, *ng*) are obtained.

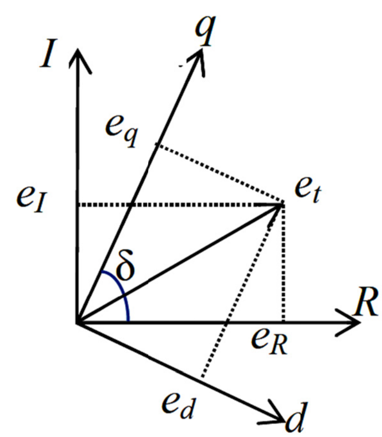

Figure 2-3: Relationship between the *d-q* frame of a single generator and the *R-I* reference frame of the system.

According to Figure 2-3, the generator voltages and currents in the *R-I* frame can be found using an orthogonal rotation matrix, say $[C(\delta_n)]$. Therefore for n^{th} generator,

$$\underline{e}_{RIn} = [C(\delta_n)]\underline{e}_{dqn} \qquad n = 1,\ 2, \ldots,\ ng \tag{2-74}$$

$$\underline{i}_{RIn} = [C(\delta_n)]\underline{i}_{dqn} \qquad n = 1,\ 2, \ldots,\ ng \tag{2-75}$$

where

$$[C(\delta_n)]_{2\times 2} = \begin{bmatrix} \sin(\delta_n) & \cos(\delta_n) \\ -\cos(\delta_n) & \sin(\delta_n) \end{bmatrix} \qquad n = 1,\ 2, \ldots,\ ng \tag{2-76}$$

$$\underline{e}_{dqn} = [e_{dn}, e_{qn}] \qquad n = 1,\ 2, \ldots,\ ng \tag{2-77}$$

$$\underline{i}_{dqn} = [i_{dn}, i_{qn}] \qquad n = 1,\ 2, \ldots,\ ng. \tag{2-78}$$

Consequently the new steady state components for n^{th} generator are:

$$\underline{e}_{0RIn} = [C(\delta_n)]\underline{e}_{0dqn} \qquad n = 1,\ 2, \ldots,\ ng \tag{2-79}$$

$$\underline{i}_{0RIn} = [C(\delta_n)]\underline{i}_{0dqn} \qquad n = 1,\ 2, \ldots,\ ng \tag{2-80}$$

where

$$\underline{e}_{0dqn} = [e_{0dn}, e_{0qn}] \qquad n = 1,\ 2, \ldots,\ ng \tag{2-81}$$

$$\underline{i}_{0dqn} = [i_{0dn}, i_{0qn}] \qquad n = 1,\ 2, \ldots,\ ng. \tag{2-82}$$

Linearizing (2-74) and (2-75) about the steady state operating point $\underline{e}_{0RIn}$ and $\underline{i}_{0RIn}$, we have:

$$\underline{\Delta e}_{dqn} = [C(\delta_n)]^T \underline{\Delta e}_{RIn} + \frac{\omega_0}{s}[C(\delta_n)]\,\underline{e}_{0RI0}\,\Delta\omega_{rn} \qquad n = 1,\ 2, \ldots,\ ng \tag{2-83}$$

$$\underline{\Delta i}_{dqn} = [C(\delta_n)]^T \underline{\Delta i}_{RIn} + \frac{\omega_0}{s}[C(\delta_n)]\,\underline{i}_{0RIn}\,\Delta\omega_{rn} \qquad n = 1,\ 2, \ldots,\ ng \tag{2-84}$$

where $\underline{\Delta e}_{RIn}$ and $\underline{\Delta i}_{RIn}$ are the voltage and current perturbations for generator n, in the R-I frame, and $\Delta\omega_{rn}$ is the perturbation rotor speed for generator n. It should be noted that $[\Delta C(\delta_n)] = [C(\delta_n)]^T \Delta\delta_n = [C(\delta_n)]^T \frac{\omega_0}{s} \Delta\omega_{rn}$.

2.3.4 *R-I* Frame Equations of *ng* Generators

Inserting (2-83) and (2-84) in (2-71) results in the current equation for n^{th} generator in the *R-I* frame:

$$\underline{\Delta i}_{RIn} = [A_n^{'}(s)]\underline{\Delta e}_{RIn} + [B_n^{'}(s)]\Delta\omega_{rn} \qquad n = 1,\ 2, \ldots,\ ng \tag{2-85}$$

where

$$[A_n^{'}]_{2\times 2} = [C(\delta_n)][A_n(s)][C(\delta_n)]^T \qquad n = 1,\ 2, \ldots,\ ng \tag{2-86}$$

$$[B_n^{'}]_{2\times 1} = \frac{\omega_0}{s}\left([C(\delta_n)][A_n(s)][C(\delta_n)]\underline{e}_{RI0n} - [C(\delta_n)]^2 \underline{i}_{RI0n}\right) + [C(\delta_n)][B_n(s)] \quad n = 1,\ 2, \ldots,\ ng \tag{2-87}$$

and $[A_n(s)]$ and $[B_n(s)]$ are defined in (2-72) and (2-73).

Equation (2-85) can be expanded for all the *ng* generators, which gives the following closed form matrix equation:

$$\underline{\Delta i}_{RI-full} = [A_{full}^{'}(s)]\ \underline{\Delta e}_{RI-full} + [B_{full}^{'}(s)]\ \underline{\Delta\omega_r} \tag{2-88}$$

where

$$\underline{\Delta i}_{RI-full} = [\underline{\Delta i}_{RI1}^T \ldots \underline{\Delta i}_{RIng}^T]^T \tag{2-89}$$

$$\underline{\Delta e}_{RI-full} = [\underline{\Delta e}_{RI1}^T \ldots \underline{\Delta e}_{RIng}^T]^T \tag{2-90}$$

are vectors of the size $2ng$, and

$$[A_{full}^{'}(s)]_{2ng\times 2ng} = \begin{bmatrix} [A_1^{'}(s)] & 0 & . & . & 0 \\ 0 & [A_2^{'}(s)] & . & . & 0 \\ . & . & . & . & . \\ . & . & . & . & . \\ 0 & . & . & 0 & [A_{ng}^{'}(s)] \end{bmatrix} \tag{2-91}$$

$$[B'_{full}(s)]_{2ng\times ng} = \begin{bmatrix} [B'_1(s)] & 0 & . & . & 0 \\ 0 & [B'_2(s)] & . & . & 0 \\ . & . & . & . & . \\ . & . & . & . & . \\ 0 & . & . & 0 & [B'_{ng}(s)] \end{bmatrix}. \tag{2-92}$$

2.4 Integrating Power System Network Equations to Generator Equations

In order to eliminate $\underline{\Delta e}_{RI\text{-}full}$ in (2-88), network equations should be incorporated. It is assumed that the network has *Nb* buses, from which the first *ng* are the generating buses. Therefore, from the bus impedance matrix we have,

$$\begin{bmatrix} e_1 \\ \vdots \\ e_{ng} \\ v_{ng+1} \\ \vdots \\ v_{Nb} \end{bmatrix} = \begin{bmatrix} Z_{bus11} & Z_{bus12} \\ Z_{bus21} & Z_{bus22} \end{bmatrix}_{Nb\times Nb} \begin{bmatrix} i_1 \\ \vdots \\ i_{ng} \\ i_{ng+1} \\ \vdots \\ i_{Nb} \end{bmatrix} \tag{2-93}$$

where $[e_{1,}\dots,e_{ng},\ e_{ng+1,}\dots,\ e_{Nb}]^T$ and $[i_{1,}\dots,\ i_{ng},\ i_{ng+1,}\dots,\ i_{Nb}]^T$ are the vectors of bus voltages and bus injected currents respectively, and Z_{busij} ($i,\ j$= 1, 2) are the sub-matrices of the bus impedance matrix.

After perturbing (2-93) we have,

$$\begin{bmatrix} \Delta e_1 \\ \vdots \\ \Delta e_{n_g} \\ \Delta v_{ng+1} \\ \vdots \\ \Delta v_{Nb} \end{bmatrix} = \begin{bmatrix} Z_{bus11} & Z_{bus12} \\ Z_{bus21} & Z_{bus22} \end{bmatrix}_{Nb\times Nb} \begin{bmatrix} \Delta i_1 \\ \vdots \\ \Delta i_{n_g} \\ \Delta i_{ng+1} \\ \vdots \\ \Delta i_{Nb} \end{bmatrix}. \tag{2-94}$$

From the first *ng* rows of (2-94), generator voltages would be extracted as,

$$\begin{bmatrix} \Delta e_1 \\ \vdots \\ \Delta e_{ng} \end{bmatrix} = [Z_{bus11}]_{ng\times ng} \begin{bmatrix} \Delta i_1 \\ \vdots \\ \Delta i_{ng} \end{bmatrix} + [Z_{bus12}]_{ng\times(Nb-ng)} \begin{bmatrix} \Delta i_{ng+1} \\ \vdots \\ \Delta i_{Nb} \end{bmatrix}. \tag{2-95}$$

At the same time, the load currents $[\Delta i_{ng+1,}\dots,\ \Delta i_{Nb}]^T$ in (2-95) can be eliminated from the second (*Nb-ng*) rows of (2-94), while considering (2-96). Equation (2-96) implies the relationship between the load voltages and the load currents. This relationship (function $f\,()$) depends on the load type, and in general can be considered as:

$$\begin{bmatrix}\Delta v_{ng+1}\\ \vdots\\ \Delta v_{Nb}\end{bmatrix} = f\left(\begin{bmatrix}\Delta i_{ng+1}\\ \vdots\\ \Delta i_{Nb}\end{bmatrix}\right). \tag{2-96}$$

Therefore, from (2-94) the load currents are:

$$\begin{bmatrix}\Delta i_{ng+1}\\ \vdots\\ \Delta i_{Nb}\end{bmatrix} = \left(f - [Z_{bus22}]_{(Nb-ng)\times(Nb-ng)}\right)^{-1} [Z_{bus21}]_{(Nb-ng)\times ng} \begin{bmatrix}\Delta i_{1}\\ \vdots\\ \Delta i_{ng}\end{bmatrix}. \tag{2-97}$$

Now replacing (2-97) for $[\Delta i_{ng+1},\ldots, \Delta i_{Nb}]^T$ in (2-95), the generator voltages are obtained,

$$\begin{bmatrix}\Delta e_{1}\\ \vdots\\ \Delta e_{ng}\end{bmatrix} = [Z_{total}] \begin{bmatrix}\Delta i_{1}\\ \vdots\\ \Delta i_{ng}\end{bmatrix} \tag{2-98}$$

where

$$[Z_{total}]_{ng\times ng} = [Z_{bus11}]_{ng\times ng} + [Z_{bus12}]_{ng\times(Nb-ng)} \times \left(f - [Z_{bus22}]_{(Nb-ng)\times(Nb-ng)}\right)^{-1} [Z_{bus21}]_{(Nb-ng)\times ng} \tag{2-99}$$

In order to extract the *R-I* components of (2-98), $[Z_{total}]$ should be decoupled into real and imaginary parts as,

$$[R_{total}]_{ng\times ng} = \text{Real } \left\{[Z_{total}]_{ng\times ng}\right\} \tag{2-100}$$

$$[X_{total}]_{ng\times ng} = \text{Imaginary } \left\{[Z_{total}]_{ng\times ng}\right\} \tag{2-101}$$

From (2-98), it can be shown that the complete generator currents and voltages in the *R-I* frame are related as,

$$\underline{\Delta e}_{RI-full} = [D]\,\underline{\Delta i}_{RI-full} \tag{2-102}$$

where

$$[D]_{2ng\times 2ng} = \begin{bmatrix}[D_{11}]_{2\times 2} & \cdots & [D_{1ng}]_{2\times 2}\\ \vdots & [D_{ij}]_{2\times 2} & \vdots\\ [D_{ng1}]_{2\times 2} & \cdots & [D_{ngng}]_{2\times 2}\end{bmatrix} \tag{2-103}$$

and

$$[D_{ij}]_{2\times 2} = \begin{bmatrix} r_{ij} & -x_{ij}\\ x_{ij} & r_{ij}\end{bmatrix} \qquad i, j = 1,\ 2, \ldots,\ ng \tag{2-104}$$

in which r_{ij} and x_{ij} are the $(i,j)^{th}$ entry of $[R_{total}]$ and $[X_{total}]$ respectively.

Finally, $\underline{\Delta e}_{RI-full}$ in (2-88) is replaced by (2-102):

$$\underline{\Delta i}_{RI-full} = [A'_{full}(s)]\ [D]\ \underline{\Delta i}_{RI-full} + [B'_{full}(s)]\ \underline{\Delta\omega_r} \tag{2-105}$$

and $\underline{\Delta i}_{RI\text{-}full}$ is derived in terms of all generators speed deviations $\underline{\Delta\omega}_r$, as:

$$\underline{\Delta i}_{RI-full} = \left([I]_{2ng\times 2ng} - [A'_{full}(s)][D]\right)^{-1}[B'_{full}(s)]\underline{\Delta\omega}_r. \tag{2-106}$$

2.5 Perturbation Generator Torque

Having $\underline{\Delta i}_{RI}$ for each generator, it is now possible to form the electrical torque variations. From (2-41):

$$\Delta T_e = \underline{\Delta i}^T[L]^T[P]^T\underline{i}_0 + \underline{i}_0^T[L]^T[P]^T\underline{\Delta i} \tag{2-107}$$

where

$$\underline{\Delta i} = [\Delta i_d, \Delta i_q, \Delta i_{fd}, \Delta i_{1d}, \Delta i_{1q}, \Delta i_{2q}]^T \tag{2-108}$$

$$\underline{i}_0 = [i_{0d}, i_{0q}, i_{0fd}, i_{01d}, i_{01q}, i_{02q}]^T \tag{2-109}$$

and $[L]$ and $[P]$ are defined in (2-34) and (2-36) respectively.

The currents in (2-108) can be easily found in terms of $\underline{\Delta\omega}_r$ from $\underline{\Delta i}_{RI}$ of (2-106). From $\underline{\Delta i}_{RI}$ for each generator, back-substitution by $[C(\delta_n)]$ of (2-76) to the *d-q* frame gives $\underline{\Delta i}_{dq}$ for each generator. Also $\underline{\Delta i}_{kdq}$ and $\underline{\Delta i}_{fd}$ are found in terms of $\underline{\Delta i}_{dq}$ from the 3rd row of (2-42) when considering (2-45). By having the currents of (2-108), the perturbation torque of (2-107) for all the *ng* generators can be arranged as,

$$\begin{bmatrix} \Delta T_{e1} \\ : \\ \Delta T_{eng} \end{bmatrix} = [A''(s)] \begin{bmatrix} \Delta\omega_{r1} \\ : \\ \Delta\omega_{rng} \end{bmatrix} \tag{2-110}$$

where $[A''(s)]$ is a full and frequency-dependent matrix. Forming $[A''(s)]$ is straight forward and is explained in Appendix B.

2.6 Damping and Synchronizing Torque Matrices

For each mode, whose modal frequency is ω_n, the rotors of every generator oscillates at the speed of ω_n. The perturbation speed can be written as an *ng*-tuple vector $\underline{\Delta\omega}_r$ in the following form:

$$\underline{\Delta\omega_r}(t) = \mathrm{Real}\left\{\underline{\overline{\Omega}} e^{j\omega_n t}\right\} \tag{2-111}$$

where

$$\underline{\overline{\Omega}} = [\overline{\Omega}_1, \overline{\Omega}_2, \ldots \overline{\Omega}_{ng}]^{\mathrm{T}} \tag{2-112}$$

in which $\overline{\Omega}_i \ (i = 1, 2, \ldots, ng)$ is a phasor quantity.

Each generator is oscillating at the perturbation speed of (2-111), which through the generator currents of (2-71) makes all other electrical variables oscillate with the same frequency, including the perturbation torque. Therefore, the vector of perturbation torques of *ng* generators would be,

$$\underline{\Delta T_e}(t) = \mathrm{Real}\left\{\underline{\overline{T}}_e e^{j\omega_n t}\right\} \tag{2-113}$$

$$\underline{\overline{T}}_e = [\overline{T_{e1}}, \overline{T_{e2}}, \ldots \overline{T}_{eng}]^T \tag{2-114}$$

where $\overline{T}_{e\,i} \ (i = 1, 2, \ldots, ng)$ is a phasor quantity.

Substituting (2-111) and (2-113) in (2-110) yields

$$\begin{bmatrix} \overline{T}_{e1} \\ \vdots \\ \overline{T}_{eng} \end{bmatrix} = [A''(\omega_n)]_{ng\times ng} \begin{bmatrix} \overline{\Omega}_1 \\ \vdots \\ \overline{\Omega}_{n_g} \end{bmatrix}. \tag{2-115}$$

On the other hand, because the rotor speed and angle deviations are related by

$$j\omega_n \Delta\delta = \omega_0 \Delta\omega_r, \tag{2-116}$$

one can define a vector of angle deviations $\underline{\Delta\delta}$:

$$\underline{\Delta\delta}(t) = \mathrm{Real}\left\{\underline{\overline{\Delta}} e^{j\omega_n t}\right\} \tag{2-117}$$

where

$$\underline{\overline{\Delta}} = [\overline{\Delta}_1 \ldots \overline{\Delta}_{n_g}]^{\mathrm{T}} \tag{2-118}$$

and $\overline{\Delta}_i \ (i = 1, 2, \ldots, ng)$ is a phasor quantity.

From (2-116), $\overline{\Omega}_i$ and $\overline{\Delta}_i$ are related by

$$j \begin{bmatrix} \overline{\Omega}_1 \\ \vdots \\ \overline{\Omega}_{ng} \end{bmatrix} = -\frac{\omega_n}{\omega_0} \begin{bmatrix} \overline{\Delta}_1 \\ \vdots \\ \overline{\Delta}_{ng} \end{bmatrix}. \tag{2-119}$$

In conclusion, the matrices of synchronizing torque coefficients $[K_S(\omega)]$ and damping torque coefficient $[K_D(\omega)]$ are derived by incorporating (2-119) into (2-115), as

$$[K_S(\omega_n)]_{ng\times ng} = \mathrm{Imaginary}\left\{[A''(\omega_n)]_{ng\times ng}\right\}(-\omega_n / \omega_0) \tag{2-120}$$

$$[K_D(\omega_n)]_{ng\times ng} = \text{Real}\{[A''(\omega_n)]_{ng\times ng}\}. \quad (2\text{-}121)$$

Once the $[K_S(\omega)]$ and $[K_D(\omega)]$ matrices are found, the reduced state matrix $[A(\omega)]_{2ng\times 2ng}$ can be formed as in (2-4).

Considering the detailed procedure of Section 2.1 to 2.6, it is realized that no approximation has been used in forming the reduced state matrix. In fact the frequency dependency in the $[A(\omega)]$ matrix ensures that the properties of the other (m-2) state-variable continue to be represented. The method has reduced the number of states without incurring inaccuracy in the dynamic behaviours.

2.7 Representative Frequency ω_K Versus Oscillating Frequency ω_n

For a predetermined frequency ω_K, which is called representative frequency, the eigenanalysis of $[A(\omega_K)]$ gives (ng-1) oscillatory modes at frequencies ω_n, n= 1, 2,…, (ng-1). At each modal frequency ω_n, all the generators are oscillating at frequency ω_n.

For the computation cost shown in Chapter 3, $[A(\omega)]$ is formed and solved only once for one representative frequency ω_K. However, the eigenvalues of $[A(\omega_K)]$ have modal frequencies ω_n, n= 1, 2,…, (ng-1), for which a single ω_K cannot be representative of. In fact, this would be the origin of discrepancies for the TFEA results: For each modal frequency ω_n, the field excitation systems, PSS and damper windings respond to frequency ω_n and not to ω_K. To observe this point, the synchronizing and damping torques of the single generator system of Figure 2-4, are shown in Figure 2-5. As can be seen, the frequency dependency of the exciter and PSS affects the synchronizing and damping torques spectrum.

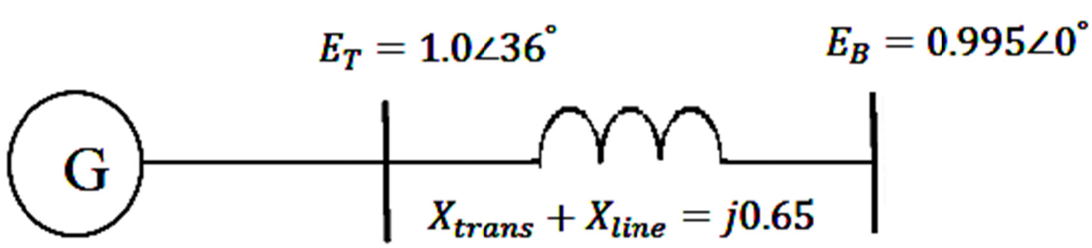

Figure 2-4: Single generator system [2].

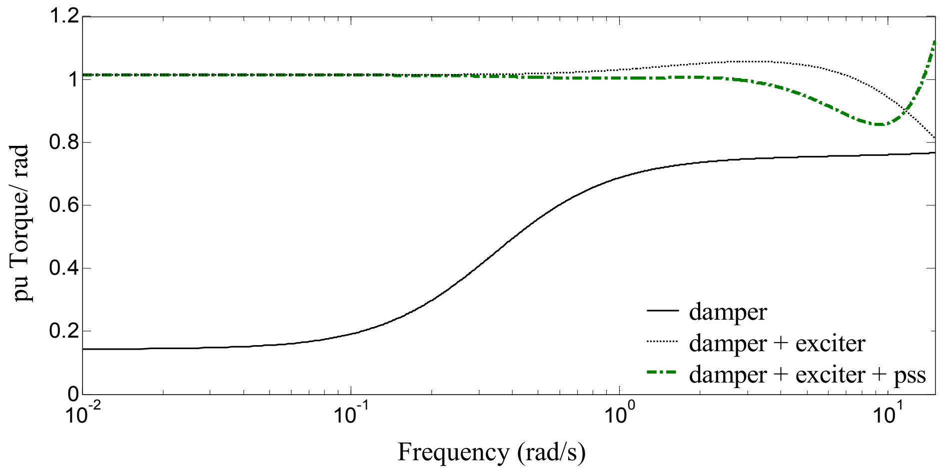

(a): Synchronizing torque coefficient.

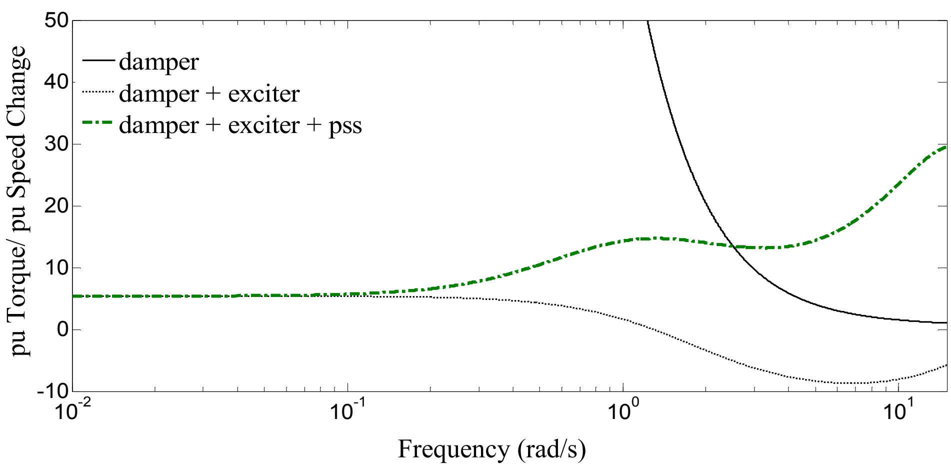

(b): Damping torque coefficient.

Figure 2-5: Torque coefficients for single generator system.

The first step of TFEA is therefore to choose ω_K, the representative frequency of the spectrum of interest. For instance, one prevailing interest is on the lowest frequency modes because their damping coefficients are very low, however, there is a disturbing note that some high frequency modes can also be lightly or negatively damped [41]. In this research, the entire electromechanical frequency range is of interest. According to [3], this range is 0.1-0.8 Hz for inter-area modes and 0.7-2 Hz for local oscillations. Therefore, a frequency range of 0.7-12.5 rad/s is considered, and a moderate frequency of 5 rad/s is chosen as ω_K. The expectation is that modes with frequencies ω_n close to ω_K are accurately predicted and this has been borne to be true from numerical evaluation. The effect of different representative frequencies on the TFEA performance will be discussed in Section 2.10.2.

2.8 Correction by the Eigenvalue Sensitivity Formula

Having pointed to an important source of inaccuracy, this section offers a computationally economical route of obtaining better estimates by applying the eigenvalue sensitivity-with-respect-to-parameter-variation formula of [41], with explanation given in [43].

For a matrix $[A]$ with an eigenvalue λ, the sensitivity formula determines the eigenvalue change $\Delta\lambda$ due to a perturbation of $\Delta[A]$ [41]:

$$\Delta\lambda = \frac{\underline{r}^T \Delta[A]\, \underline{u}}{\underline{r}^T\ \underline{u}} \tag{2-122}$$

where the vectors $\underline{u}$ and $\underline{r}$ are the eigenvectors of $[A]$ and $[A]^T$ respectively. The vectors $\underline{u}$ and $\underline{r}$ are sometimes called the right and left eigenvectors of $[A]$ [44].

$$[A]\,\underline{u} = \lambda\, \underline{u} \tag{2-123}$$

$$[A]^T\, \underline{r} = \lambda\, \underline{r} \tag{2-124}$$

From TFEA, the eigenvalues $\lambda_n=\sigma_n \pm j\omega_n$ and the eigenvectors $\underline{u}_n$ and $\underline{r}_n$, n=1, 2..., (ng-1), of $[A(\omega_K)]$ are retained. If the n^{th} mode is of interest, a new $[A(\omega_n)]$ is formed evaluated at the frequency ω_n. For the n^{th} mode with right eigenvector $\underline{u}_n$ and left eigenvector $\underline{r}_n$ of $[A(\omega_K)]$, the correction for $[A]=[A(\omega_n)]$ is based on small perturbation $\Delta[A]=[A(\omega_n)]-[A(\omega_K)]$ in (2-122). Therefore, the eigenvalue sensitivity correction is,

$$\Delta\lambda_n = \frac{\underline{r}_n^T([A(\omega_n)] - [A(\omega_K)])\underline{u}_n}{\underline{r}_n^T \underline{u}_n} \tag{2-125}$$

and the new improved eigenvalue estimation is,

$$\lambda_{n\_imp} = \lambda_n + \Delta\lambda_n \tag{2-126}$$

where λ_n is the n^{th} eigenvalue of $[A(\omega_K)]$.

2.9 Numerical Results

In order to establish the feasibility of the method, it is necessary to provide unimpeachable eigenvalue references for comparison. The model of the test references represents the damper windings, the excitation system and PSS of each generator as state-space equations. In general, each generator with exciter and PSS, is modeled by m=11 state-variables. This matrix is the full state matrix $[A]_{11ng\times 11ng}$ as in (1-4). The 11 state variables include six flux variables, rotor angle, rotor speed and three control states from exciter and PSS. From the (11ng) modes, (ng-1) pair of complex conjugate electromechanical modes are sorted out for comparison with the results of the TFEA method. The (ng-1) electromechanical eigenvalues of the full state matrix are the benchmark results for comparison.

The TFEA results are from the eigenanalysis of the reduced state matrix $[A(\omega_K)]_{2ng\times 2ng}$, where ω_K is chosen 5 rad/s. The eigenvectors of $[A(\omega_K)]$ are retained for improved accuracy estimation using the eigenvalue sensitivity formula of (2-125).

Eigenanalysis of both the reduced and full state matrices are solved in MATLAB by QR Algorithm [18].

2.9.1 Single-Generator System

To start with a basic example, the single generator model of Figure 2-4 is considered in this section. The generator data and the operating conditions, taken from [2], are presented in Table 2-1 and Table 2-2 respectively. The values are in per unit. It is assumed that the generator is equipped with the exciter and PSS modeled in Figure 2-2, with the parameters in Table 2-3.

Table 2-1: Generator parameters in per unit for the system of Figure 2-4.

L_{ad}	L_{aq}	$L_{leakage}$	L_{fd}	L_{1d}	L_{1q}	L_{2q}	R_a	R_{fd}	R_{1d}	R_{1q}	R_{2q}
1.4	1.36	0.16	0.15	0.14	0.07	0.11	0.003	0.0006	0.024	0.006	0.022

Table 2-2: Operating conditions for the system of Figure 2-4.

i_{d0} (pu)	i_{q0} (pu)	e_{d0} (pu)	e_{q0} (pu)	e_{fd0} (pu)	δ_0 (deg)
0.83	0.45	0.68	0.73	2.395	79^{o}

Table 2-3: Exciter and PSS parameters.

K_A	$T_R(s)$	K_{ST}	$T_w(s)$	$T_1(s)$	$T_2(s)$
200	0.02	9.5	1.4	0.154	0.033

The TFEA method is applied to this system to find $[K_S(\omega)]$ and $[K_D(\omega)]$ and form the reduced $[A(\omega)]$ matrix. This system has only one electromechanical mode, as shown in Table 2-5 for three different cases of Table 2-4. The purpose of case studies in Table 2-4 is to gather data which shed insights on the method. For example, exciters are known to give rise to negative damping while the PSS is to resolve it. The case studies of Table 2-4 are used through the entire chapter.

Table 2-4: Different case studies based on the generator model.

Case number	Damper windings	Exciter	PSS
1	✓	×	×
2	✓	✓	×
3	✓	✓	✓

Table 2-5: Eigenvalue estimation results for the single generator system.

Case number	Benchmark results of $[A]_{11\times 11}$	$\lambda(\omega_K=5)$ of $[A(\omega_K)]_{2\times 2}$	$\lambda_{imp} = \lambda(\omega_K=5)+\Delta\lambda$ of (2-126)
1	$-0.17\pm j6.47$	$-0.29\pm j6.43$	$-0.19\pm j6.45$
2	$0.53\pm j7.38$	$0.51\pm j7.49$	$0.55\pm j7.36$
3	$-1.08\pm j6.8$	$-1.05\pm j7.1$	$-1.15\pm j6.85$

Table 2-5 has four columns. The first column lists the case number from Table 2-4. The second column is the benchmark result obtained by the eigenanalysis of the full state matrix from [2]. The third column is the eigenvalue estimation by TFEA for the representative frequency ω_K=5 rad/s and the last column shows the improved estimation of eigenvalue from (2-126), when $\Delta\lambda$ is calculated from (2-125).

Comparing the results in Table 2-5, it is observed that the final result λ_{imp}, is in good agreement with the benchmark result.

2.9.2 Multi-Generator Power Systems

Three different multi-generator power systems are used in this research: the 4-generator and 16-generator test systems taken from [11] and the 69-generator system taken from [45]. The power system size is increased to see if the proposed method is applicable and effective for larger networks.

The generators dynamic model, transmission lines and the load models are the same for the three test systems. The transmission lines are modeled as pi-line model of Figure 2-6. The power system loads are assumed to be constant, therefore, in small perturbation Δi_{load}=0 (i.e., (Δi_{ng+1},..., Δi_{Nb}) in (2-95)).

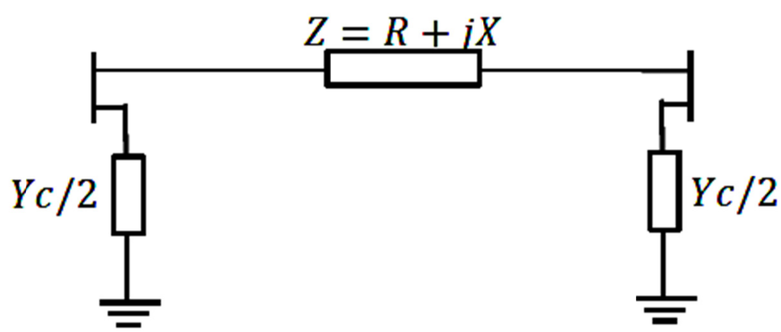

Figure 2-6: Pi-line model [46].

All generators are equipped with the exciter and PSS modeled in Figure 2-2. The complete power system data including the operating conditions, as well as the exciter and PSS parameters are given in Appendix C. The power system operating condition is the result of the load flow analysis. The load flow program used in this research is the MatNetFlow provided by Rogers, also known as "Cherry Tree Scientific Software" [11, 47]. The turbine/governor model is not considered so the mechanical torque is assumed constant. No other system devices such as DC links or Flexible AC Transmission System (FACTS) stabilizers [48] are considered.

2.9.3 4-Generator Test System

The 4-generator or two-area test system of Figure 2-7 has 13 buses and 14 transmission lines [11]. The eigenanalysis results for this system are shown in Table 2-6. This system has three electromechanical oscillatory modes as shown in this Table 2-6.

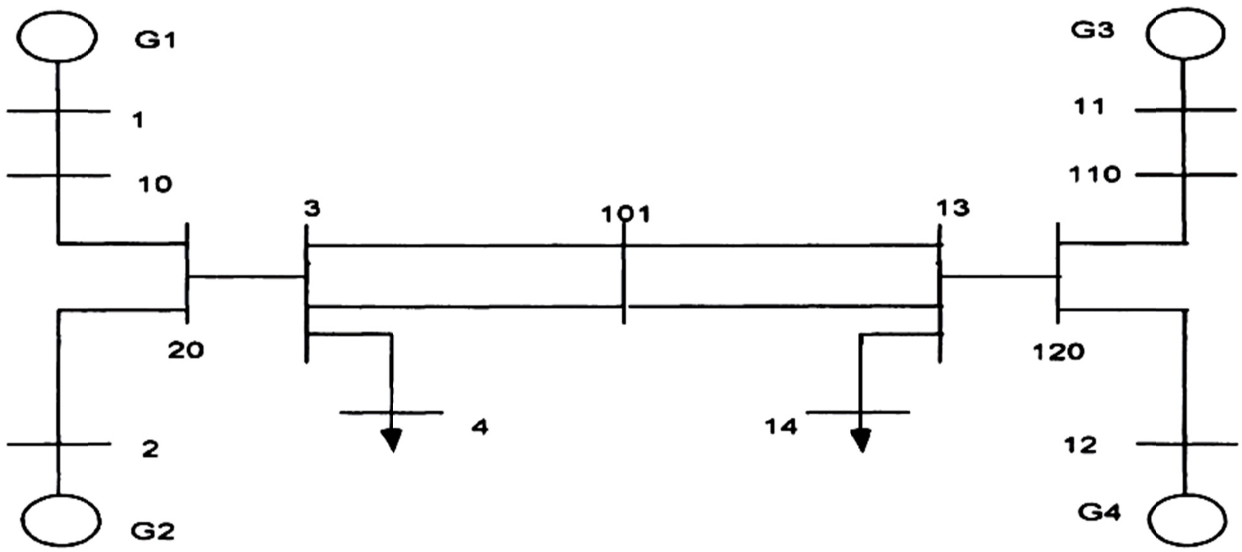

Figure 2-7: 4-Generator test system [11].

Table 2-6: Eigenvalue estimation results for 4-generator system.

Mode number		1	2	3
Case 1	Benchmark results	-0.15±j2.79	-0.88±j6.45	-0.59±j6.72
	$\lambda(\omega_K=5)$	-0.061±j2.81	-1.05±j6.12	-0.78±j6.52
	$\lambda_{imp}=\lambda+\Delta\lambda$	-0.15±j2.78	-0.84±j6.31	-0.58±j6.66
Case 2	Benchmark results	0.073±j3.46	-1.00±j6.66	-0.67±j7.11
	$\lambda(\omega_K=5)$	0.10±j3.45	-1.19±j6.12	-0.97±j6.69
	$\lambda_{imp}=\lambda+\Delta\lambda$	0.075±j3.46	-0.94±j6.41	-0.65±j6.98
Case 3	Benchmark results	-0.27±j3.37	-2.41±j6.40	-2.29±j6.75
	$\lambda(\omega_K=5)$	-0.26±j3.29	-2.41±j5.6	-2.40±j6.20
	$\lambda_{imp}=\lambda+\Delta\lambda$	-0.27±j3.37	-2.21±j5.9	-2.18±j6.44

The three cases come from Table 2-4. In each case in Table 2-6, the predictions under ω_K=5 rad/s are shown in the second row, which are obtained form $A[(\omega_K=5)]_{8\times8}$. To improve the estimation, the sensitivity formula is applied and the improved predictions listed in the third row show perfect agreement with the first row: The damping prediction error for modes 2 and 3 of Case 3 is approximately 8%. The rest of the results have less than 5% prediction error compared to the benchmark results.

2.9.4 16-Generator Test System

From the 4-generator system, tests have been conducted on the 16-generator system of [11], which belongs to a 68-bus system as shown in Figure 2-8.

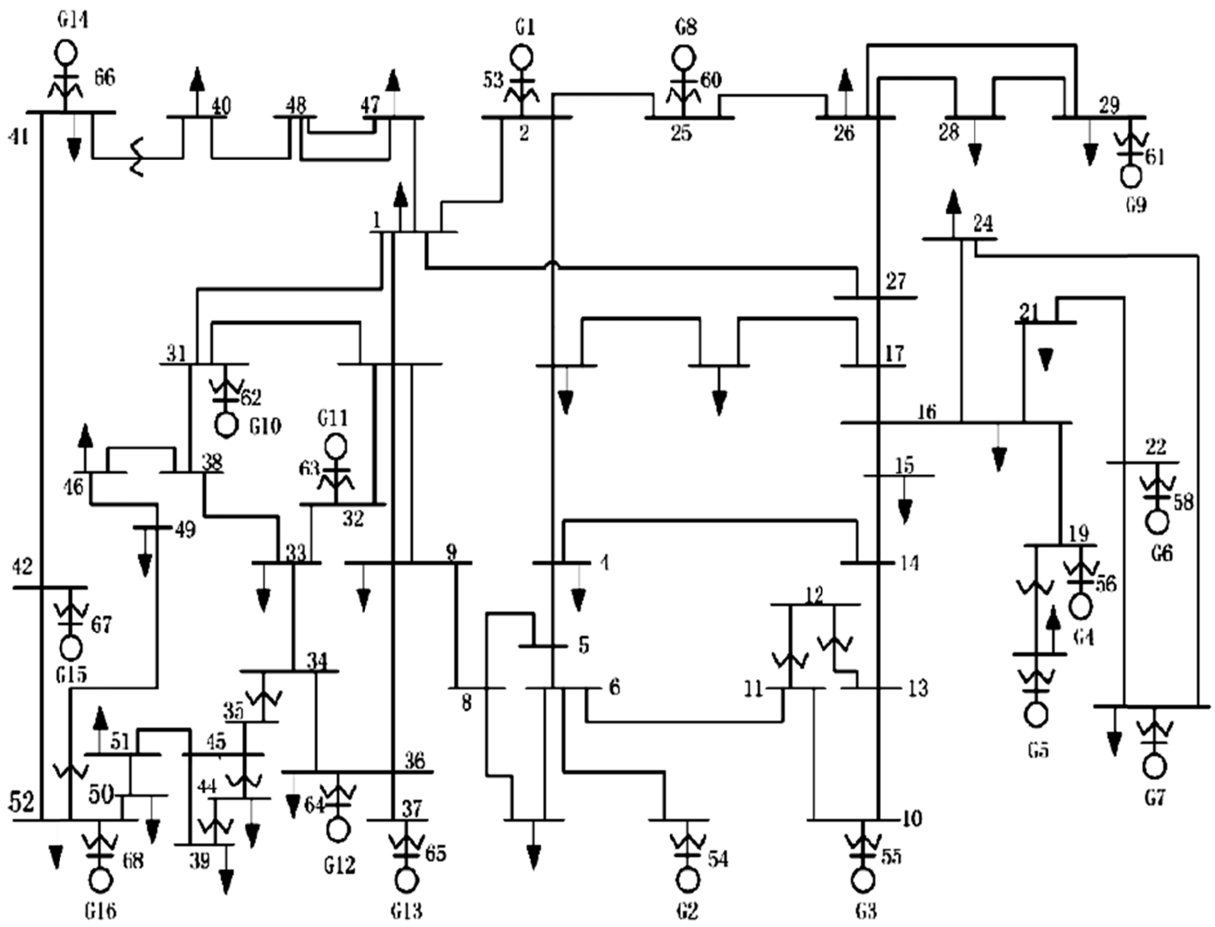

Figure 2-8: 16-generator test system [11] .

This system has 15 oscillatory electromechanical modes as shown in Table 2-7. This table is formatted in the same way as Table 2-6: for each case the first row being the benchmark for comparison; the second row shows the eigenanalysis results from $[A(\omega_K\text{=}5)]_{32\times32}$ and the third row is the improvement based on the sensitivity formula. The best overall agreement is found in the low frequency and low damping modes, which are fortunate because they are also the modes of concern for stability predictions.

Table 2-7: Eigenvalue estimation results for 16-generator system.

Mode number		1	2	3	4	5	6	7	8	9	10	11	12	13	14	15
Case 1	Benchmark results	-0.94 ±j0.89	-0.28 ±j2.04	-0.10 ±j2.90	-0.18 ±j4.79	-0.27 ±j5.57	-0.31 ±j6.15	-0.51 ±j6.88	-0.39 ±j7.10	-0.49 ±j7.76	-0.33 ±j7.84	-0.65 ±j8.15	-0.92 ±j9.07	-0.92 ±j9.30	-0.81 ±j10.85	-0.65 ±j11.03
	$\lambda(\omega_K=5)$	-0.51 ±j0.93	-0.07 ±j2.08	-0.04 ±j2.90	-0.16 ±j4.79	-0.32 ±j5.54	-0.41 ±j6.10	-0.71 ±j6.70	-0.66 ±j6.98	-0.94 ±j7.50	-0.62 ±j7.78	-1.07 ±j7.78	-1.74 ±j8.42	-1.80 ±j8.60	-1.02 ±j10.60	-1.99 ±j10.50
	$\lambda_{imp}=\lambda+\Delta\lambda$	-0.91 ±j0.95	-0.28 ±j2.01	-0.097 ±j2.91	-0.17 ±j4.79	-0.28 ±j5.55	-0.31 ±j6.13	-0.51 ±j6.82	-0.39 ±j7.07	-0.49 ±j7.67	-0.34 ±j7.84	-0.62 ±j8.08	-0.90 ±j8.96	-0.95 ±j9.22	-0.87 ±j10.8	-0.61 ±j11.01
Case 2	Benchmark results	0.08 ±j1.15	0.13 ±j2.82	0.07 ±j3.26	-0.13 ±j4.85	0.07 ±j7.00	0.35 ±j7.25	-0.38 ±j7.66	0.27 ±j7.96	0.07 ±j8.33	0.15 ±j8.69	-0.68 ±j8.95	-0.66 ±j9.82	-0.43 ±j10.11	-0.91 ±j10.72	0.21 ±j11.86
	$\lambda(\omega_K=5)$	0.06 ±j1.10	0.11 ±j2.79	0.08 ±j3.25	-0.11 ±j4.86	-0.17 ±j6.99	0.24 ±j7.30	-0.85 ±j7.30	-0.15 ±j8.04	-0.31 ±j8.30	-0.63 ±j8.64	-1.71 ±j7.9	-2.1 ±j8.68	-1.88 ±j9.1	-0.73 ±j10.5	-1.60 ±j11.57
	$\lambda_{imp}=\lambda+\Delta\lambda$	0.09 ±j1.15	0.13 ±j2.82	0.07 ±j3.25	-0.12 ±j4.85	0.07 ±j7.01	0.35 ±j7.26	-0.39 ±j7.59	0.28 ±j7.98	0.09 ±j8.3j	0.15 ±j8.74	-0.81 ±j8.83	-0.75 ±j9.78	-0.60 ±j10.08	-0.87 ±j10.56	0.22 ±j12.04
Case 3	Benchmark results	-0.08 ±j1.11	-0.07 ±j2.79	-0.17 ±j3.19	-0.35 ±j4.81	-1.02 ±j6.58	-1.16 ±j6.78	-1.86 ±j7.20	-2.14 ±j7.64	-1.22 ±j7.74	-2.38 ±j8.14	-1.33 ±j8.54	-3.91 ±j8.66	-4.63 ±j8.72	-1.31 ±j10.69	-1.90 ±j10.97
	$\lambda(\omega_K=5)$	-0.12 ±j0.79	-0.09 ±j2.68	-0.17 ±j3.13	-0.34 ±j4.78	-1.23 ±j6.67	-1.37 ±j6.83	-2.30 ±j6.86	-2.30 ±j7.78	-1.50 ±j7.86	-3.13 ±j7.9	-2.21 ±j7.74	-4.80 ±j7.10	-5.80 ±j6.71	-1.00 ±j10.50	-3.50 ±j10.80
	$\lambda_{imp}=\lambda+\Delta\lambda$	-0.06 ±j1.23	-0.07 ±j2.79	-0.17 ±j3.18	-0.35 ±j4.78	-1.11 ±j6.54	-1.27 ±j6.73	-1.97 ±j6.91	-1.99 ±j7.68	-1.30 ±j7.66	-2.63 ±j8.05	-1.53 ±j8.55	-4.02 ±j8.10	-4.95 ±j8.21	-1.10 ±j10.65	-2.10 ±j10.67

Cases 1, 2 and 3 correspond to each generator connected to the exciter and/or the PSS as described in Table 2-4. In Case 2, a number of modes have positive real parts and therefore the system is unstable. However, these modes are stabilized by the introduction of PSS in Case 3.

The results of Case 3 in Table 2-7 are plotted in Figure 2-9 for a visual check of the accuracy of the predictions. In this figure the blue stars are the benchmark results, the green plus are the eigenanalysis results of $[A(\omega_K\text{=}5)]$ and the red triangles are the modified eigenvalues from the sensitivity corrections. Overlap of the blue stars and red triangles show excellent agreement between the benchmark and modified eigenvalues, specifically for the low frequency modes.

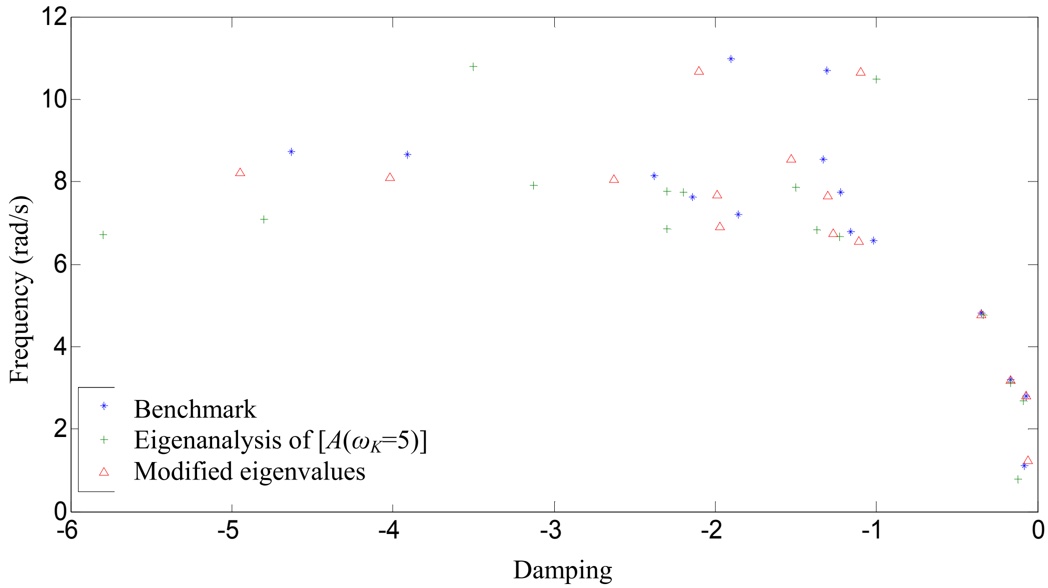

Figure 2-9: Complex plane for the results of Case 3 in Table 2-7.

The summary of the prediction accuracy is provided in Table 2-8 for the results of Table 2-7. In this table the error of the TFEA results for damping and frequency predictions are obtained by comparing the improved eigenvalue λ_{imp}, with the benchmark results.

Table 2-8: Error of the TFEA predictions for 16-generator system.

	Damping	Frequency
Case 1	All modes have less than 6% error.	All modes have less than 7%.
Case 2	10 modes have less than 10% error. Maximum error is limited to 39%.	All modes have less than 2%.
Case 3	4 modes have less than 5% error. 12 modes have less than 10% error. Maximum error is limited to 25%.	8 modes have less than 1% error. Maximum error is limited to 10%.

2.9.5 69-Generator Test System

The 69-generator system of Figure 2-10 has 300 buses [45]. This system is considered big enough for educational purposes [49].The numerical results for this system are shown in Table 2-9. This table shows the result when exciters and PSSs are in operation which corresponds to Case 3 in Table 2-4. The representative frequency is chosen to ω_K=5 rad/s. The

68 electromechanical modes of the benchmark results are shown in column 2 and 6. The initial estimation from eigenanalysis of $[A(\omega_K=5)]_{138\times138}$ are in columns 3 and 7. More accurate results, obtained by the sensitivity correction, are provided in columns 4 and 8.

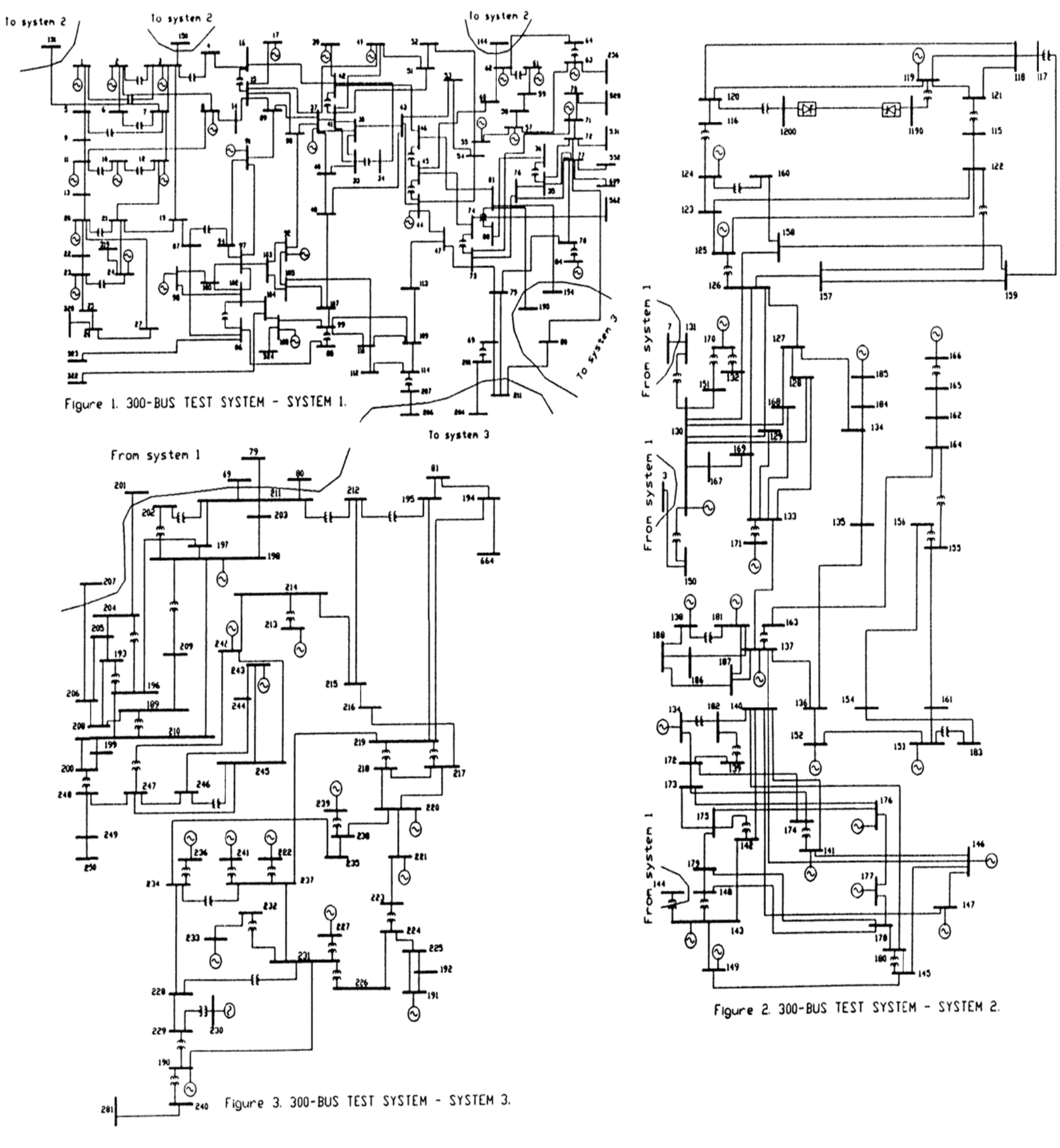

Figure 2-10: 69-generator test system [45].

Table 2-9: Eigenvalue estimation results for 69-generator system.

Mode number	Benchmark results	$\lambda(\omega_K=5)$	$\lambda_{imp}=\lambda+\Delta\lambda$	Mode number	Benchmark results	$\lambda(\omega_K=5)$	$\lambda_{imp}=\lambda+\Delta\lambda$
1	-0.08±j1.78	-0.19±j1.96	-0.11±j1.80	35	-0.79±j7.73	-1.58±j7.35	-0.79±j7.66
2	-0.2±j2.38	-0.23±j2.54	-0.21±j2.41	36	-0.86±j7.75	-1.29±j7.44	-0.85±j7.69
3	-0.12±j2.90	-0.14±j2.97	-0.12±j2.91	37	-0.82±j7.90	-1.24±j7.45	-1.00±j7.71
4	-0.16±j3.05	-0.13±j3.10	-0.16±j3.05	38	-1.04±j7.90	-1.35±j7.44	-1.00±j7.75
5	-0.17±j4.05	-0.14±j4.06	-0.17±j4.05	39	-1.15±j7.89	-2.15±j7.29	-1.11±j7.78
6	-0.32±j4.88	-0.30±j4.85	-0.31±j4.85	40	-0.89±j7.96	-1.60±j7.44	-0.79±j7.85
7	-0.4±j5.33	-0.42±j5.28	-0.39±j5.29	41	-0.99±j7.99	-1.21±j7.64	-0.87±j7.88
8	-0.4±j5.55	-0.45±j5.49	-0.39±j5.51	42	-0.97±j8.02	-1.33±j7.63	-0.99±j7.91
9	-0.08±j5.59	-0.06±j5.6	-0.08±j5.60	43	-1.07±j8.07	-1.47±j7.62	-0.94±j7.93
10	-0.52±j5.77	-0.64±j5.65	-0.51±j5.69	44	-1.00±j8.12	-1.47±j7.63	-0.98±j8.02
11	-0.39±5.79	-0.48±j5.73	-0.39±j5.75	45	-0.87±j8.14	-1.90±j7.69	-0.85±j8.08
12	-0.38±j5.82	-0.47±j5.73	-0.37±j5.77	46	-1.26±j8.15	-1.59±j7.69	-1.21±j8.02
13	-0.25±j5.85	-2.61±j5.18	-0.24±j5.85	47	-1.19±j8.20	-1.79±j7.61	-1.21±j8.02
14	-0.52±j6.06	-0.23±j5.85	-0.51±j6.00	48	-1.32±j8.28	-1.31±j7.84	-1.28±j8.14
15	-0.56±j6.10	-0.63±j5.95	-0.56±j6.02	49	-1.01±j8.39	-1.61±j7.99	-0.99±j8.3
16	-0.58±j6.12	-0.74±j5.94	-0.58±j6.03	50	-0.87±j8.44	-1.48±j8.02	-0.86±j8.37
17	-0.47±j6.21	-0.79±j5.96	-0.46±j6.16	51	-1.08±j8.48	-1.70±j8.00	-1.05±j8.38
18	-0.55±j6.32	-0.62±j6.11	-0.54±j6.26	52	-0.92±j8.93	-1.74±j8.43	-0.91±j8.87
19	-0.48±j6.38	-0.70±j6.17	-0.49±j6.33	53	-1.24±j8.91	-1.85±j8.38	-1.20±j8.79
20	-0.62±j6.52	-0.69±j6.27	-0.61±j6.45	54	-1.11±j8.99	-1.55±j8.41	-1.15±j8.82
21	-0.56±j6.78	-0.85±j6.32	-0.55±j6.74	55	-1.12±j9.10	-2.10±j 8.40	-1.12±j9.01
22	-0.56±j6.84	-0.76±j6.64	-0.56±j6.78	56	-1.04±j9.31	-1.97±j8.74	-1.03±j9.24
23	-2.12±j6.59	-0.88±j6.67	-2.19±j5.59	57	-1.22±j9.69	-2.42±j8.87	-1.19±j9.61
24	-0.79±j6.96	-1.07±j6.72	-0.77±j6.89	58	-1.15±j9.71	-2.32±j8.97	-1.14±j9.64
25	-0.67±j6.97	-0.99±j6.74	-0.67±j6.88	59	-1.14±j9.96	-2.39±j9.24	-1.13±j9.89
26	-0.64±j7.06	-0.97±j6.84	-0.64±j6.98	60	-1.19±j10.22	-2.52±j9.42	-1.19±j10.19
27	-0.63±j7.08	-1.90±j6.65	-0.62±j7.02	61	-1.27±j10.66	-2.88±j9.68	-1.26±j10.68
28	-0.78±j7.09	-0.89±j6.89	-0.78±j7.12	62	-1.39±j10.74	-2.94±j9.75	-1.37±j10.73
29	-0.65±j7.24	-1.16±j6.97	-0.64±j7.19	63	-1.52±j11.67	-3.52±j10.48	-1.48±j11.71
30	-0.87±j7.25	-1.07±j6.97	-0.84±j7.16	64	-1.54±j11.79	-3.64±j10.45	-1.53±j11.85
31	-0.71±j7.39	-1.02±j7.16	-0.69±j7.33	65	-2.07±j12.59	-4.67±j10.59	-2.02±j12.70
32	-0.91±j7.44	-0.94±j7.06	-1.01±j7.26	66	-2.28±j12.99	-5.13±j10.75	-2.21±j13.14
33	-0.71±j7.49	-1.14±j7.24	-0.70±j7.43	67	-2.05±j13.13	-4.86±j11.12	-1.99±j13.29
34	-0.80±j7.51	-1.23±j7.20	-0.79±j7.42	68	-2.21±j13.49	-5.09±j11.37	-2.13±j13.67

The results of Table 2-9 are plotted in Figure 2-11 to visually show that the modified eigenvalues (red triangles) are in very close agreement with benchmark results (blue stars).The prediction error is given in Table 2-10. The damping prediction error is limited to 5% for 63 out of 68 modes. High error observed for few high frequency modes, which are of less concern.

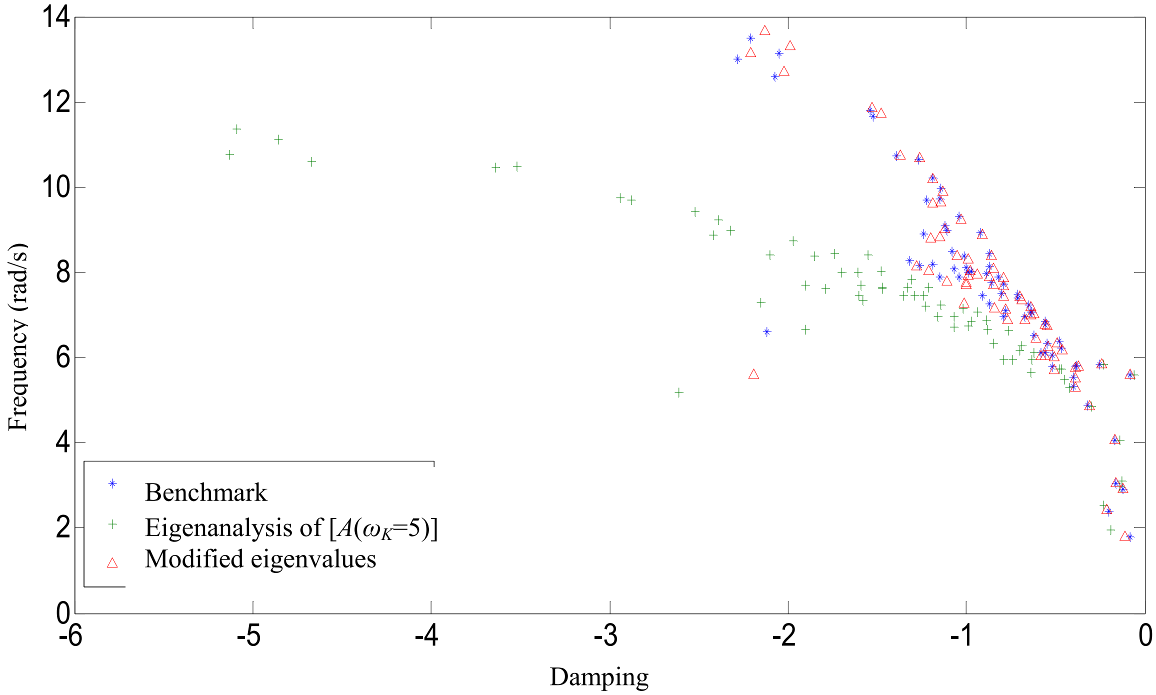

Figure 2-11: Complex plane for the results of Table 2-9.

Table 2-10: Error of the TFEA predictions for 69-generator system.

	Damping	Frequency
Case 3	63 modes have less than 5% error. Maximum error is 37%.	67 modes have less than 3% error. One mode has 15% error.

2.10 Discussion of the Accuracy of the TFEA Method

In this section, it will be shown that the nature of frequency dependency of the method would not cause accuracy problems. The discussion is based on the TFEA results of the 16-generator system.

2.10.1 Sufficient Accuracy of Predictions

Depending on the accuracy criteria and application of TFEA results, one can conclude if the TFEA accuracy is "sufficient" or not. The power system requires assurance that the system is stable in small signal perturbation. This means that only the damping factor of the eigenvalue closest to imaginary axis counts. It does not matter whether the eigenvalues of the remaining modes are inaccurate. If another technique, such as Nyquist stability criterion is used, stability is assured when the open loop transfer function does not encircle any eigenvalue or the -1 point [4, 50]. The designer is oblivious of the other eigenvalues.

Although the prediction errors in Tables 2-8 and 2-10 provide good means of knowing the accuracy of the TFEA method, the relationship between accuracy and small signal stability criteria must be remembered. For example, with the explanations above, the accuracy of heavily damped modes are not important.

Another point is the application of TFEA results. As mentioned in Chapter 1, the initial objective of this research is to present estimates of all the electromechanical modes so the user can choose the few dominant (least damped) ones which he will use in more accurate methods like the Modified Arnoldi Method (MAM) [16], to compute the eigenvalues precisely.

Considering Case 3 of Table 2-7, the user attention, on scanning the second row, is drawn to -0.09 of mode 2 as the least damped mode. For assurance, an improved estimate is sought and this requires applying the sensitivity method which yields the value of -0.07 equal to the benchmark result. What is useful is that the estimate based on the representative frequency ω_K=5 rad/s, is "good enough" to call attention to the fact that mode 2 is a dominant and least damped mode.

Also for the heavily damped modes, the TFEA accuracy is sufficient to classify them as non-dominant modes. For example, for mode 15 the damping is -3.5. Accurate prediction using eigenvalue sensitivity correction, as shown in the third row, is -2.1 which is close to the benchmark value of -1.9. However, the initial damping estimation is "good enough" to classify mode 15 as a non-dominant mode.

2.10.2 Choice of Representative Frequency

Choice of representative frequency ω_K is the first step of applying the TFEA method. Numerical results of Section 2.9 acknowledge that only the modes whose modal frequencies are close to the representative frequency ω_K are accurate. The experiment done in this section shows the effect of different representative frequencies on the TFEA results.

Considering the 16-generator system, Table 2-11 lists the eigenvalues of modes 1, 2 and 3 (lowest modal frequencies) and modes 14 and 15 (highest modal frequencies), obtained by TFEA for three representative frequencies ω_K=1.0, 5.0 and 10.0 rad/s. For ω_K=1.0 rad/s, the estimates of the damping of the lowest frequency modes are reasonable and the sensitivity correction results (fourth column) are very good. On the other hand, the entries of mode 15 are left blank because eigenvalue subroutine yields real rather than complex conjugate numbers. In other words, the prediction is poor because the frequency 10.9 rad/s is too distant from ω_K=1.0 rad/s. Similarly, for ω_K=10.0 rad/s, there is no prediction for mode 1, because the frequency of 1.11 rad/s of mode 1, is too different from ω_K=10.0 rad/s. For the high frequency modes, the estimates of damping coefficients of modes 14 and 15 are reasonable.

For a spread of frequency between 1.11 to 10.9 rad/s, ω_K=5.0 rad/s is a good representative frequency. Depending on the expected frequencies of the dominant modes, the user is helped by choosing ω_K close to it.

Table 2-11: Choice of representative frequency ω_K.

Mode number	Benchmark results	$\lambda(\omega_K=1)$	$\lambda_{imp}=\lambda+\Delta\lambda$	$\lambda(\omega_K=5)$	$\lambda_{imp}=\lambda+\Delta\lambda$	$\lambda(\omega_K=10)$	$\lambda_{imp}=\lambda+\Delta\lambda$
1	-0.08±j1.11	-0.08±j1.12	-0.08±j1.12	-0.12±j0.79	-0.06±j1.23		
2	-0.07±j2.79	-0.02±j2.87	-0.09±j2.79	-0.09±j2.68	-0.07±j2.79	-0.14±j2.28	-0.06±j2.85
3	-0.17±j3.19	-0.32±j3.14	-0.18±j3.20	-0.17±j3.13	-0.17±j3.18	-0.21±j2.75	-0.16±j3.25
14	-1.31±j10.69	-1.03±j10.20	-1.10±j10.80	-1.00±j10.5	-1.10±j10.65	-1.06±j10.73	-1.07±j10.78
15	-1.90±j10.9			-3.5±j10.8	-2.10±j10.67	-2.16±j10.86	-2.14±j10.7

2.10.3 Perturbation of Eigenvectors

The eigenvalue sensitivity method depends on small perturbation linearization. The accuracy of the estimate of (2-125) relies on the invariability of the eigenvectors for frequencies ω_n close to ω_K.

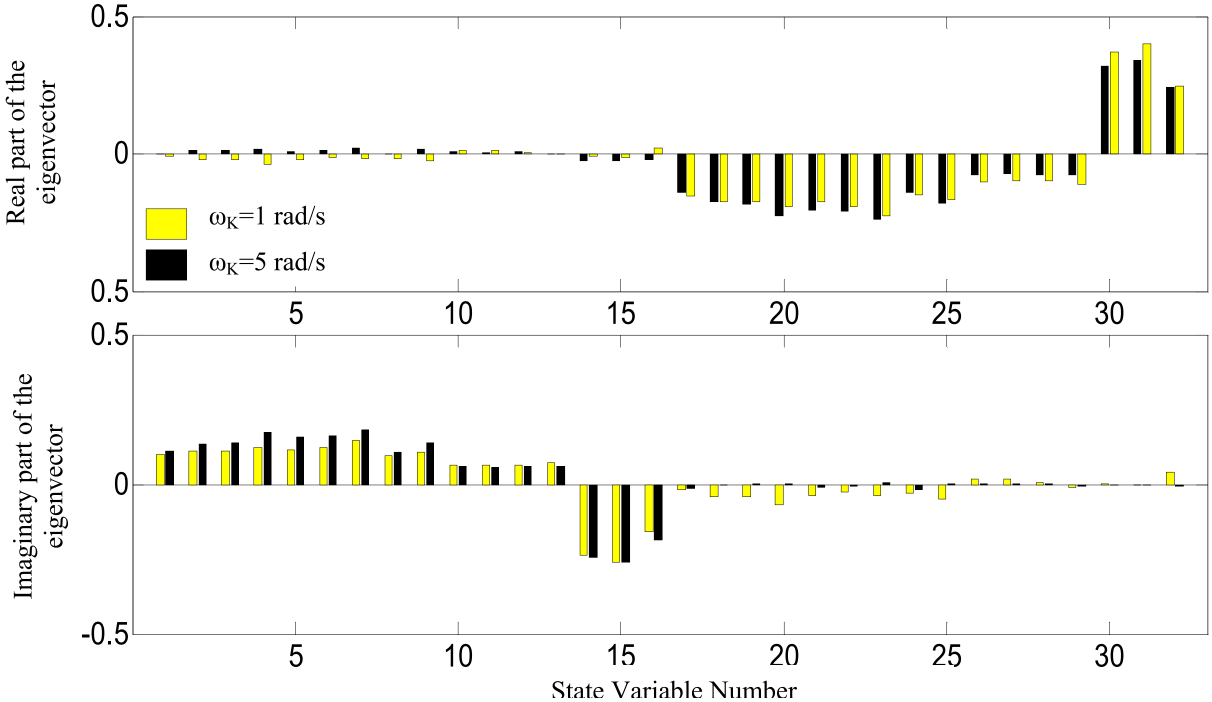

Figure 2-12: Complex eigenvector for mode 1, Case 3 of Table 2-7, 16-generator system.

The bar graphs in Figure 2-12 compare the 32 real parts and the 32 imaginary parts of the 16 generator complex eigenvectors for mode 1, Case 3 of Table 2-7. It is shown for two representative frequencies: ω_K=1.0 and ω_K=5.0 rad/s. Each bar corresponds to one state variable; the first 16 bars are associated with the generators rotor angle while the rest relate to the rotor speed variation. If the accuracy of the lowest frequency modes are of interest, for instance, it is necessary to use the eigenvectors of ω_K=1.0. If ω_K=5.0, the differences as shown in Figure 2-12 would lower the accuracy.

2.11 TFEA Robustness

Robustness of eigenanalysis methods is important to verify the method accuracy under different system conditions [40]. In this section, the robustness of TFEA method is tested for lightly and heavily loaded systems. This includes three loadings for the 16-generator system and two loadings for the 69-generator system, as shown in Table 2-12.

Table 2-12: Loading cases for TFEA robustness test.

16-generator system				69-generator system		
Original loading (MW)	Loading 1 (MW)	Loading 2 (MW)	Loading 3 (MW)	Original loading (MW)	Loading 4 (MW)	Loading 5 (MW)
18000	6300	11700	23400	23600	15300	29700

The eigenanalysis results for the first three loadings of Table 2-12 are shown in Table 2-13. The results demonstrate that the dominant modes are predicted accurately irrespective of the level of loading. The results of Loadings 4 and 5 are shown graphically in Figure 2-13 and Figure 2-14. The scale is sufficient to show that the dominant modes, which are closest to the imaginary axis, are close to the benchmark results.

Table 2-13: Eigenvalue estimation results for 16-generator system under different loadings.

Mode number		1	2	3	4	5	6	7	8	9	10	11	12	13	14	15
Loading 1	Benchmark results	-0.09 $\pm j2.49$	-0.20 $\pm j3.43$	-0.34 $\pm j4.10$	-0.29 $\pm j4.98$	-1.09 $\pm j6.29$	-1.26 $\pm j6.68$	-1.73 $\pm j6.98$	-2.17 $\pm j7.23$	-0.95 $\pm j7.76$	-2.04 $\pm j7.84$	-2.52 $\pm j7.81$	-3.54 $\pm j7.44$	-3.76 $\pm j8.56$	-0.89 $\pm j8.66$	-1.60 $\pm j11.16$
	$\lambda_{imp}=\lambda+\Delta\lambda$	-0.09 $\pm j2.49$	-0.20 $\pm j3.42$	-0.34 $\pm j4.08$	-0.29 $\pm j4.96$	-1.25 $\pm j6.15$	-1.31 $\pm j6.47$	-3.36 $\pm j5.46$	-2.41 $\pm j6.23$	-1.00 $\pm j7.71$	-1.85 $\pm j6.77$	-2.25 $\pm j7.54$	-2.59 $\pm j6.69$	-4.26 $\pm j6.69$	-0.96 $\pm j8.66$	-1.86 $\pm j11.35$
Loading 2	Benchmark results	-0.09 $\pm j2.19$	-0.21 $\pm j3.29$	-0.24 $\pm j4.00$	-0.32 $\pm j4.91$	-1.17 $\pm j6.50$	-1.41 $\pm j6.73$	-2.11 $\pm j7.21$	-1.95 $\pm j7.33$	-2.56 $\pm j7.81$	-1.18 $\pm j7.74$	-3.69 $\pm j8.23$	-2.00 $\pm j8.37$	-4.69 $\pm j8.43$	-0.94 $\pm j9.73$	-1.84 $\pm j10.96$
	$\lambda_{imp}=\lambda+\Delta\lambda$	-0.09 $\pm j2.20$	-0.21 $\pm j3.29$	-0.25 $\pm j4.00$	-0.33 $\pm j4.89$	-1.28 $\pm j6.35$	-1.53 $\pm j6.63$	-2.37 $\pm j6.69$	-2.09 $\pm j7.24$	-2.14 $\pm j7.49$	-1.28 $\pm j7.72$	-3.76 $\pm j6.96$	-2.86 $\pm j7.58$	-5.65 $\pm j6.43$	-1.04 $\pm j9.73$	-2.17 $\pm j11.09$
Loading 3	Benchmark results	-0.16 $\pm j2.39$	0.05 $\pm j2.93$	-0.35 $\pm j4.67$	-0.78 $\pm j6.58$	-0.97 $\pm j6.88$	-1.52 $\pm j7.12$	-1.04 $\pm j7.61$	-1.69 $\pm j7.94$	-0.69 $\pm j8.72$	-0.88 $\pm j8.91$	-2.19 $\pm j8.46$	-3.57 $\pm j8.46$	-4.60 $\pm j8.88$	-0.27 $\pm j10.08$	-1.50 $\pm j10.59$
	$\lambda_{imp}=\lambda+\Delta\lambda$	-0.16 $\pm j2.41$	0.06 $\pm j2.94$	-0.36 $\pm j4.65$	-0.90 $\pm j6.59$	-1.08 $\pm j6.88$	-1.71 $\pm j7.04$	-1.17 $\pm j7.61$	-1.87 $\pm j7.99$	-0.78 $\pm j8.60$	-0.95 $\pm j8.81$	-2.42 $\pm j8.48$	-3.89 $\pm j8.19$	-5.23 $\pm j8.45$	-0.31 $\pm j10.09$	-1.78 $\pm j10.58$

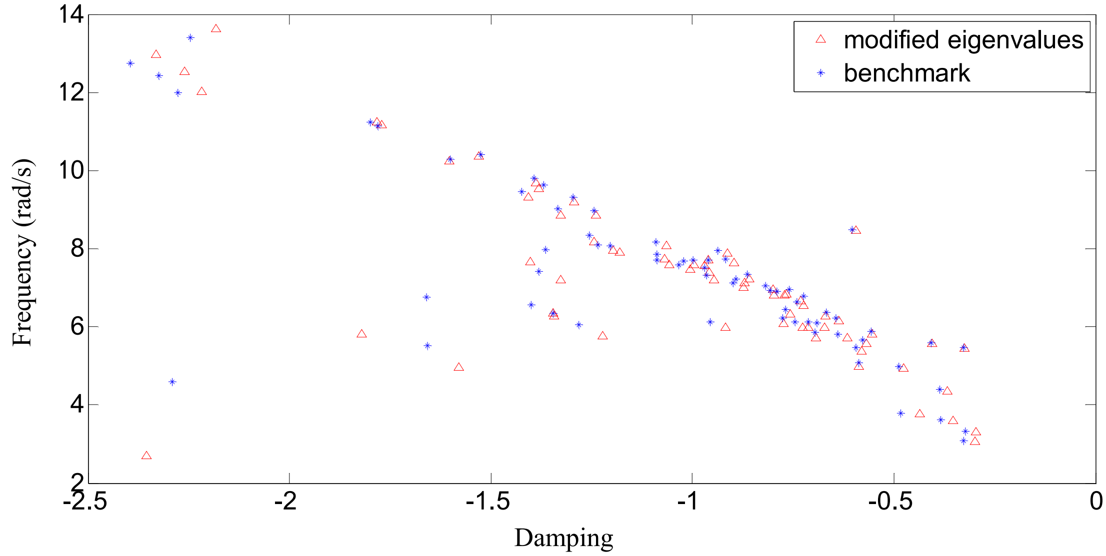

Figure 2-13: Complex plane for the results of 69-generator system under loading Case 4.

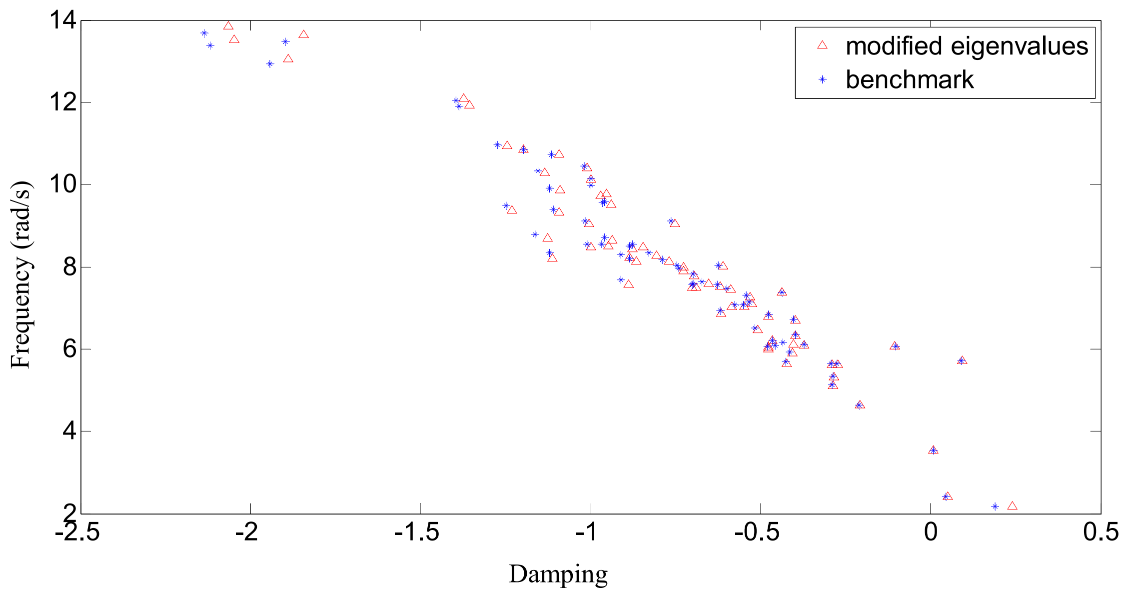

Figure 2-14: Complex plane for the results of 69-generator system under loading Case 5.

Table 2-14 summarizes the prediction error based on the results of Loading 1 to Loading 5. This table with Table 2-8 and Table 2-10 show that the TFEA method is robust for different system loadings, because the TFEA method predicts the same level of accuracy in all of the three tables for different system operations.

Table 2-14: Error of the TFEA predictions for five different loadings.

	Damping	Frequency
Loading 1	9 modes have less than 10% error. Maximum error is limited to 26%.	10 modes have less than 5% error. Maximum error is limited to 22%.
Loading 2	5 modes have less than 5 % error. 14 modes have less than 20% error.	13 modes have less than 10% error. Maximum error is limited to 23%.
Loading 3	7 modes have less than 10 % error. All modes have less than 20% error.	All modes have less than 5 % error.
Loading 4	62 modes have less than 5% error. Maximum error is 11%.	65 modes have less than 3% error. Maximum error is 38%.
Loading 5	63 modes have less than 5% error. Maximum error is 25%.	64 modes have less than 3% error. Maximum error is 8%.

2.12 Chapter Summary

The chapter has described a two-stage method of estimating the electromechanical eigenvalues of interconnected power systems. The first stage consists of evaluating all the eigenvalues and eigenvectors of a $2ng\times2ng$ $[A(\omega_K)]$ matrix evaluated at a representative frequency ω_K. From the damping coefficients of all the electromechanical modes, the dominant modes are identified. For added reliability, the second stage offers a computationally economical method of obtaining more accurate estimation of the eigenvalues selected from the first stage. Although the eigenvalue sensitivity formula is well known, it is applied to obtain improved estimates, without having to re-compute the eigenvalues.

The accuracy of the estimations has been tested against the benchmark results computed from a full state matrix which models the damper windings, exciters and power system stabilizers (PSSs). The numerical results from different test systems have shown acceptable accuracy of the proposed method. A discussion of accuracy in Section 2.10 also showed that the feature of frequency dependency of TFEA would not cause accuracy problems. The chapter is concluded by an important discussion of TFEA robustness under different system loadings. Next chapter will elaborate on the TFEA computational efficiency.

Chapter Three

3. TFEA Computational Efficiency

3.1 Overview

This chapter elaborates on the computation count and efficiency of the TFEA method and the eigenvalue sensitivity. In Chapter 2, the TFEA method was introduced as a frequency-dependent eigenanalysis method for large power systems. The eigenvalues $\lambda_n=\sigma_n \pm j\omega_n$ and the right and left eigenvectors $\underline{u}_n$ and $\underline{r}_n$ (n=1, 2…, ng) of $[A(\omega_K)]$ are retained. If the n^{th} mode is of interest, a new $[A(\omega_n)]$ is evaluated at frequency ω_n. An improved estimate of the eigenvalue is then obtained by applying the eigenvalue sensitivity formula of (2-125). It will be shown in this chapter that the cost in applying the sensitivity formula can be reduced significantly by using a curve fitting interpolation method.

The numerical results of this research were obtained on a conventional PC with a memory of 4 GB. However, the elapsed CPU time is not a measurement of computational efficiency as it changes from one PC to another. The efficiency of an algorithm such as TFEA can be estimated by counting the number of elementary operations performed by the algorithm, in which an elementary operation requires a fixed amount of time to perform [18]. The computation count is expressed using *big O notation*, which excludes coefficients and lower order terms [51].

All of the subroutines of the TFEA package were written by the author as part of his research work. The TFEA package contains several MATLAB subroutines.

3.2 Computation Count

The total computation count for the eigenanalysis, determined by TFEA and applying sensitivity formula, can be derived from the following five steps.

Step 1: Forming $[A(\omega_K)]$

The major computation cost in forming the $[A(\omega_K)]$ matrix is in solving the $2n_g$ equation set of (2-105) for currents. For ng generators, the computation cost is on the order of $(2ng)^3$.

Step 2: Solving eigenvalues and eigenvectors of $[A(\omega_K)]$

The most computationally intensive part is in solving the eigenvalues (λ_1, λ_2,…, λ_{ng}) and the eigenvectors ($\underline{u}_1$, $\underline{u}_2$,…, $\underline{u}_{ng}$) of $[A(\omega_K)]$ matrix. The computation cost is on the order of $(2ng)^3$.

Step 3: Solving eigenvectors of $[A(\omega_K)]^T$

The transpose matrix $[A(\omega_K)]^T$ has the same eigenvalues as $[A(\omega_K)]$. In solving its eigenvectors ($\underline{r}_1$, $\underline{r}_2$, …, $\underline{r}_{ng}$), the cost is $(2ng)^3$.

The eigenvalues (λ_1, λ_2,…, λ_{ng}) and eigenvectors ($\underline{u}_1$, $\underline{u}_2$,…, $\underline{u}_{ng}$) and ($\underline{r}_1$, $\underline{r}_2$, …, $\underline{r}_{ng}$) are solved only once, and they are retained for the application of the sensitivity formula.

Step 4: Improved estimation of eigenvalue for mode n

To improve the accuracy of mode n, using eigenvalue sensitivity, it is necessary to form the $[A(\omega_n)]$ matrix. The major computational burden lies again in solving the $2ng$ equation set of (2-105) and the cost is on the order of $(2ng)^3$.

Step 5: Applying Sensitivity Formula

Computing the sensitivity formula of (2-125) is trivial, because $\underline{u}_n$ and $\underline{r}_n$ are available from the storage of ($\underline{u}_1$, $\underline{u}_2$,…, $\underline{u}_{ng}$) and ($\underline{r}_1$, $\underline{r}_2$, …, $\underline{r}_{ng}$) in Step 3.

Table 3-1 summarizes the computation count of the five steps and show the total count and speed-up efficiency, compared to full state matrix eigenanalysis. This increase in speed is $166/(ng+3)$ if a sensitivity correction is applied to all ng modes (worst case). In the case of no sensitivity corrections, the increase is approximately 56.

Table 3-1: Computation count.

Computation Step	TFEA			Correction by sensitivity for one mode		TFEA (with no sensitivity)	TFEA+ sensitivity applied to all *ng* modes	Eigenanalysis of the full state matrix $[A]_{(11ng\times 11ng)}$
	Step 1	Step2	Step3	Step4	Step5			
Computation Count	$(2ng)^3$	$(2ng)^3$	$(2ng)^3$	$(2ng)^3$	-	$(3)(2ng)^3$	$(ng+3)(2ng)^3$	$(11ng)^3$
Speed-up Efficiency (compared to eigenanalysis of full state matrix)						$(11ng)^3/(3)(2ng)^3 \approx 56$	$(11ng)^3/(ng+3)(2ng)^3 = 166/(ng+3)$	

3.3 Discussion of Speed-up Efficiency

In Table 3-1, when sensitivity correction is applied to all of the modes, there is no increase in speed when *ng* is greater than 163. However, the advantage of TFEA is similar to those of selective eigenanalysis methods, such as AESOPS and MAM, in which only a few modes must be known accurately. Therefore, few sensitivity corrections are needed in practice.

Moreover, in situations such as for online dynamic security assessment, there can be a speed increase of 56 because sensitivity correction of TFEA can be undertaken by parallel computing with supercomputers. This means that the accuracy of each mode is improved separately by the processing unit assigned to it, and the real-time computation count is $3\times(2ng)^3$. Therefore, the increase in speed for *ng* corrections compared to full state matrix analysis, will be approximately $(11ng)^3/3\times(2ng)^3 \approx 56$.

To have a better understanding, the actual elapsed CPU times for the results of Section 2.9 are presented in Table 3-2.

Table 3-2: CPU time.

	Eigenanalysis of the full state matrix $[A]_{(11ng\times 11ng)}$	TFEA with sensitivity correction applied to all *ng* modes
16-generator system	0.09 sec	0.008 sec
69-generator system	2.77 sec	0.85 sec

3.4 Improving the Computation Count by Applying Curve Fitting Interpolation to the TFEA Method

3.4.1 Contribution of Curve Fitting Interpolation

The interpolation method is a simple but important contribution to methodology. It is a contribution to experimental research that comes from combining observation with intuition in software experimentation.

According to Table 3-1, the cost of sensitivity correction for each mode ω_n lies in the formation of the matrix $[A(\omega_n)]$. If the correction sensitivity formula is applied to all ng modes, the total cost is $ng \times (2ng)^3$, which is a relatively high cost. To reduce such computation cost, a simple curve fitting interpolation will be applied during the procedure of evaluating $[A(\omega_n)]$.

Because forming the matrix $[A(\omega_n)]$ relies on arithmetic rules, the elements $a_{ij}(\omega_n)$ of $[A(\omega_n)]$ are expected to change continuously with frequency. These changes are shown in Section 3.4.3. However, since the author does not have the required mathematical training, a proof cannot be presented to demonstrate the robustness of interpolation. The contribution consists of evaluating $[A(\omega)]$ for only a small number of frequencies (called sampling frequencies), and using curve fitting to span the frequency gaps between the sampling frequencies. The accuracy of the method relies on the closeness of sampling points and the range over which the sensitivity formula is accurate.

3.4.2 Implementation of Curve Fitting Interpolation

The curve fitting interpolation method implies that $[A(\omega)]$ be computed not for all ng frequencies but only for a very small number of sampling frequencies. Then, interpolation is applied for the full range of frequencies between the sampling frequencies, which is achieved by the following three steps.

Step 1: Choosing sampling frequencies

For the electromechanical frequency range of 0.7-12.5 rad/s, the sampling frequencies are chosen as ω_{sample}= 1, 2, 3, 4, 5, 6, 7, 8, 9, 10 rad/s. The number of sampling frequencies is n_{sample}=10.

Step 2: Forming $[A(\omega_{sample})]$

$[A(\omega)]$ is calculated for all of the sampling frequencies: $[A(\omega_{sample}=1)]$,…, $[A(\omega_{sample}=10)]$.

Step 3: Forming $[A(\omega_n)]$

For the n^{th} mode, $[A(\omega_n)]$ can be found by interpolating the matrices of $[A(\omega_{sample})]$ calculated in step 2, as:

$$[A(\omega_n)] = [A(\omega_{sample})] + \left([A(\omega_{sample}+1)] - [A(\omega_{sample})]\right) \times (\omega_n - \omega_{sample}) \quad \text{for } \begin{cases} \omega_{\text{sample}} < \omega_{\text{n}} < \omega_{\text{sample}} + 1 \\ 1 \le \omega_n \le 10 \ \text{ rad/s} \end{cases}$$

$$[A(\omega_n)] = [A(\omega_{sample} = 10)] + \left([A(\omega_{sample} = 10)] - [A(\omega_{sample} = 9)]\right) \times (\omega_n - 10) \text{ for } \omega_{\text{n}} > 10 \ \text{ rad/s.} \tag{3-1}$$

3.4.3 Smoothness of $[A(\omega)]_{2ng\times 2ng}$

The accuracy of the interpolation method depends on the smoothness of the entries of $[A(\omega)]$. According to the TFEA in Chapter 2, the $[A(\omega)]$ matrix has four sub-matrices: the important ones are $[a_{21}(\omega)]$ and $[a_{22}(\omega)]$. For the 69-generator system, $[a_{21}(\omega)]$ and $[a_{22}(\omega)]$ are 69×69 frequency-dependent matrices. The feasibility of interpolation depends on the smoothness of these sub-matrices. To show this, Figures 3-1 and 3-2 show 10 random diagonal entries of $[a_{21}(\omega)]$ and $[a_{22}(\omega)]$, respectively. This process is repeated for the off-diagonal entries in Figures 3-3 and 3-4. According to these figures, it can be observed that the elements of $[a_{21}(\omega)]$ and $[a_{22}(\omega)]$ are smooth curves such that the proposed curve fitting interpolation could be implemented and utilized successfully.

It should be emphasized that these curves are obtained by having ω_{sample}= 1, 2,…, 10 rad/s, forming $[A(\omega_{sample})]_{2ng\times 2ng}$ and using curve fitting to plot these figures. A small “kink” around ω=5 rad/s is observed in all four of the figures. Investigation shows that the “kink” is due to frequency-dependent elements such as exciter and PSS. It is not related to ω_K=5 rad/s.

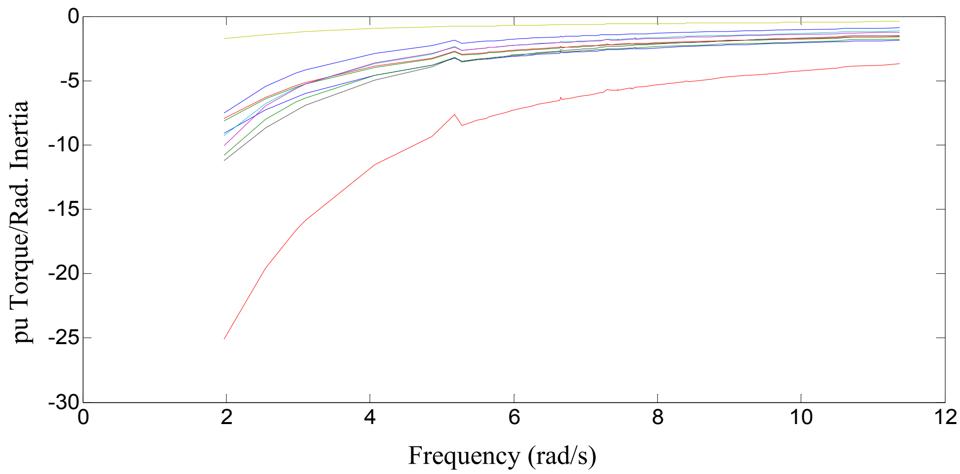

Figure 3-1: 10 random diagonal entries of $[a_{21}(\omega)]_{69\times 69}$.

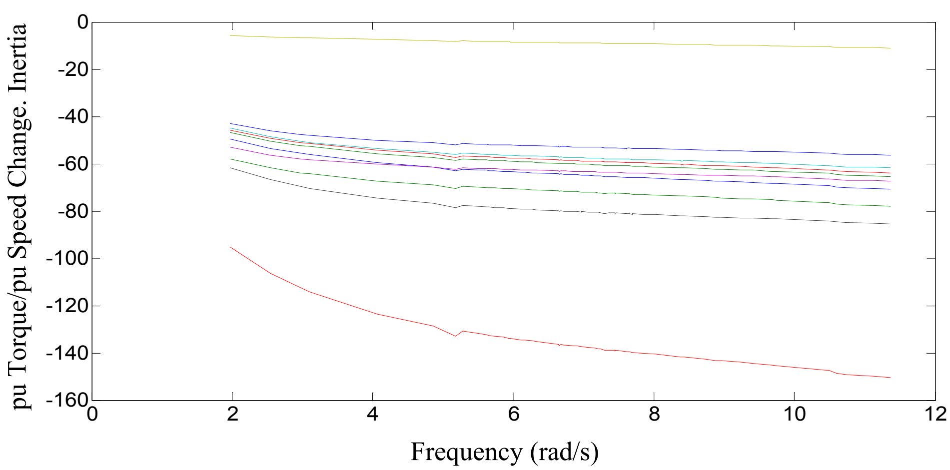

Figure 3-2: 10 random diagonal entries of $[a_{22}(\omega)]_{69\times 69}$.

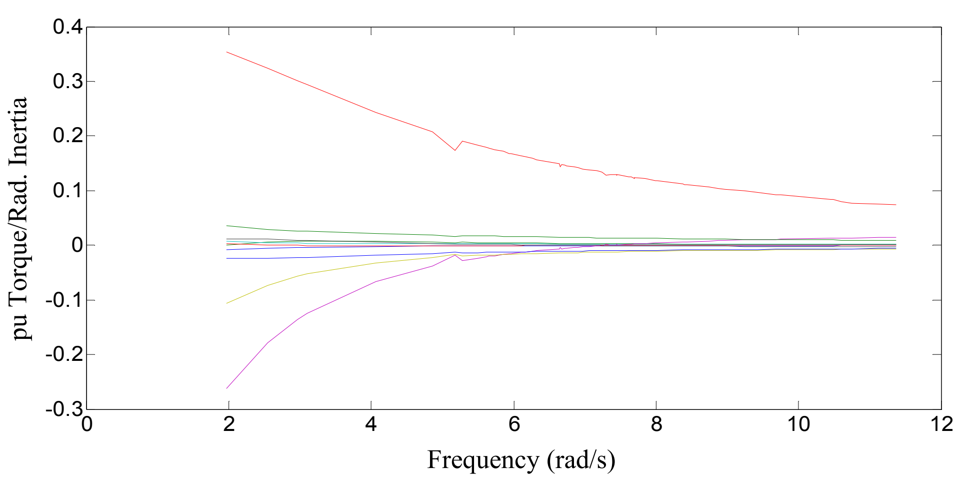

Figure 3-3: 10 random off-diagonal entries of $[a_{21}(\omega)]_{69\times 69}$.

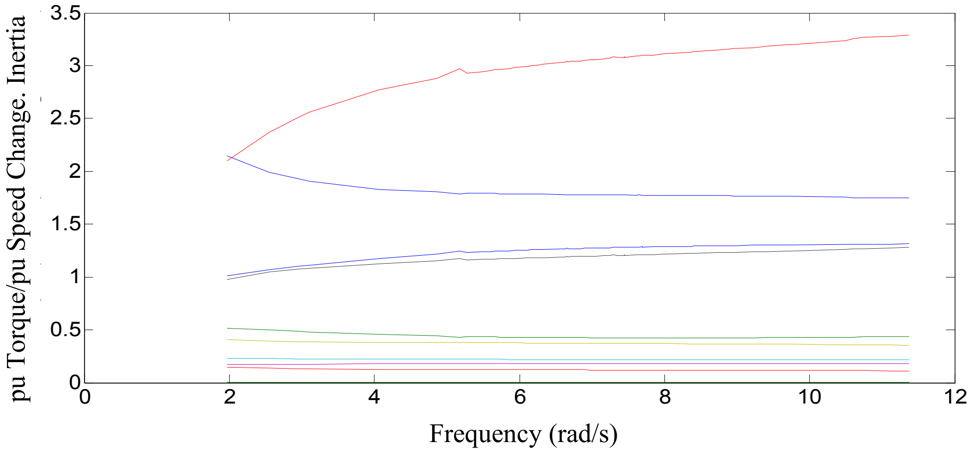

Figure 3-4: 10 random off-diagonal entries of $[a_{22}(\omega)]_{69\times 69}$.

3.4.4 Numerical Results

To examine the proposed method of interpolation, the two test systems from Chapter 2 are used: the 16-generator and the 69-generator test systems. The operating conditions, the system parameters and the exciter/PSS model are the same as in Chapter 2.

Table 3-3 shows the complete results for the 16-generator system, when the sensitivity method is applied to all 15 modes for both without and with interpolation. In this table, the first three columns are taken from Table 2-7, Case 3. The 3rd column of Table 3-3 is based on determining $\Delta\lambda_1$ by the sensitivity formula of (2-125), when $[A(\omega_n)]$ is found without interpolation. In contrast, after forming $[A(\omega_n)]$ using the curve fitting interpolation of (3-1), $\Delta\lambda_2$ is obtained by applying the sensitivity formula, and the final results are placed in the 4th column. In both cases, the total modified eigenvalue is λ_{imp}.

The prediction error for the results of Table 3-3 is indicated in Table 3-4. According to these tables, the modified eigenvalues obtained with interpolation (λ_{imp2}) are in good agreement with the modified eigenvalues obtained without interpolation (λ_{imp1}).

Table 3-3: Applying sensitivity correction by interpolation, 16-generator system.

Benchmark results	$\lambda(\omega_K=5)$	$\lambda_{imp1}=\lambda+\Delta\lambda_1$ (without interpolation)	$\lambda_{imp2}=\lambda+\Delta\lambda_2$ (with interpolation)
-0.08±*j*1.11	-0.12±*j*0.79	-0.06±*j*1.23	-0.06±*j*1.23
-0.07±*j*2.79	-0.09±*j*2.68	-0.07±*j*2.79	-0.07±*j*2.78
-0.17±*j*3.19	-0.17±*j*3.13	-0.17±*j*3.18	-0.18±*j*3.18
-0.35±*j*4.81	-0.34±*j*4.78	-0.35±*j*4.78	-0.34±*j*4.78
-1.02±*j*6.58	-1.23±*j*6.67	-1.11±*j*6.54	-1.11±*j*6.54
-1.16±*j*6.78	-1.37±*j*6.83	-1.27±*j*6.73	-1.29±*j*6.73
-1.86±*j*7.20	-2.30±*j*6.86	-1.97±*j*6.91	-1.93±*j*6.90
-2.14±*j*7.64	-2.30±*j*7.78	-1.99±*j*7.68	-1.98±*j*7.67
-1.22±*j*7.74	-1.50±*j*7.86	-1.30±*j*7.66	-1.32±*j*7.66
-2.38±*j*8.14	-3.13±*j*7.90	-2.63±*j*8.05	-2.65±*j*8.05
-1.33±*j*8.54	-2.20±*j*7.74	-1.53±*j*8.55	-1.54±*j*8.55
-3.91±*j*8.66	-4.80±*j*7.10	-4.02±*j*8.10	-4.09±*j*8.10
-4.63±*j*8.72	-5.80±*j*6.71	-4.95±*j*8.21	-4.99±*j*8.20
-1.31±*j*10.69	-1.00±*j*10.50	-1.10±*j*10.65	-1.10±*j*10.6
-1.90±*j*10.97	-3.50±*j*10.80	-2.10±*j*10.67	-2.11±*j*10.68

Table 3-4: Error of the TFEA predictions with curve fitting interpolation, 16-generator system.

	Damping	Frequency
Error of λ_{imp2} relative to λ_{imp1}	All modes have less than 5% error.	All modes have less than 1% error.
Error of λ_{imp2} relative to benchmark results	8 modes have less than 10% error. Maximum error is 25%.	8 modes have less than 1% error. Maximum error is limited to 10%.

To appreciate the accuracy and efficiency of the method, it is necessary to test the method on a larger system. Table 3-5 shows the results for the 69-generator system. The corresponding columns of this table are taken from Table 2-9. The columns of Table 3-5 are formatted in the same way as in Table 3-3.

Table 3-5: Applying sensitivity correction by interpolation, 69-generator system.

Benchmark results	$\lambda(\omega_K=5)$	$\lambda_{imp1}=\lambda+\Delta\lambda_1$	$\lambda_{imp2}=\lambda+\Delta\lambda_2$	Benchmark results	$\lambda(\omega_K=5)$	$\lambda_{imp1}=\lambda+\Delta\lambda_1$	$\lambda_{imp2}=\lambda+\Delta\lambda_2$
-0.08±j1.78	-0.19±j1.96	-0.11±j1.80	-0.058±j1.72	-0.79±j7.73	-1.58±j7.35	-0.79±j7.66	-0.79±j7.66
-0.2±j2.38	-0.23±j2.54	-0.21±j2.41	-0.18±j2.08	-0.86±j7.75	-1.29±j7.44	-0.85±j7.69	-0.86±j7.68
-0.12±j2.90	-0.14±j2.97	-0.12±j2.91	-0.12±j2.89	-0.82±j7.90	-1.24±j7.45	-1.00±j7.71	-1.01±j7.71
-0.16±j3.05	-0.13±j3.10	-0.16±j3.05	-0.17±j3.01	-1.04±j7.90	-1.35±j7.44	-1.00±j7.75	-1.00±j7.75
-0.17±j4.05	-0.14±j4.06	-0.17±j4.05	-0.18±j3.95	-1.15±j7.89	-2.15±j7.29	-1.11±j7.78	-1.11±j7.78
-0.32±j4.88	-0.30±j4.85	-0.31±j4.85	-0.31±j4.84	-0.89±j7.96	-1.60±j7.44	-0.79±j7.85	-0.80±j7.85
-0.4±j5.33	-0.42±j5.28	-0.39±j5.29	-0.39±j5.28	-0.99±j7.99	-1.21±j7.64	-0.87±j7.88	-0.87±j7.89
-0.4±j5.55	-0.45±j5.49	-0.39±j5.51	-0.39±j5.50	-0.97±j8.02	-1.33±j7.63	-0.99±j7.91	-0.99±j7.91
-0.08±j5.59	-0.06±j5.6	-0.08±j5.60	-0.09±j5.59	-1.07±j8.07	-1.47±j7.62	-0.94±j7.93	-0.94±j7.93
-0.52±j5.77	-0.64±j5.65	-0.51±j5.69	-0.51±j5.68	-1.00±j8.12	-1.47±j7.63	-0.98±j8.02	-0.98±j8.02
-0.39±j5.79	-0.48±j5.73	-0.39±j5.75	-0.39±j5.734	-0.87±j8.14	-1.90±j7.69	-0.85±j8.08	-0.85±j8.08
-0.38±j5.82	-0.47±j5.73	-0.37±j5.77	-0.37±j5.77	-1.26±j8.15	-1.59±j7.69	-1.21±j8.02	-1.21±j8.02
-0.25±j5.85	-2.61±j5.18	-0.24±j5.85	-0.25±j5.85	-1.19±j8.20	-1.79±j7.61	-1.21±j8.02	-1.21±j8.01
-0.52±j6.06	-0.23±j5.85	-0.51±j6.00	-0.51±j6.00	-1.32±j8.28	-1.31±j7.84	-1.28±j8.14	-1.28±j8.14
-0.56±j6.10	-0.63±j5.95	-0.56±j6.02	-0.56±j6.01	-1.01±j8.39	-1.61±j7.99	-0.99±j8.3	-0.97±j8.31
-0.58±j6.12	-0.74±j5.94	-0.58±j6.03	-0.57±j6.03	-0.87±j8.44	-1.48±j8.02	-0.86±j8.37	-0.86±j8.37
-0.47±j6.21	-0.79±j5.96	-0.46±j6.16	-0.46±j6.15	-1.08±j8.48	-1.70±j8.00	-1.05±j8.38	-1.05±j8.38
-0.55±j6.32	-0.62±j6.11	-0.54±j6.26	-0.54±j6.26	-0.92±j8.93	-1.74±j8.43	-0.91±j8.87	-0.91±j8.87
-0.48±j6.38	-0.70±j6.17	-0.49±j6.33	-0.49±j6.32	-1.24±j8.91	-1.85±j8.38	-1.20±j8.79	-1.20±j8.79
-0.62±j6.52	-0.69±j6.27	-0.61±j6.45	-0.61±j6.44	-1.11±j8.99	-1.55±j8.54	-1.05±j8.89	-1.05±j8.89
-0.56±j6.78	-0.85±j6.32	-0.55±j6.74	-0.55±j6.74	-1.12±j9.10	-2.10±j8.40	-1.12±j9.01	-1.12±j9.01
-0.56±j6.84	-0.76±j6.64	-0.56±j6.78	-0.56±j6.78	-1.04±j9.31	-1.97±j8.74	-1.03±j9.24	-1.03±j9.24
-2.12±j6.59	-0.88±j6.67	-2.19±j5.59	-2.19±j5.59	-1.22±j9.69	-2.42±j8.87	-1.19±j9.61	-1.20±j9.61
-0.79±j6.96	-1.07±j6.72	-0.77±j6.89	-0.77±j6.89	-1.15±j9.71	-2.32±j8.97	-1.14±j9.64	-1.14±j9.64
-0.67±j6.97	-0.99±j6.74	-0.67±j6.88	-0.67±j6.88	-1.14±j9.96	-2.39±j9.24	-1.13±j9.89	-1.13±j9.89
-0.64±j7.06	-0.97±j6.84	-0.64±j6.98	-0.64±j6.98	-1.19±j10.22	-2.52±j9.42	-1.19±j10.19	-1.19±j10.20
-0.63±j7.08	-1.90±j6.65	-0.62±j7.02	-0.62±j7.02	-1.27±j10.66	-2.88±j9.68	-1.26±j10.68	-1.26±j10.65
-0.78±j7.09	-0.89±j6.89	-0.78±j7.12	-0.78±j7.12	-1.39±j10.74	-2.94±j9.75	-1.37±j10.73	-1.37±j10.73
-0.65±j7.24	-1.16±j6.97	-0.64±j7.19	-0.64±j7.19	-1.52±j11.67	-3.52±j10.48	-1.48±j11.71	-1.49±j11.71
-0.87±j7.25	-1.07±j6.97	-0.84±j7.16	-0.84±j7.17	-1.54±j11.79	-3.64±j10.45	-1.53±j11.85	-1.53±j11.85
-0.71±j7.39	-1.02±j7.16	-0.69±j7.33	-0.69±j7.33	-2.07±j12.59	-4.67±j10.59	-2.02±j12.70	-2.03±j12.70
-0.91±j7.44	-0.94±j7.06	-1.01±j7.26	-1.01±j7.27	-2.28±j12.99	-5.13±j10.75	-2.21±j13.14	-2.21±j13.14
-0.71±j7.49	-1.14±j7.24	-0.70±j7.43	-0.70±j7.43	-2.05±j13.13	-4.86±j11.12	-1.99±j13.29	-2.00±j13.29
-0.80±j7.51	-1.23±j7.20	-0.79±j7.42	-0.79±j7.42	-2.21±j13.49	-5.09±j11.37	-2.13±j13.67	-2.14±j13.67

Table 3-6 shows the errors for the results of Table 3-5. It is observed that λ_{imp1} and λ_{imp2} are in good agreement. The acceptable numerical results as well as the expected smoothness of $[A(\omega)]$, demonstrate the feasibility and the effectiveness of the interpolation method.

Table 3-6: Error of the TFEA predictions with curve fitting interpolation, 69-generator system.

	Damping	Frequency
Error of λ_{imp2} relative to λ_{imp1}	62 modes have less than 2% error. Maximum error is 15%.	67 modes have less than 2% error. Maximum error is 13%.
Error of λ_{imp2} relative to benchmark results	59 modes have less than 5% error. 8 modes have error between 5 and 10%. Maximum error is 27%.	66 modes have less than 5% error. Maximum error is 15%.

3.4.5 Computation Count with Curve Fitting Interpolation

Since the number of electromechanical modes is much greater than the number of sampling frequencies, it is expected that the curve fitting interpolation will significantly improve the computation count.

According to the results in Section 3.4.3, the sampling frequencies of ω_{sample}= 1, 2,…, 10 rad/s (n_{sample}=10) are sufficient for the range of 0.7-12.5 rad/s. In other words, because the usual frequency range of power system eigenanalysis is 0.7-12.5 rad/s [3], the sampling frequencies are chosen regardless of the system size and topology, which is the most important advantage of this method. A comparison of the computation counts is provided in Table 3-7.

Table 3-7: Computation count for applying interpolation in forming $[A(\omega_n)]$.

	Without interpolation (from Table 3-1)	With interpolation
Eigenanalysis by TFEA method: applying sensitivity correction to all ng modes	$(3+ng)(2ng)^3$	$(3+n_{sample})(2ng)^3$

Therefore, the speed up efficiency of interpolation method from Table 3-7 is,

$$\frac{(3+ng)(2ng)^3}{(3+n_{sample})(2ng)^3}=\frac{(3+ng)}{(3+n_{sample})}. \quad (3\text{-}2)$$

According to Table 3-1, the TFEA method has a speed up efficiency of 166/(ng+3). Therefore, considering (3-2), the total increase in speed with interpolation, compared to the QR analysis of the full state matrix, would be,

$$\frac{166}{(ng+3)} \times \frac{(3+ng)}{\left(3+n_{sample}\right)} = \frac{166}{\left(3+n_{sample}\right)}. \tag{3-3}$$

For n_{sample}=10, it would be approximately 13 times faster than conventional QR analysis of the full state matrix. It should be reemphasized that this increase in speed is for the worst case, in which the sensitivity formula is applied to modify all ng modes. The interesting point is that the speed-up efficiency of (3-3) depends only on n_{sample}, which is a fixed number regardless of the number of generators, ng, and the states per generator, m.

3.6 Conclusion of TFEA Advantages

The TFEA method has been introduced and tested in Chapters 2 and 3. Based on the results of these chapters the following conclusion can be made regarding the advantages of the TFEA method.

3.6.1 TFEA for Power System Security Assessment

Because power system outage affects gross national productivity, there is a need for continuous power system security assessment. TFEA has potential as one of the next-generation on-line methods for power system analysis tools, such as DSA Tools offered by Powertech [52], to assess all forms of stability in close to real time.

Currently, the Modified Arnoldi Method (MAM) is the workhorse for small signal stability analysis because it has both speed and accuracy for large-dimension matrices. However, its application is limited to a few eigenvalues. Because only the eigenvalues closest to the imaginary axis of the complex s-plane affect stability, MAM is adequate in principle. In practice, one does not know a priori which modes are lowly damped.

Since the TFEA method solves all the electromechanical eigenvalues, it can be used to identify the modes that have low damping. The eigenvalues of modes with modal frequencies ω_n distant from ω_K are inaccurate. Improving their accuracy by the sensitivity method is an option. Usually, it is unnecessary because stability is determined by the eigenvalue closest to the imaginary axis. In application, the TFEA is first used to scan all of the modes to identify the few with the smallest real parts. If required, improvement of accuracy by the sensitivity method is applied to only the few ones. Therefore, the method is fast. If all of the eigenvalues must be determined accurately, one can turn to the curve fitting interpolation method.

3.6.2 Summary

The TFEA method:

- Avoids redundant calculation, because it does not find any eigenvalue more than once;
- Is not iterative, so it does not have the issue of convergence;
- Does not require any initial guess or estimation;
- Does not require any preconditioning transformation as in MAM and Inverse Iterations; and
- Is adaptive to any system complexity: the power system elements such as exciter, PSS, governor, and FACTS devices could be easily accounted for with the method. The state matrix order is always $2ng$, regardless of the power system model and complexity.

Finally, the advantages of eigenanalysis by the TFEA method could be summarized as:

- Good estimate of all of the electromechanical modes;
- Improvement in computational efficiency;
- Selective eigenanalysis, as it can find more accurate result for selected modes by applying the sensitivity formula;
- The use of different approaches to improve the overall computational efficiency when applying the sensitivity formula, such as the proposed interpolation method and parallel computation; and
- Near real-time assessment of small disturbance stability.

Chapter Four

4. Selective Eigenanalysis by Applying Modified Arnoldi Method (MAM) to TFEA

4.1 Overview

Small signal stability is assured when all the modes of the linearized [A]-matrix are positively damped. However, the only important oscillatory modes are the few that have the lowest damping factors. This shows the importance of special methods introduced in Section 1.4 that can efficiently find a limited and selected number of eigenvalues. The Modified Arnoldi Method (MAM) is one of the most successful ones in power system applications [16].

In contrast, a production program for eigenvalue estimation of power systems could incorporate more than one algorithm. A good example is provided in Section 1.4.2, in which the Inverse Iterations method is used to improve the convergence of the AESOPS algorithm. The Program for Eigenvalue Analysis of Large Systems (PEALS) in [40] also employs the two methods of the AESOPS algorithm and the Modified Arnoldi Method (MAM) to compute eigenvalues.

This chapter draws attention to applying MAM to [$A(\omega_K)$] formed by TFEA for the efficient calculation of a limited and selected number of eigenvalues. It is shown that when the interest lies only in oscillatory modes around a specific frequency ω_n, then the TFEA method is sufficiently accurate if $\omega_K \approx \omega_n$, and there is no need to apply the sensitivity formula of (2-125).

4.2 Contributions

The first contribution of this chapter is to investigate whether the TFEA can be combined with the well-known method of MAM. The second contribution is to reduce the computation cost for selective eigenanalysis.

Computation cost reduction comes from applying MAM to the reduced $2ng\times2ng$ matrix of $[A(\omega_K)]$, instead of the higher rank full state matrix, as shown in Figure 4-1. In this figure, the blocks on the left show the steps for applying MAM to TFEA. $[A(\omega_K)]$ is formed and passed on to MAM stage, which produces a lower rank $[H]_{p\times p}$ matrix. The QR method is then applied to obtain the eigenvalues of $[H]$. To compare, the blocks on the right follow the same steps except that MAM is applied to the full state matrix.

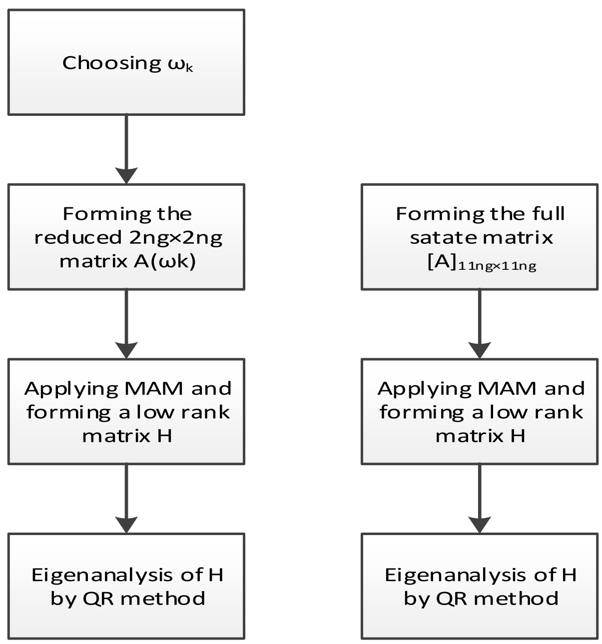

Figure 4-1: Applying MAM to $[A(\omega_K)]$ and to the full state matrix.

4.3 Modified Arnoldi Method (MAM)

4.3.1 Background on MAM

The Arnoldi method is the most efficient method for determining a set of dominant eigenvalues (i.e., largest moduli) of an unsymmetrical matrix, and it has been successfully applied to large power systems. The Arnoldi method was first introduced in [15]. However, because of its poor numerical properties, it was not successful initially, and it required several modifications to be satisfactory [16]. Different modifications to the Arnoldi method have been presented. The algorithm used in this research was taken from [16] and it is called the Modified Arnoldi Method (MAM). Another recent modification is the Implicit Restarted Modified Arnoldi (IRMA) of [53, 54]. Based on IRMA, the Arnoldi Package (ARPACK) of [55] computes a few eigenvalues and their eigenvectors of large, sparse matrices. It is beyond the scope of this research to review these methods.

4.3.2 Implementation for TFEA Application

The Arnoldi method is based on building the dominant invariant subspace of a matrix [A]. The subspace is built as a unitary Krylov subspace [34, 35]. The process starts with a single random vector $\underline{x}$ and then proceeds by calculating the second vector as [A]$\underline{x}$ and orthonormalizing it relative to $\underline{x}$, and so on. During this process an upper Hessenberg projection matrix [H] of order p is automatically obtained, where p is the number of Krylov steps and is much smaller than the rank of original matrix [A] [35]. An upper Hessenberg matrix has zero entries below the first sub-diagonal.

Chiefly, the procedure forms an orthogonal basis $V_p=\{v_1,v_2,\ldots, v_p\}$ for the Krylov subspace of [A], $\kappa_p(A,\underline{x})$, through a lower rank upper Hessenberg transformation matrix [H]:

$$AV_p = V_p H_p \tag{4-1}$$

$$\kappa_p(A,\underline{x}) = \{\underline{x}, A\underline{x}, A^2\underline{x}, \ldots, A^{p-1}\underline{x}\}. \tag{4-2}$$

Equation (4-1) implies that the eigenvalues of [H] are approximates of the dominant eigenvalues of [A]. The dominant eigenvalues are those with the largest moduli. Choosing the number of Krylov steps, p, depends on the number of desired eigenvalues.

When the desired eigenvalues are not the dominant ones, a transformation should be applied to [A] matrix to transform the desired eigenvalues into dominant ones. A simple way is to use the spectral transformation of (4-3) when the eigenvalues around λ_t are of interest [16]:

$$[A_t] = ([A] - \lambda_t [I])^{-1}. \tag{4-3}$$

This transforms the eigenvalue λ_A of [A] to

$$\lambda_{At} = \frac{1}{(\lambda_A - \lambda_t)} \tag{4-4}$$

or consequently

$$\lambda_A = \frac{1}{\lambda_{At}} + \lambda_t \qquad (4\text{-}5)$$

where, for this research, $[I]$ is the $2ng \times 2ng$ identity matrix, $[A]=[A(\omega_K)]$, and $\lambda_t=(j\omega_K)$ because the eigenvalues around ω_K are of interest.

The complete procedure performed in this chapter can be summarized as follows.

1- The desired frequency range, ω_K is chosen.

2- $[A(\omega_K)]$ is formed by the TFEA method.

3- $[A_t]$ is formed as in (4-3).

4- The order of $[H]$ is chosen, depending on the number of desired eigenvalues.

5- MAM is applied to $[A_t]$, and $[H]$ is formed.

6- The eigenvalues of $[H]$ are calculated by a QR algorithm.

7- The desired eigenvalues of $[A(\omega_K)]$ are retrieved as in (4-5).

4.4 Numerical Results

To evaluate the proposed method, the 69-generator test system of [45] has been used. The operation conditions, system parameters and the exciter/PSS model are the same as in Chapter 2. Table 4-1 shows the results of applying MAM for four different ω_K for the frequency range of 1-6 rad/s. For each ω_K, $[A(\omega_K)]$ is formed, and MAM is applied to determine the selected eigenvalues. The selected eigenvalues are those around ω_K.

The first column of Table 4-1 shows the benchmark values, which are the results of QR eigenanalysis of the full state matrix. For each ω_K in this table there are two columns: the first column shows the eigenvalues of $[A(\omega_K)]$, and the second column, under $[H]$, shows the eigenvalues of MAM applied to $[A(\omega_K)]$. Only the eigenvalues around ω_K are presented as the desired modes. There is good agreement between the results in the two columns, confirming that MAM can be successfully applied to TFEA. Although the overall estimation for each ω_K is acceptable, the best results are high-lighted in yellow.

Table 4-1: Applying MAM to $[A(\omega_K)]$ for the 69-generator test system.

Benchmark values	$\omega_K=2$		$\omega_K=3$		$\omega_K=4$		$\omega_K=5$	
	$A(\omega_K)$	$[H]$ (p=20)	$A(\omega_K)$	$[H]$ (p=20)	$A(\omega_K)$	$[H]$ (p=20)	$A(\omega_K)$	$[H]$ (p=20)
$-0.08\pm j1.78$	$-0.11\pm j1.79$	$-0.11\pm j1.79$	$-0.18\pm j1.82$	$-0.18\pm j1.82$	$-0.19\pm j1.89$	$-0.21\pm j1.88$	$-0.19\pm j1.96$	$-0.19\pm j1.96$
$-0.2\pm j2.38$	$-0.15\pm j2.39$	$-0.15\pm j2.39$	$-0.23\pm j2.42$	$-0.23\pm j2.42$	$-0.24\pm j2.48$	$-0.25\pm j2.49$	$-0.23\pm j2.54$	$-0.23\pm j2.54$
$-0.12\pm j2.90$	$-0.08\pm j2.89$	$-0.08\pm j2.89$	$-0.12\pm j2.91$	$-0.12\pm j2.91$	$-0.13\pm j2.94$	$-0.13\pm j2.94$	$-0.14\pm j2.97$	$-0.14\pm j2.97$
$-0.16\pm j3.05$	$-0.18\pm j3.01$	$-0.18\pm j3.01$	$-0.16\pm j3.04$	$-0.16\pm j3.04$	$-0.14\pm j3.07$	$-0.14\pm j3.07$	$-0.13\pm j3.1$	$-0.13\pm j3.1$
$-0.17\pm j4.05$	$-0.36\pm j3.96$	$-0.3\pm j3.95$	$-0.22\pm j4.02$	$-0.22\pm j4.02$	$-0.17\pm j4.04$	$-0.17\pm j4.05$	$-0.14\pm j4.06$	$-0.14\pm j4.06$
$-0.32\pm j4.88$			$-0.63\pm j4.74$	$-0.63\pm j4.74$	$-0.41\pm j4.82$	$-0.41\pm j4.81$	$-0.30\pm j4.85$	$-0.30\pm j4.85$
$-0.4\pm j5.33$					$-0.59\pm j5.22$	$-0.59\pm j5.22$	$-0.42\pm j5.28$	$-0.42\pm j5.28$
$-0.4\pm j5.55$					$-0.62\pm j5.44$	$-0.62\pm j5.44$	$-0.45\pm j5.49$	$-0.45\pm j5.49$
$-0.08\pm j5.59$					$-0.002\pm j5.65$	$-0.002\pm j5.65$	$-0.059\pm j5.61$	$-0.059\pm j5.61$
$-0.52\pm j5.77$					$-0.69\pm j5.66$	$-0.66\pm j5.66$	$-0.64\pm j5.65$	$-0.64\pm j5.65$
$-0.39\pm j5.79$					$-0.68\pm j5.67$	$-0.69\pm j5.67$	$-0.48\pm j5.73$	$-0.48\pm j5.73$
$-0.38\pm j5.82$					$-0.85\pm j5.86$	$-0.87\pm j\,5.87$	$-0.47\pm j5.73$	$-0.47\pm j5.73$
$-0.25\pm j5.85$					$-0.23\pm j5.86$	$-0.23\pm j\,5.86$	$-0.23\pm j5.86$	$-0.23\pm j5.86$
$-0.52\pm j6.06$							$-0.63\pm j5.95$	$-0.63\pm j5.95$
$-0.56\pm j6.10$							$-0.74\pm j5.94$	$-0.74\pm j5.94$

4.5 Computation Speed-up Gain

According to [56] the cost of forming the upper Hessenberg matrix of $[H]_{p\times p}$ with MAM is on the order of np^2, where n and p are the ranks of original matrices $[A]_{n\times n}$ and $[H]_{p\times p}$ respectively. Therefore, the speed up efficiency when applying MAM to $[A(\omega_K)]_{2ng\times 2ng}$ instead of $[A]_{11ng\times 11ng}$ would be 11/2=5.5.

4.6 Choosing *p*

Before applying MAM, the order of [*H*] should be determined depending on the number of desired eigenvalues. As explained in [16], there is not a specific rule for choosing *p*. As *p* increases, the number of accurate eigenvalues increases, as well as computation cost, making a trade-off in choosing *p*. To test the effect of *p*, MAM is applied to determine the low frequency modes. The representative frequency is chosen as ω_K=2, and MAM is evaluated for *p*=5, *p*=10 and *p*=15. Table 4-2 summarizes the results for the frequency range of 1-3 rad/s; the first column shows the benchmark values while the other columns show the results of MAM. From this table, it can be observed that for *p*=5, only 2 eigenvalues are found, while more eigenvalues are calculated by increasing *p* to 10 and then to 15.

Table 4-2: Effect of *p* in MAM.

Benchmark values	[*H*] (*p*=5)	[*H*] (*p*=10)	[*H*] (*p*=15)
-0.08±*j*1.78	-0.11±*j*1.79	-0.11±*j*1.79	-0.11±*j*1.79
-0.20±*j*2.38	-0.15±*j*2.39	-0.15±*j*2.39	-0.15±*j*2.39
-0.12±*j*2.90	-	-0.08±*j*2.89	-0.08±*j*2.89
-0.16±*j*3.05	-	-	-0.18±*j*3.01

4.7 Conclusion

The Modified Arnoldi Method (MAM) [16] is a well-known, accurate method in finding limited numbers of eigenvalues. It has been shown that, for a selected desired number of eigenvalues around a specific frequency ω_K, the input to MAM could be $[A(\omega_K)]$ instead of the full state matrix of $[A]_{11ng\times 11ng}$. This process led to a more efficient calculation, while preserving the accuracy. Rather than efficiency, the ability of TFEA to be combined with MAM showed the prospective development opportunities for TFEA.

Chapter Five

5. Application of TFEA in PSS Tuning: Contributions and Methodology

5.1 Overview

This chapter presents the application of TFEA method in power system stabilizer (PSS) tuning. This research shows that the time-saving TFEA method can be combined with eigenvalue sensitivity concepts and optimization techniques to yield a fast and robust method for coordinated tuning of gains and time constants. The proposed tuning method is first applied to PSS gain tuning. Tuning is followed by simultaneous gain and time constants tuning.

This chapter is organized as follows. A review of work previously accomplished and a background on PSS design and tuning are presented in Section 5.2. Section 5.2.2 presents a brief review of PSS tuning using eigenvalue sensitivity principles, which forms the basis of this research. The contribution is presented in Section 5.3. The method employed begins in Section 5.4 with PSS tuning implementation explained in Section 5.5. A chapter summary is provided in Section 5.6. The numerical results and validation tests based on the contribution and methodology of this chapter are given in Chapter 6.

5.2 Introduction

5.2.1 Classic Design of Power System Stabilizer (PSS)

As electric utilities have interconnected to take advantage of economies of scale, the size increase has resulted in weakened dynamic systems with low frequency and lightly damped oscillatory modes. Power system stabilizers (PSSs) were developed to increase system damping by introducing a perturbation torque proportional to the perturbation angular velocity of the rotor [57, 58].

Early feedback design was not successful until it was realized that there is a large phase lag due to the long time-constant of the field winding. The PSS operation of a single generator was explained as phase-compensation of the transfer function between the voltage reference input to the Automatic Voltage Regulator (AVR) and the electrical torque developed on the shaft of the generator [57, 59]. The method is called the P-Vr method, and it is based on the concept of synchronizing and damping torques [57, 59].

GEP (Generator, Excitation and Power systems) and the method of residues are the other classic phase compensation methods for PSS design. GEP is similar to P-Vr and is based on the measurement of the voltage reference of the AVR/exciter and the generator terminal voltage. However, determining the stabilizer gains with this method is not considered as robust [59, 60, 61].

The method of residues, allows the “poles” of partial fractions of a transfer function to predict the damping factor and the oscillating frequency [62, 63, 64]. Residues yield only a limited number of phase angles that can be used with confidence for design purposes. The remaining residues for rotor modes are affected by the variability of participation factor angles and by interactions from other generators [61].

From PSS designed for the operation of a single-generator, attention is next turned to the tuning of the stabilizers of multi-generator power system [58, 65]. In this regard, the coordination among stabilizers is important because it is believed to constitute the origin for some damping deterioration [66].

5.2.2 Coordinated Tuning of Local PSSs Using Eigenvalue Sensitivity

Different research groups have considered the problem of coordinating the settings of local PSSs to improve the overall dynamic performance of the system [67, 68, 69, 70]. Iterative methods based on eigenvalue sensitivities, have been used widely as a result of modal analysis to determine the eigenvalue shift due to a change in PSS parameters [44, 71, 72, 73, 74]. In this regard, linear programming has proved successful for the problem of PSS gain coordination [71, 72, 75, 76].

The proposed method in this research is similar to the method of [76] , which has used the concept of induced torque coefficients (ITCs) to form the eigenvalue sensitivity. However, the torque coefficients in this research are obtained by the TFEA method. The important feature of both ITC and TFEA is that the interactions between any stabilizer and any generator in the system can be quantified. This ability is important because such interactions can enhance or degrade the damping of certain electromechanical modes [66].

Independently, others have developed techniques for the coordination of stabilizers based on the calculation of eigenvalue shifts from the residues [63, 71, 77, 78].

5.2.3 Recent Developments in Stabilizer Design

In recent years, many design methods have been centered around new control concepts. Research has been done on PSS design, based on probabilistic sensitivity indices [79], the linear parameter varying approach [80], Adaptive Control [81, 82], Neural Network [83, 84] and Genetic Algorithm [79, 85]. An important development is the identification technique of [85], based on standard Prony analysis [86]. The method is claimed to have the ability to extract crucial dynamic characteristics from a system of any size to develop a robust controller. The objective is to reduce the system order, as with the TFEA method. The difference is that Prony depends on high observability and controllability indices whereas TFEA models the intrinsic dynamics of the generator, with the exciter and the PSS as transfer functions.

With the advent of Flexible AC Transmission Systems (FACTS), damping improvement is sought in coordinating the power electronic controllers of FACTS to supplement the capabilities of individual PSSs [66, 87, 88]. Additionally, the development of phase measurement units

(PMUs) offers wide-area measurements, by which large power systems can be stabilized using a central controller that is effectively a "Global PSS" [89, 90] that augments the damping from local PSSs. These methods are not addressed in the research of this thesis.

5.3 Contribution

The contribution of this research is to show that a combination of (i) computationally efficient Transfer Function and Eigenfunction Analysis (TFEA) method, (ii) the eigenvalue sensitivity concept and (iii) optimization techniques makes a powerful tool for the coordinated tuning of power system stabilizers to meet the stability objectives of the power system. The distinguishing feature of the research is the TFEA method, which brings about computational efficiency.

Eigenvalue sensitivity formulation ensures full controllability of the perturbation vector of electromechanical eigenvalue shifts, by the perturbation vector of parameter changes. Therefore, PSS gain and time constants can be tuned, as perturbation parameters, for the desired eigenvalue shifts. The tuning depends on the powerful optimization techniques available in MATLAB [91, 92]. The MATLAB optimization algorithms have linear programming and non-linear programming capabilities, which enable PSSs gains and time constants to be simultaneously tuned to meet the stability objectives [93].

The tuning research of this chapter is performed in two steps, as shown in Table 5-1. The method is first applied to PSS gain tuning to demonstrate the feasibility of the method. With positive experience in tuning a few parameters, research is encouraged to continue to complete the tuning of gains and time constants simultaneously. The computation tool allows different stability concerns to be addressed as objective functions of optimization under constraints, as shown in Table 5-1.

Table 5-1: Stability objectives of PSS tuning.

Tuning type	Test system used	Objective of PSS tuning
PSSs gains	69-generator system	Achieving desired damping shift. Maximizing damping improvement for the low frequency modes (optimization by linear programming).
PSSs gains and time constants	16-generator system 69-generator system	Minimizing the PSSs gains (optimization by non-linear programming). Maximizing damping improvement for the low frequency modes (optimization by non-linear programming).

5.4 Outline of Method

5.4.1 PSS Perturbation Parameters

The PSS model used in this research is PSS2B from IEEE std. 421.5 [94, 95]. From the 4 settings in Table I in [94], the authors have chosen Setting 1, which is shown in Figure 5-1. The parameters are the gain K_{ST} and the four time constants T_1, T_2, T_3 and T_4. All the ng generators are equipped with the same PSS model. Therefore, for a system with ng generators, the parameters form ng-tuple vectors $\underline{K}_{ST}$, $\underline{T}_1$, $\underline{T}_2$, $\underline{T}_3$ and $\underline{T}_4$.

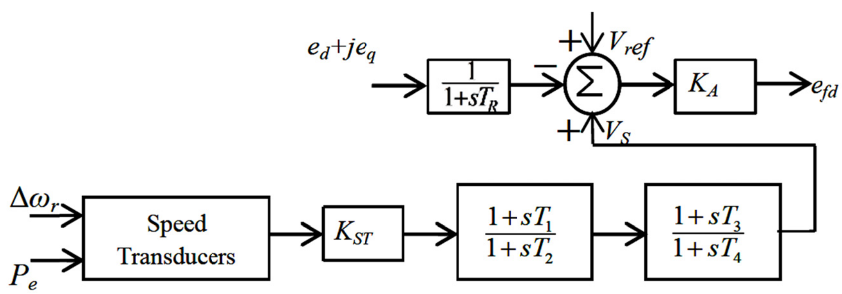

Figure 5-1: Exciter and PSS model for the study of PSS tuning [94].

To allow for perturbation Δpa in the tuning study, each parameter is written as $pa=pa^0+\Delta pa$, where pa^0 is the value of the original design. Thus, for the PSS gain and time constants of ng generators,

$$\underline{K}_{ST} = \underline{K}_{ST}^0 + \underline{\Delta K}_{ST} \tag{5-1}$$

$$\underline{T}_1 = \underline{T}_1^0 + \underline{\Delta T}_1 \tag{5-2}$$

$$\underline{T}_2 = \underline{T}_2^0 + \underline{\Delta T}_2 \tag{5-3}$$

$$\underline{T}_3 = \underline{T}_3^0 + \underline{\Delta T}_3 \tag{5-4}$$

$$\underline{T}_4 = \underline{T}_4^0 + \underline{\Delta T}_4 \tag{5-5}$$

where the original and perturbation parameters form the vectors of

$$\underline{K}_{ST}^0 = [K_{ST1}^0, \ldots, K_{STng}^0]^T \tag{5-6}$$

$$\underline{T}_1^0 = [T_{11}^0, \ldots, T_{1ng}^0]^T \tag{5-7}$$

$$\underline{T}_2^0 = [T_{21}^0, \ldots, T_{2ng}^0]^T \tag{5-8}$$

$$\underline{T}_3^0 = [T_{31}^0, \ldots, T_{3ng}^0]^T \tag{5-9}$$

$$\underline{T}_4^0 = [T_{41}^0, \ldots, T_{4ng}^0]^T \tag{5-10}$$

$$\underline{\Delta K}_{ST} = [\Delta K_{ST1}, \ldots, \Delta K_{STng}]^T \tag{5-11}$$

$$\underline{\Delta T}_1 = [\Delta T_{11}, \ldots, \Delta T_{1ng}]^T \tag{5-12}$$

$$\underline{\Delta T}_2 = [\Delta T_{21}, \ldots, \Delta T_{2ng}]^T \tag{5-13}$$

$$\underline{\Delta T}_3 = [\Delta T_{31}, \ldots, \Delta T_{3ng}]^T \tag{5-14}$$

$$\underline{\Delta T}_4 = [\Delta T_{41}, \ldots, \Delta T_{4ng}]^T . \tag{5-15}$$

The parameters together are represented by a 5×*ng* tuple vector $\underline{pa}$. The perturbation parameters are represented by the vector $\underline{\Delta pa}$,

$$\underline{pa} = \underline{pa}^0 + \underline{\Delta pa} \tag{5-16}$$

$$\underline{pa} = [\underline{K}_{ST}^T, \underline{T}_1^T, \underline{T}_2^T, \underline{T}_3^T, \underline{T}_4^T]^T \tag{5-17}$$

$$\underline{pa}^0 = [\underline{K}_{ST}^{0T}, \underline{T}_1^{0T}, \underline{T}_2^{0T}, \underline{T}_3^{0T}, \underline{T}_4^{0T}]^T \tag{5-18}$$

$$\underline{\Delta pa} = [\underline{\Delta K}_{ST}^T, \underline{\Delta T}_1^T, \underline{\Delta T}_2^T, \underline{\Delta T}_3^T, \underline{\Delta T}_4^T]^T . \tag{5-19}$$

The eigenvalues shifts due to perturbation parameters of (5-11)-(5-15) would be obtained in the general form of

$$\underline{\Delta \lambda} = f(\underline{\Delta pa}) \tag{5-20}$$

where $\underline{\Delta \lambda}$ is the (*ng*-1) tuple vector of the eigenvalue shifts as

$$\underline{\Delta \lambda} = [\Delta \lambda_1, \ldots, \Delta \lambda_{ng-1}]^T . \tag{5-21}$$

5.4.2 Modeling Excitation System and Power System Stabilizer to Insert PSS Parameters into Equations

Based on the transfer functions of the exciter and PSS in Figure 5-1, Δe_{fd} can be written as

$$\Delta e_{fd} = G_{exc}(s)\,\underline{\Delta e}_{dq} + G_{pss}(s)\,\Delta\omega_r \tag{5-22}$$

where

$$G_{pss}(s) = K_A K_{ST}\frac{1+sT_1}{1+sT_2}\frac{1+sT_3}{1+sT_4}. \tag{5-23}$$

G_{exc} is the transfer function of the exciter, with the gain of K_A, defined in (2-68). $\underline{\Delta e}_{dq}$ is the vector of terminal voltage defined in (2-43) and $\Delta\omega_r$ is the perturbation rotor speed. The parameters K_{st}, T_1,T_2,T_3 and T_4 in (5-23) are defined in (5-1)-(5-5) which carry the perturbed parameters. Now, the field voltage of (5-22), which contains the PSS perturbed parameters, is used by the TFEA method to form $[A(\omega_n)]$. As shown in the next section, $[A(\omega_n)]$ will be used in the sensitivity formula to determine the eigenvalue shift.

5.4.3 Eigenvalue Shift: Implicit and Explicit Evaluation of Δλ

The eigenvalue sensitivity formula of (2-122) repeated below plays the key role in forming the eigenvalue shift:

$$\Delta\lambda = \frac{\underline{r}^T \Delta[A]\,\underline{u}}{\underline{r}^T\,\underline{u}} \tag{5-24}$$

To estimate $\Delta\lambda$ for the n^{th} mode due to the PSSs parameters of (5-1)-(5-5), the correction $\Delta[A]$ in the eigenvalue sensitivity formula of (5-24) would be

$$\Delta[A] = [A(\omega_n, \underline{K}_{ST}^0 + \underline{\Delta K}_{ST}, \underline{T}_1^0 + \underline{\Delta T}_1, \underline{T}_2^0 + \underline{\Delta T}_2, \underline{T}_3^0 + \underline{\Delta T}_3, \underline{T}_4^0 + \underline{\Delta T}_4)] - [A(\omega_n, \underline{K}_{ST}^0, \underline{T}_1^0, \underline{T}_2^0, \underline{T}_3^0, \underline{T}_4^0)] \tag{5-25}$$

where $[A(\omega_n, \underline{K}_{ST}^0, \underline{T}_1^0, \underline{T}_2^0, \underline{T}_3^0, \underline{T}_4^0)]$ is the original matrix before parameter perturbation, and $[A(\omega_n, \underline{K}_{ST}^0 + \underline{\Delta K}_{ST}, \underline{T}_1^0 + \underline{\Delta T}_1, \underline{T}_2^0 + \underline{\Delta T}_2, \underline{T}_3^0 + \underline{\Delta T}_3, \underline{T}_4^0 + \underline{\Delta T}_4)]$ is the matrix after parameter perturbations. Both matrices are evaluated at the frequency of ω_n. The eigenvectors $\underline{r}$ and $\underline{u}$ are obtained from $[A(\omega_K, \underline{K}_{ST}^0, \underline{T}_1^0, \underline{T}_2^0, \underline{T}_3^0, \underline{T}_4^0)]$.

From (5-25) for each mode, the eigenvalue shift takes the implicit form of

$$\Delta\lambda_n = f_n(\omega_n, \underline{\Delta K}_{ST}, \underline{\Delta T}_1, \underline{\Delta T}_2, \underline{\Delta T}_3, \underline{\Delta T}_4) \qquad for\ n = 1,\ 2, ...,\ (ng\text{ - }1). \tag{5-26}$$

Considering the PSS transfer function of (5-23), it is realized that (5-26) is a non-linear function of time constants. However, for gain tuning only, (5-26) would be a linear function of PSSs gains and can be formed explicitly as

$$\underline{\Delta\lambda} = [C]\underline{\Delta K}_{ST} \tag{5-27}$$

where $[C]$ is a real $(ng\text{-}1)\times npa$ matrix, $(ng\text{-}1)$ is the total number of electromechanical modes, and npa is the number of PSSs gains to be modified.

As the interest of this research is only in the damping part, we have

$$\underline{\Delta\sigma} = [D]\underline{\Delta K}_{ST} \tag{5-28}$$

where

$$[D] = real([C]). \tag{5-29}$$

For a specific $\underline{\Delta\sigma}$, (5-28) allows $\underline{\Delta K}_{ST}$ to be determined as

$$\underline{\Delta K}_{ST} = ([D]^T[D])^{-1}[D]^T\,\underline{\Delta\sigma} \tag{5-30}$$

where $([D]^T[D])^{-1}[D]^T$ is called the generalized (pseudo) inverse of $[D]$ [35].

5.4.4 Choice of Representative Frequency

The accuracy of eigenvalue sensitivity of (5-24) depends on the eigenvectors $\underline{r}$ and $\underline{u}$. It was shown in Chapter 2 that these eigenvalues are computed only once (i.e., from $[A(\omega_K{=}5)]$) for economic reasons. However, for better accuracy in PSS tuning, three ω_K are used in this chapter, as in Table 5-2.

The representative frequency ω_K is like a portable magnifying glass, which can be held over any region in which accuracy is needed. From the results of Section 2.10, the choice of ω_K for accurate estimation of eigenvalues in the modal frequency range is shown in Table 5-2.

Table 5-2: Choosing ω_K according to the frequency range.

Representative frequency (rad/s)	Modal frequency range (rad/s)
$\omega_{K1}=2$	0.5-3.5
$\omega_{K2}=5$	3.5-7
$\omega_{K3}=8$	over 7

5.5 Implementation of PSS Tuning

5.5.1 Gain Tuning

For the PSS gain tuning in this research, it is assumed that the time constants are set from a prior manufacturer PSS design and the task is to tune the gains to fulfill a specific damping objective (i.e., $\underline{pa}^0 \neq 0$ in (5-18)). According to Table 5-1, the first objective of PSS gain tuning is to verify whether any desired damping is achievable from (5-30).

The second objective, however, returns to the goal of increasing the damping of the few least damped modes. There is concern that, as the power system continues to grow in size, the power system will weaken, resulting in low frequency modes, which are usually lightly damped [94]. This research explores whether the damping of the low frequency modes can be improved by relaxing the damping constraints placed on the modes that have higher damping. Tuning is based on maximizing the damping of the target modes (i.e., low frequency modes) under constraints.

The objective function is

$$\min\left\{-\sum_j W_j \Delta\sigma_j^2\right\} \qquad j = \text{target modes} \tag{5-31}$$

where W_j is the weighting factor of the j^{th} mode, and $\Delta\sigma$ is a linear function of PSSs gains from (5-28).

5.5.2 Simultaneous Tuning of Gains and Time Constants: Iterative Tuning by Optimization Using Non-linear Programming

For a realistic multiple PSS design, the tuning procedure should consist not only of the gains but also of the time constants, with no pre-set manufacturer design (i.e. $\underline{pa}^0=0$ in (5-18)). This requirement is fulfilled by formulating them as objective functions under constraints, which are solved by an optimization algorithm, based on searching in the parameter space of $\Delta\underline{pa}$. Remembering (5-26), when considering the time constants the problem involves applying a non-linear programming. The optimization algorithm used is the Sequential Quadratic Programming (SQP) method [93] from a built-in MATLAB function.

The SQP method represents the state of the art in non-linear programming methods by outperforming every other tested method in terms of efficiency, accuracy, and percentage of successful solutions [96]. With each iteration of SQP, a Quadratic Programming (QP) sub-problem is solved to determine the search direction for a line search procedure. The QP sub-problem is formed by an approximation of the Hessian of the Lagrangian function, using a quasi-Newton updating method [97, 98].

To illustrate how the proposed method can be applied for simultaneous gain and time constants tuning, this section focuses on two design objectives of Table 5-1.

Objective 1- This objective follows the design philosophy of [76] which states, "low stabilizer gains reduce not only the effect of limiting in the stabilizer, AVR and excitation systems, but also Mvar swings on generators for small disturbances". In tuning objective, the PSSs gains are minimized under the constraint that the damping ratios for all the electromechanical modes are at least 5%. Therefore,

$$\min\left\{\sum_j W_j K_{STj}\right\} \qquad j = 1, 2, ..., ng \tag{5-32}$$

subject to

$$\frac{\sigma_f}{\omega_f} \leq -5\% \qquad \text{for all electromechanical modes.} \tag{5-33}$$

W_j is the weighting factor that can be unity, or it can be chosen in such a manner to bias the solutions in favor of the most effective stabilizers [76]. In addition, σ_f and ω_f are the final damping and oscillation frequency, respectively, after the PSS tuning:

$$\underline{\sigma}_f = real\ (\underline{\lambda}_0 + \underline{\Delta\lambda}) \tag{5-34}$$

$$\underline{\omega}_f = imaginary\ (\underline{\lambda}_0 + \underline{\Delta\lambda}) \tag{5-35}$$

where $\underline{\lambda}_0$ is the vector of original eigenvalues with no PSS, and $\underline{\Delta\lambda}$ is the vector of eigenvalue shifts obtained from (5-26).

Objective 2- Similar to Section 5.5.1, the tuning objective is to maximize the damping of few target modes (i.e., low frequency modes) by

$$\min\left\{-\sum_j W_j \Delta\sigma_j^2\right\} \qquad j = \text{target modes.} \tag{5-36}$$

where $\Delta\sigma$ is the real part of (5-26). The constraint on the damping factors of the non-target modes is the 5% damping ratio limit:

$$\frac{\sigma_f}{\omega_f} \leq -5\% \qquad \text{for non-target modes.} \tag{5-37}$$

For both tuning objectives, the eigenanalysis of the system shows whether the damping requirements are fulfilled by the PSS tuning. If the optimization constraints are not met, the tuning can be continued for more iterations.

The iterative tuning procedure can be summarized as follows.

I- Set the initial PSSs parameters of (5-18) to zero, $\underline{pa}^0=0$.

At each iteration j (j=1, 2,…):

II- Set the PSSs parameters to $\underline{pa}^{j-1}$, apply the TFEA method to form the reduced $[A(\omega_K)]$, and then apply the QR algorithm to obtain $\underline{\lambda_0}$ and the right and left eigenvectors;

III- From the sensitivity formula in (5-26), the eigenvalue shift $\underline{\Delta\lambda}$ and consequently the objective function are formed.

IV- $\underline{\Delta pa}$ is calculated, fulfilling the objective function and the constraints. The tuning parameters are set as $\underline{pa}^j= \underline{pa}^{j-1}+\underline{\Delta pa}$.

V- Considering $\underline{pa}^j$, new eigenvalues are calculated by the QR algorithm. If the constraints are all satisfied, the search in parameter space is complete. Otherwise, repeat from step II.

VI- The final tuning parameters are $\underline{pa}= \underline{pa}^j$.

5.6 Chapter Summary

This chapter has presented a tool for coordinated tuning of PSS for large power systems. The tool consists of the TFEA method, eigenvalue sensitivity analysis and optimization.

Developed from the TFEA method and the eigenvalue sensitivity method of Chapter 2, the method has formulated $\underline{\Delta\lambda}=f(\underline{\Delta pa})$. The eigenvalue shifts of selected modes are specified in $\underline{\Delta\lambda}$, and the parameters of selected stabilizers are specified in $\underline{\Delta pa}$.

The methodology has been introduced in two steps: PSS gain tuning; and simultaneous PSS gain and time constants tuning. For each type of tuning, two objective functions have been proposed to verify the tuning method. Several test results based on the objective functions are explained in Chapter 6.

Chapter Six

6. Application of TFEA in PSS Tuning: Validation Tests and Discussions

6.1 Overview

This chapter presents the validation tests for the PSS tuning method of Chapter 5. The procedure is performed separately for gain tuning and simultaneous gain and time constants tuning based on the objectives of Chapter 5. The tests are conducted on the 16-generator and 69-generator systems of Chapter 2. All the generators are equipped with the exciter and PSS modeled in Figure 5-1 and the power system operating conditions are the same as in Chapter 2, provided in Appendix C.

6.2 Test Results for PSS Gain Tuning on 69-Generator Test System

The philosophy of PSS gain tuning is that the initial values of the PSSs parameters are known from some prior design. These values are taken from Appendix C for the gains and time constants. In validating the PSS gain tuning of Section 5.5, the benchmark used consists of the eigenvalues of the full state matrix of the 69-generator system.

The [D] matrix of (5-28) is formed to provide the linear relationship between the damping factor shifts $\underline{\Delta\sigma}$ and the perturbation gains $\underline{\Delta K_{ST}}$. According to Table 5-1, two tests are conducted. The numerical results are presented in this section.

Test 1: Achieving desired damping shift

According to (5-30), one can find $\underline{\Delta K_{ST}}$ for a specification of $\underline{\Delta\sigma}$. In this test, desired damping improvement values are assigned to the first five modes and no changes are specified for the other modes, as

$$\underline{\Delta\sigma}_{68\times1} = [-0.06, -0.1, -0.06, -0.08, -0.08, 0, ..., 0]^T \tag{6-1}$$

The test results are shown in Table 6-1. Based on $\underline{K_{ST}}^0$, the original eigenvalues are solved from the full state matrix. The eigenvalues of the 5 target modes are entered in the second column of Table 6-1. From the desired damping improvement of (6-1), $\underline{\Delta K_{ST}}$ is solved from (5-30). The gains ($\underline{K_{ST}}^0+\underline{\Delta K_{ST}}$) are inserted in the full state matrix and new eigenvalues are solved by the QR method. The benchmark damping improvement in the fourth column is the differences of the real parts of the new and original eigenvalues. The close agreement between the desired and benchmark damping improvements validates the application of: (i) eigenvalue sensitivity method and (ii) the generalized inverse method, which to the author's knowledge is seldom used.

Table 6-1: Results of desired damping improvements for 69-generator system.

Mode number	Original eigenvalue	Desired damping improvement from (6-1)	Benchmark damping improvement
1	-0.080±j1.78	-0.06	-0.065
2	-0.198±j2.38	-0.10	-0.11
3	-0.123±j2.91	-0.06	-0.06
4	-0.160±j3.05	-0.08	-0.083
5	-0.172±j4.05	-0.08	-0.078

Test 2: Maximizing damping improvement

Tuning consists of modifying the PSS gains to maximize the damping of a few target modes. According to Section 5.5.1, the minimization objective function is (5-31) with W_j=1,

$$\min\left\{-\sum \Delta\sigma_j^2\right\} \quad j = 1,2,3,4,5 \tag{6-2}$$

and the gain constraints of

$$-15\%\underline{K_{ST}^0} \le \underline{\Delta k_{ST}} \le 15\%\underline{K_{ST}^0}. \tag{6-3}$$

The target modes are j= 1, 2,…,5 which have the lowest frequencies and damping. The constraint of (6-3) is chosen to keep the final PSS gain close to $\underline{K_{ST}}^0$. The problem is solved in MATLAB using a linear optimization algorithm. The tuning is performed for 5 case studies. Cases 1 to 4 differ in the damping constraints placed on the non-target modes.

$$\text{Case 1: } \Delta\sigma_i = 0 \qquad i \neq j \tag{6-4}$$

$$\text{Case 2: } \Delta\sigma_i \leq 30\%\left|\sigma_{i0}\right| \qquad i \neq j \tag{6-5}$$

$$\text{Case 3: } \Delta\sigma_i \leq 0 \qquad i \neq j \tag{6-6}$$

$$\text{Case 4: } \Delta\sigma_i \textit{ free} \qquad i \neq j \tag{6-7}$$

Case 5: The gains of all 69 generators are set to the maximum.

In (6-5), σ_{i0} is the original damping before gain tuning. Table 6-2 summarizes the results of the five case studies. In each case of this table, there is a row for benchmark damping shift and a row for estimated damping shift. They are respectively from eigenanalysis of the full state matrix and $[A(\omega_K)]$ matrix of TFEA, after $\underline{\Delta K_{ST}}$ have been solved by optimization. The results are shown for the five target modes as well as modes 9, 13, 30, 46 and 68, which have been randomly chosen to check if the constraints of (6-4)-(6-7) are fulfilled.

Case 1: The goal is to find the maximum possible damping improvement for the 5 target modes while keeping the damping of other modes unchanged. Table 6-2 shows that there is small improvement in the target modes. This is for the strict constraint of (6-4). The non-target modes, 9, 13, 30, 46 and 68 have no damping change, as required by (6-4). Figure 6-1 shows the results of perturbation gains ΔK_{STn}, plotted against the generator numbering, n=1, 2,…, 69. This figure shows that only 5 gains have reached the maximum limit of 15% and 35 gains have decreased.

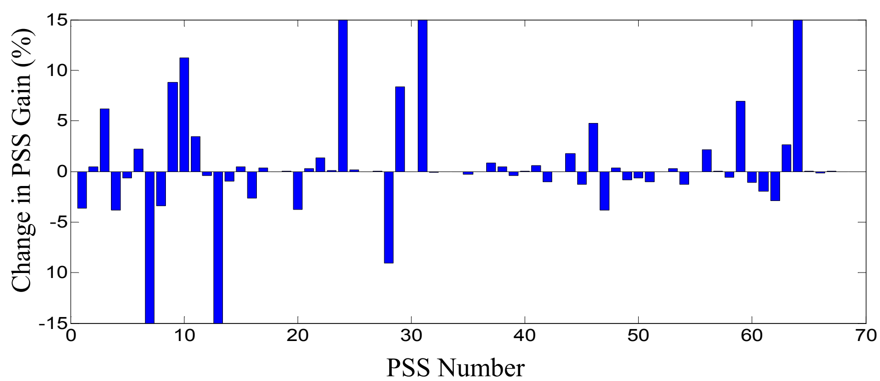

Figure 6-1: Change in PSSs gains from optimization results of Case 1.

Table 6-2: Maximum damping improvement for 69-generator system.

Mode number		1	2	3	4	5	9	13	30	46	68
Original benchmark		-0.08 $\pm j1.78$	-0.20 $\pm j2.38$	-0.12 $\pm j2.90$	-0.165 $\pm j3.05$	-0.17 $\pm j4.05$	-0.08 $\pm j5.59$	-0.25 $\pm j5.85$	-0.87 $\pm j7.25$	-1.26 $\pm j8.15$	-2.21 $\pm j13.49$
Case 1	Benchmark damping shift	-0.03	-0.12	-0.042	-0.011	-0.031	0	0	0	0	0
	Estimated damping shift	-0.028	-0.09	-0.047	-0.009	-0.030	0	0	0	0	0
Case 2	Benchmark damping shift	-0.11	-0.15	-0.09	-0.077	-0.064	0.01	0.03	0	0.004	-0.035
	Estimated damping shift	-0.11	-0.12	-0.086	-0.070	-0.063	0.012	0.006	0	0.003	-0.043
Case 3	Benchmark damping shift	-0.11	-0.15	-0.089	-0.075	-0.062	-0.01	0	0	0	-0.025
	Estimated damping shift	-0.11	-0.12	-0.081	-0.068	-0.062	-0.009	0	0	0	-0.03
Case 4	Benchmark damping shift	-0.12	-0.15	-0.093	-0.08	-0.06	0.013	0.03	0	0.004	-0.04
	Estimated damping shift	-0.11	-0.12	-0.086	-0.07	-0.06	0.014	0.007	0	0.003	-0.05
Case 5	Benchmark damping shift	-0.12	-0.15	-0.09	-0.077	-0.064	0.055	0.08	0	0.004	-0.09
	Estimated damping shift	-0.11	-0.12	-0.088	-0.071	-0.064	0.054	0.04	0	0.004	-0.10

Case 2: In this optimization, the non-target modes are permitted to decrease in their damping by 30%. The relaxation of (6-5) allows damping improvement over Case 1. The damping of 6 modes have deteriorated including modes 9, 13 and 46 as shown in Table 6-2. From Figure 6-2, 41 gains have reached their maximum gain limit while no PSS has its gain decreased.

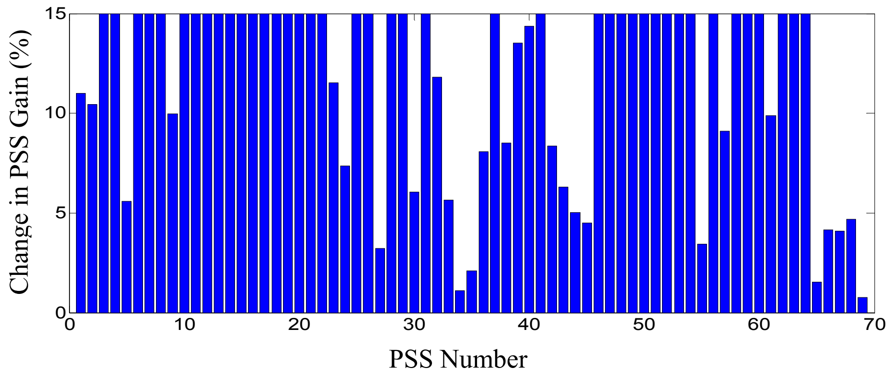

Figure 6-2: Change in PSSs gains from optimization results of Case 2.

Case 3: In this optimization, the damping of non-target modes are allowed to remain unchanged or improve. The results in Table 6-2 for the target modes are very similar to Case 2. However, there is no damping deterioration for any mode. Figure 6-3 shows that 32 gains have reached the maximum gain limit while the gains of 2 PSSs have decreased.

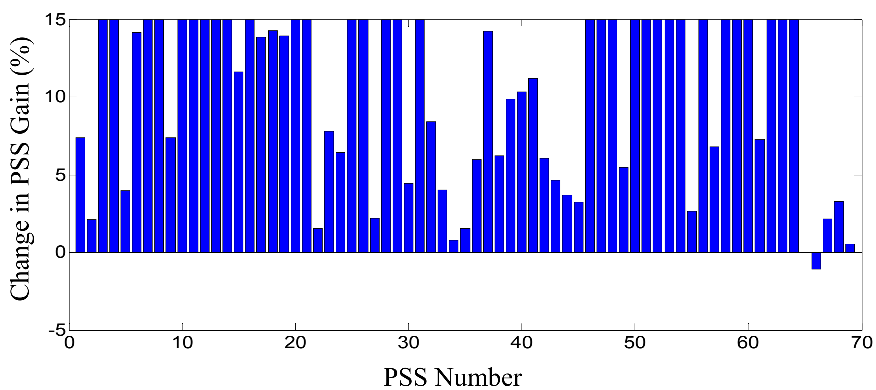

Figure 6-3: Change in PSSs gains from optimization results of Case 3.

Case 4: In this study, there is no constraint placed on the damping shifts of non-target modes. Consequently, some damping deterioration is observed in non-target modes while damping improvements of the target modes are similar to Cases 2 and 3. In this case, 39 gains have reached the maximum limit and no gain has decreased, as shown in Figure 6-4.

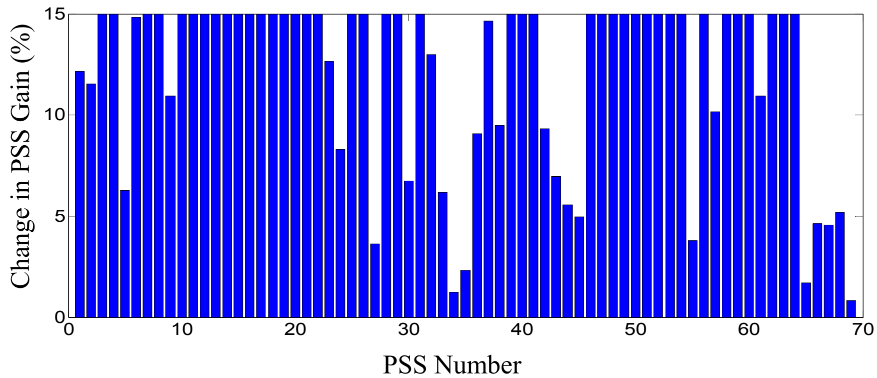

Figure 6-4: Change in PSSs gains from optimization results of Case 4.

Case 5: From examining the gains of 69 PSSs in the four case studies, improvement in damping seems to come from increasing the gains to their maximum limit. To test this, the gains of all the 69 generators are set to the maximum limit. Comparing the results of Case 5 in Table 6-2 with the results of Cases 1 to 4, there is not much difference in damping improvements for the target modes. What is significant is that the damping of modes 9, 13 and 46 are lowered. The deterioration can be from stabilizer interactions as reported in [66]. However, as increasing all the PSSs gains does not improve the damping for all modes, tuning based on optimizing under constraints, such as in Case 3, is a better method.

6.3 Test Results for Simultaneous Tuning of PSSs Gains and Time Constants

The tuning is performed based on the two objective functions of Section 5.5.2. The PSS tuning for each objective is conducted on the 16-generator and 69-generator systems. For each test system the tuning robustness is analysed based on the tuning results. The iterative tuning steps are explained in Section 5.5.2. Unlike PSS gain tuning there is no prior design in this study.

6.3.1 Boundaries for Tuning Parameters

It is found that the optimization algorithm does not converge to a solution when parameter limits are not set. Setting lower and upper bounds on the parameter limits require extensive field experience. Considering the different design covered in [94], the following ranges for the PSSs parameters are chosen:

$$0 < K_{ST} \leq 20 \tag{6-8}$$

$$0.08 \leq T_1 \leq 0.12 \tag{6-9}$$

$$0.01 \leq T_2 \leq 0.04 \tag{6-10}$$

$$0.08 \leq T_3 \leq 0.12 \tag{6-11}$$

$$0.01 \leq T_4 \leq 0.04. \tag{6-12}$$

6.3.2 16-Generator Test System, Objective 1: Minimizing the PSSs Gains

The tuning results of Objective 1, for the 16-generator system, are shown in Table 6-3. The system has 15 electromechanical modes. The tuning procedure is accomplished in two similar iterations. At each iteration an optimization problem is solved to find the PSSs parameters in order to minimize the sum of the gains of (5-32) considering the constraints of (5-33) and the parameters ranges of (6-8)-(6-12). There are three columns under each iteration in Table 6-3. The first column shows the eigenvalue prediction results obtained from TFEA. The second column shows the benchmark results from the QR eigenanalysis of the full state matrix and the third column shows the benchmark damping ratio.

First, it should be noticed that the TFEA results in the first column of each iteration are in very good agreement with the associated benchmark results. To be more precise by comparing the predicted and benchmark results of the second iteration, it is realized that the damping prediction for 8 out of 15 modes has less than 5% error, three modes have approximately 15% error and the maximum error happens for the last mode and it is 18%. For the frequency prediction, on the other hand, the maximum error is limited to 3%.

The next step is to check the damping ratios to see if the design constraint of (5-33) has been achieved. From Iteration 1 of Table 6-3 the damping ratio of 5 modes are below 5%. In Iteration 2, all the modes have a minimum of 5% damping ratio and the tuning procedure is complete. All other modes (rather than electromechanical modes) are carefully observed to be positively damped.

The sum of the gains after Iteration 2 is 92.5, giving an average gain of 5.43. The gains cannot be lowered further because 2 generators in Iteration 2 have damping ratio of 5.1%, close to the constraint of (5-33). The tuning results of the PSSs parameters after Iteration 2 are shown in

Figure 6-5 to Figure 6-9 for the gains and time constants. Figure 6-6 to Figure 6-9 show that the time constants tend to migrate to the boundaries of (6-9)-(6-12). This is discussed in Section 6.4.

Table 6-3: Results of PSS tuning for Objective 1, 16-generator system.

	Iteration 1			Iteration 2		
Mode number	Predicted results after PSS tuning	Benchmark results after PSS tuning	Benchmark damping ratio (%)	Predicted results after PSS tuning	Benchmark results after PSS tuning	Benchmark damping ratio (%)
1	-0.076±*j*1.47	-0.076±*j*1.46	5.2	-0.13±*j*1.46	-0.13±*j*1.45	8.9
2	-0.31±*j*2.95	-0.29±*j*2.95	9.83	-0.40±*j*2.91	-0.37±*j*2.92	12.6
3	-0.17±*j*3.53	-0.15±*j*3.54	4.2	-0.20±*j*3.51	-0.18±*j*3.52	5.1
4	-0.27±*j*4.77	-0.26±*j*4.79	5.4	-0.35±*j*4.73	-0.34±*j*4.74	7.1
5	-0.28±*j*6.90	-0.26±*j*6.91	3.7	-0.40±*j*6.76	-0.39±*j*6.77	5.7
6	-0.53±*j*7.02	-0.47±*j*6.96	6.7	-0.62±*j*7.02	-0.53±*j*6.97	7.6
7	-0.55±*j*7.44	-0.56±*j*7.53	7.4	-1.48±*j*7.17	-1.28±*j*7.16	17.8
8	-0.52±*j*7.68	-0.46±*j*7.69	5.9	-0.57±*j*7.36	-0.58±*j*7.44	7.7
9	-0.41±*j*7.97	-0.37±*j*7.99	4.6	-0.63±*j*7.86	-0.54±*j*7.87	6.8
10	-0.41±*j*8.17	-0.38±*j*8.21	4.6	-0.42±*j*8.17	-0.42±*j*8.21	5.1
11	-1.10±*j*8.44	-1.08±*j*8.72	12.3	-1.12±*j*8.4	-1.07±*j*8.66	12.3
12	-0.91±*j*9.92	-0.93±*j*9.88	9.4	-2.86±*j*9.18	-2.57±*j*9.48	27.1
13	-0.90±*j*9.82	-0.82±*j*10.04	8.1	-1.03±*j*9.36	-1.02±*j*9.55	10.6
14	-1.06±*j*9.37	-1.04±*j*9.58	10.8	-1.41±*j*9.69	-1.34±*j*9.79	13.6
15	-0.54±*j*11.02	-0.46±*j*11.09	4.1	-0.69±*j*10.84	-0.58±*j*10.94	5.3

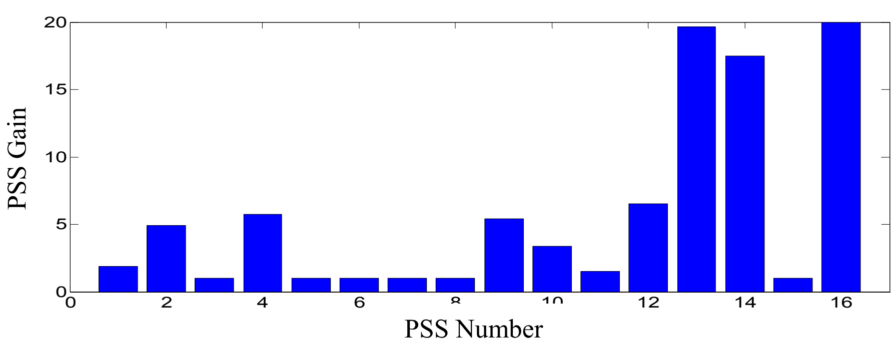

Figure 6-5: Results of PSSs gains: 16-generator system, Objective 1.

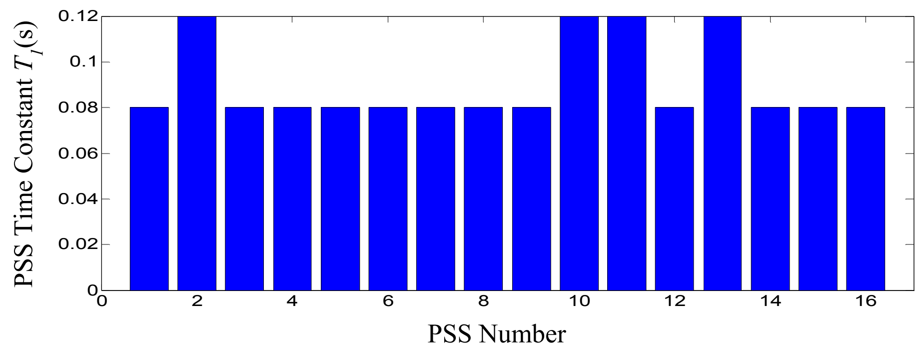

Figure 6-6: Results of PSSs time constants T_1: 16-generator system, Objective 1.

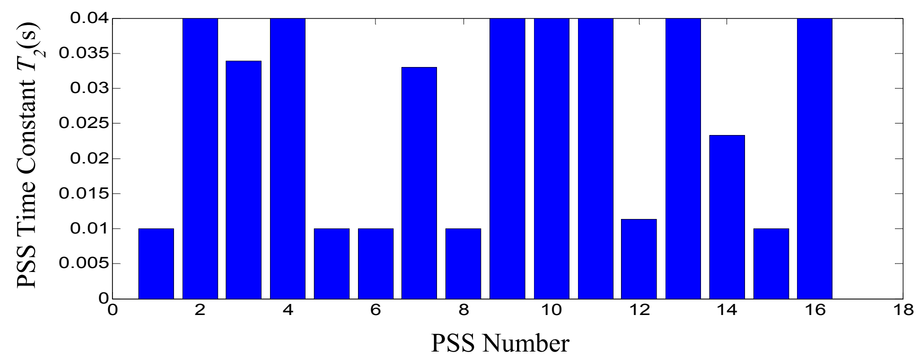

Figure 6-7: Results of PSSs time constants T_2: 16-generator system, Objective 1.

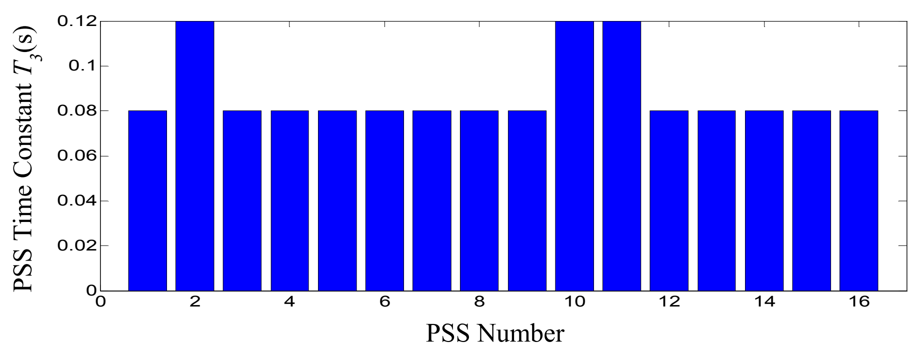

Figure 6-8: Results of PSSs time constants T_3: 16-generator system, Objective 1.

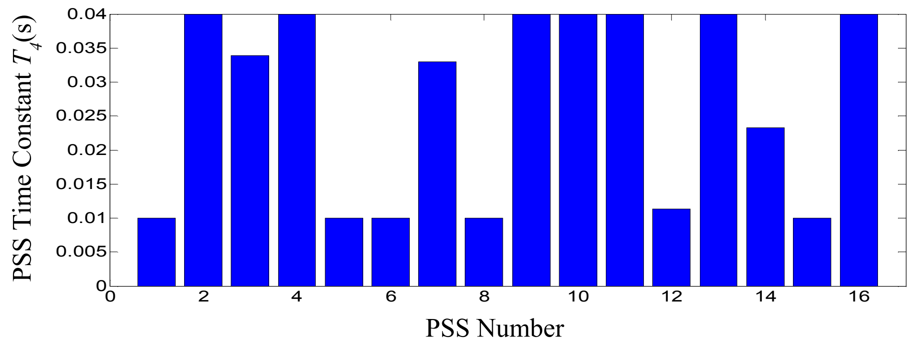

Figure 6-9: Results of PSSs time constants T_4: 16-generator system, Objective 1.

6.3.3 16-Generator Test System, Objective 2: Maximizing Damping Improvement for the Low Frequency Modes

The objective of PSS tuning in this case is to maximize the damping of the low frequency modes. Therefore, the target modes in (5-36) are the first three modes and j=1, 2, 3 with weighting factor W_j=1. The tuning constraints in (5-37) provides a 5% damping ratio for other electromechanical modes. The boundaries for PSSs parameters are in (6-8)-(6-12).

The results are shown in Table 6-4. This table is organized as Table 6-3. Table 6-4 shows the damping ratio of the low frequency modes are significantly larger than those of Table 6-3. Tuning accuracy is obtained by comparing the predicted and benchmark results. From Iteration 2, the damping prediction for 7 modes has less than 5% error and the rest have less than 12% error except for mode 6 which has 17% error. For the frequency prediction, the error is less than 3% except for mode 5 which has an error of 11%. It is seen in Iteration 1 of Table 6-4 that modes 11 and 15 have damping ratios less than 5%. After Iteration 2 all modes have damping ratios over 5%. After the design, all the system modes obtained from the full state matrix are checked to be stable. In this design the sum of the gains after Iterations 1 and 2 are 185 and 188 respectively, which shows a very small change that is sufficient to improve the damping for modes 11 and 15.

Table 6-4: Results of PSS tuning for Objective 2, 16-generator system.

	Iteration 1			Iteration 2		
Mode number	Predicted results after PSS tuning	Benchmark results after PSS tuning	Benchmark damping ratio (%)	Predicted results after PSS tuning	Benchmark results after PSS tuning	Benchmark damping ratio (%)
1	-0.18±*j*1.45	-0.18±*j*1.43	12.5	-0.18±*j*1.45	-0.18±*j*1.43	12.6
2	-0.44±*j*2.90	-0.41±*j*2.91	14.1	-0.44±*j*2.90	-0.41±*j*2.91	14.1
3	-0.55±*j*3.51	-0.49±*j*3.50	14.0	-0.55±*j*3.51	-0.49±*j*3.50	14.0
4	-0.38±*j*4.73	-0.36±*j*4.75	7.5	-0.38±*j*4.73	-0.36±*j*4.75	7.5
5	-3.02±*j*5.98	-3.27±*j*5.36	61.0	-3.02±*j*5.98	-3.27±*j*5.36	61.0
6	-2.25±*j*6.11	-2.03±*j*5.90	34.4	-2.39±*j*6.06	-2.03±*j*5.90	34.4
7	-4.10±*j*6.29	-3.68±*j*6.28	58.5	-4.09±*j*6.29	-3.68±*j*6.28	58.6
8	-3.13±*j*6.27	-2.83±*j*6.55	43.2	-3.03±*j*6.40	-2.83±*j*6.55	43.2
9	-4.03±*j*6.40	-3.86±*j*6.98	55.30	-4.05±*j*6.39	-3.86±*j*6.98	55.3
10	-2.07±*j*7.09	-1.71±*j*7.30	23.4	-1.74±*j*7.31	-1.71±*j*7.30	23.4
11	-0.21±*j*8.23	-0.21±*j*8.23	2.5	-0.45±*j*8.15	-0.44±*j*8.16	5.3
12	-1.47±*j*8.26	-1.47±*j*8.22	17.8	-1.43±*j*8.25	-1.46±*j*8.22	17.7
13	-1.04±*j*8.27	-1.07±*j*8.45	12.6	-1.04±*j*8.28	-1.07±*j*8.47	12.6
14	-2.78±*j*10.29	-2.92±*j*10.55	27.6	-2.78±*j*10.29	-2.93±*j*10.56	27.7
15	-0.50±*j*11.54	-0.46±*j*11.52	3.9	-0.62±*j*11.48	-0.57±*j*11.47	5.0

The PSSs parameters after Iteration 2 are shown in Figure 6-10 to Figure 6-14 for the gains and the time constants. Comparing Figure 6-5 and Figure 6-10, it is clear that the higher gains of Objective 2 lead to higher damping. From Figure 6-11 to Figure 6-14, the time constants tend to migrate to the limits set by (6-9)-(6-12).

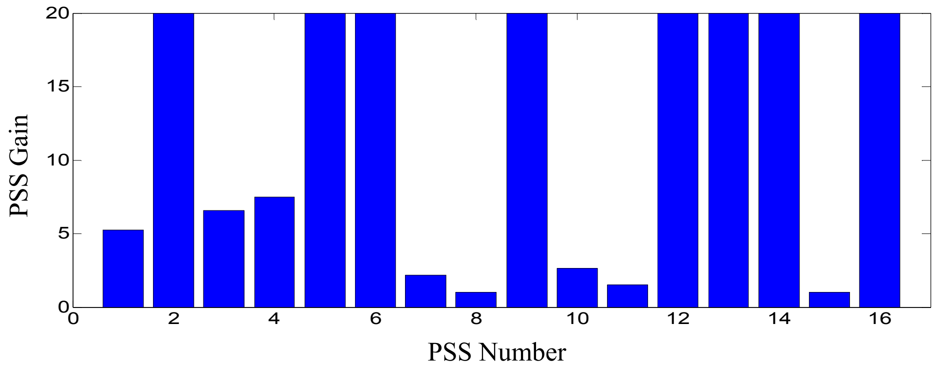

Figure 6-10: Results of PSSs gains: 16-generator system, Objective 2.

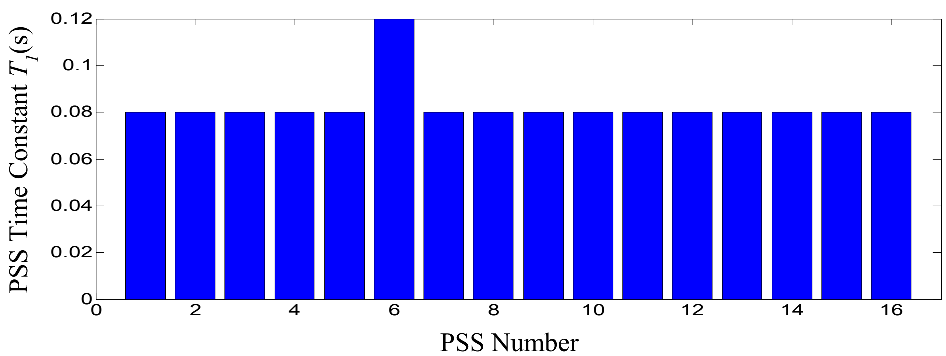

Figure 6-11: Results of PSSs time constants T_1: 16-generator system, Objective 2.

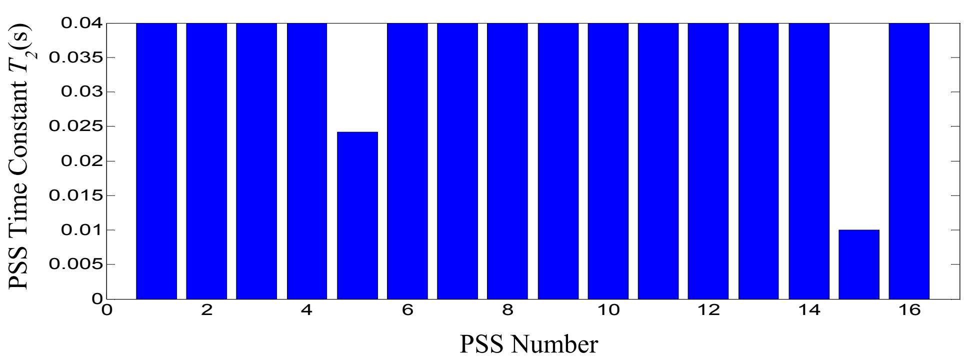

Figure 6-12: Results of PSSs time constants T_2: 16-generator system, Objective 2.

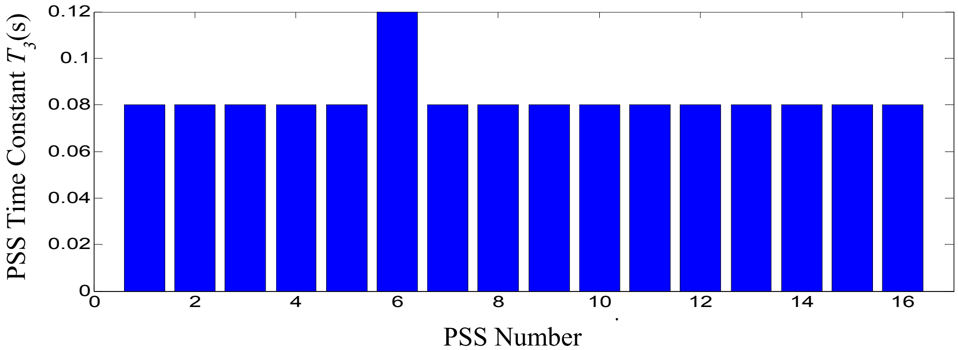

Figure 6-13: Results of PSSs time constants T_3: 16-generator system, Objective 2.

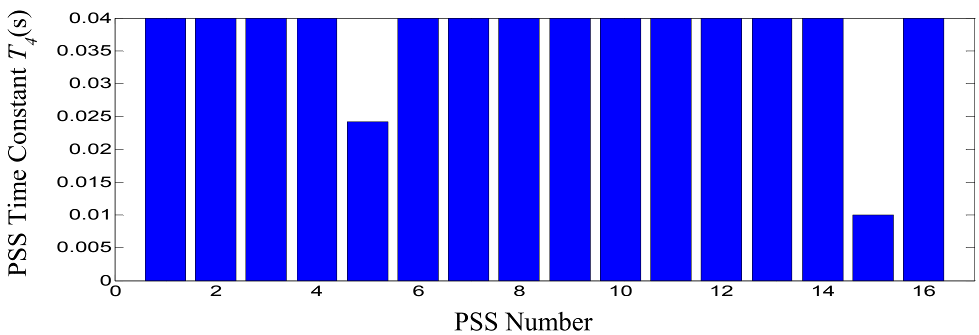

Figure 6-14: Results of PSSs time constants T_4: 16-generator system, Objective 2.

6.3.4 Tuning Robustness for the 16-Generator System

When a power system encounters fault(s) and transmission lines are disconnected, the tuned PSS should ensure that the degraded power system continues to be stable. When a line is disconnected, a new load flow problem is solved to determine the new operating conditions. The test is performed to check the robustness of PSS tuning of Section 6.3.3.

According to [11], the 16-generator system has two regions connected with three lines, simply shown in Figure 6-15. Three fault cases are considered: in Case 1, line 1-2 is disconnected; in Case 2, lines 1-5 is disconnected and in Case 3, both lines are out of service and region 1 and region 2 hold together through line 4-3.

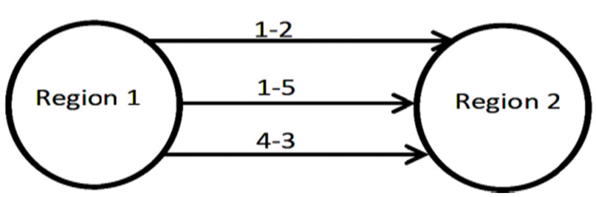

Figure 6-15: Two-region connection for the 16-generator system.

The eigenanalysis results of the three case studies are shown in Table 6-5 for the low frequency modes. As shown in this table, the damping ratios of the lowest frequency modes are over 5%. The other modes are all positively damped.

Table 6-5: Eigenanalysis results under different operating conditions, 16-generator system.

Case 1	Mode	$-0.08\pm j0.86$	$-0.21\pm j2.69$	$-0.40\pm j3.04$
	Damping ratio (%)	9.3	7.8	13.1
Case 2	Mode	$-0.09\pm j0.71$	$-0.23\pm j2.43$	$-0.42\pm j3.02$
	Damping ratio (%)	12.7	9.5	13.9
Case 3	Mode	$-0.13\pm j1.12$	$-0.23\pm j2.02$	$-0.42\pm j2.98$
	Damping ratio (%)	11	11.4	14

6.3.5 69-Generator System, Objective 1: Minimizing the PSSs Gains

The study of Section 6.3.2 for the 16-generator system is repeated for the 69-generator system of [45]. The objective function is minimizing the gains as in (5-32) with the damping ratio constraints of (5-33) and parameters ranges of (6-8)-(6-12). Instead of listing the eigenvalues as in Table 6-3, the locations of 68 eigenvalues in Figure 6-16 summarizes the results of the method. All the eigenvalues lie on or to the left of the red line representing the 5% damping ratio limit. The sum of the gains is 345 as shown in Figure 6-18, which gives an average gain of 5. Similar to the tuning of the 16-generator system, the tuning is completed in two iterations.

In Figure 6-16, there are many plus (predicted) and circle (benchmark) signs which overlap or are close together indicate the results accuracy. Comparing the damping from TFEA and benchmark results, there are 34 modes with less than 5% error and 16 modes with error between 5-10%. Three modes exceed the error of 15%. For the results of oscillation frequency, 39 modes have less than 5% error and the maximum error is limited to 10%. The tuning results for the PSSs parameters after Iteration 2 are shown in Figure 6-18 to Figure 6-22 for the gains and time constants.

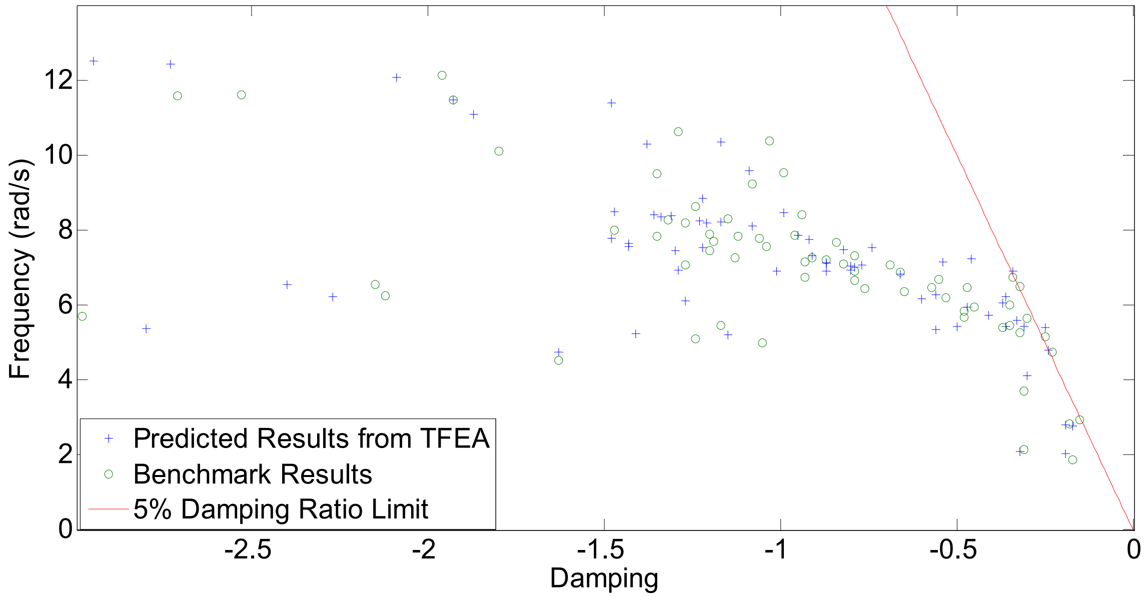

Figure 6-16: Complex plane for the tuning results of Objective 1, 69-generator system.

Figure 6-17 shows the time domain response to a perturbation disturbance. The solid line is $\Delta\omega(t)$ calculated for the generator 44. The two dashed curves are damped responses of the slowest and the fastest modes.

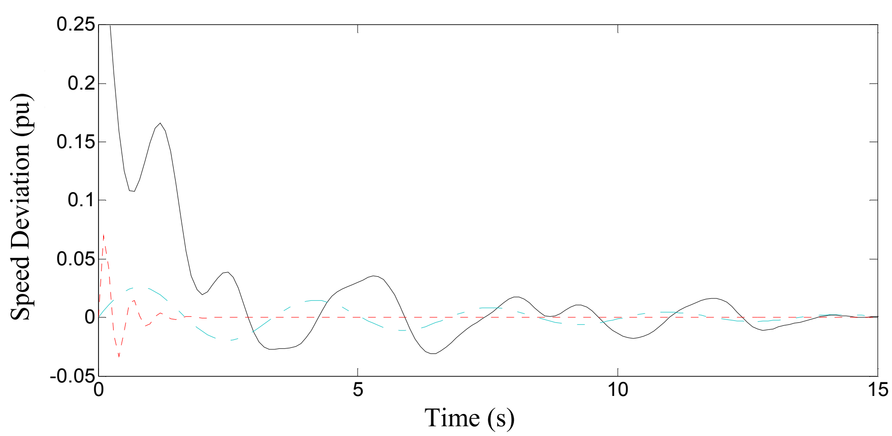

Figure 6-17: Time domain damping of $\Delta\omega_{44}(t)$ after tuning for Objective 1.

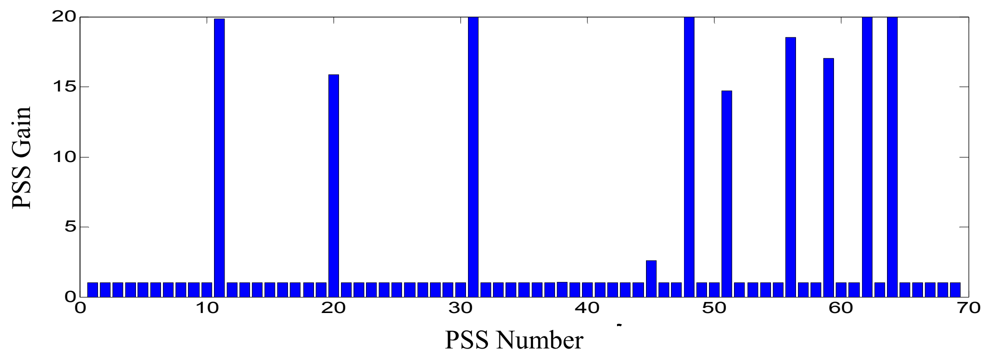

Figure 6-18: Results of PSSs gains: 69-generator system, Objective 1.

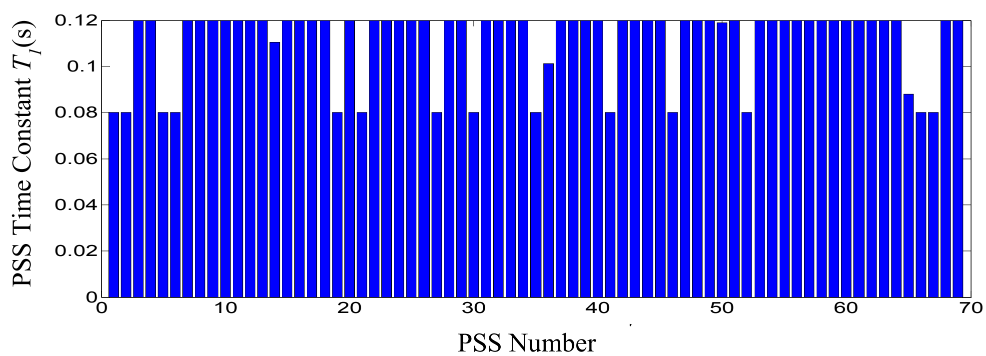

Figure 6-19: Results of PSSs time constants T_1: 69-generator system, Objective 1.

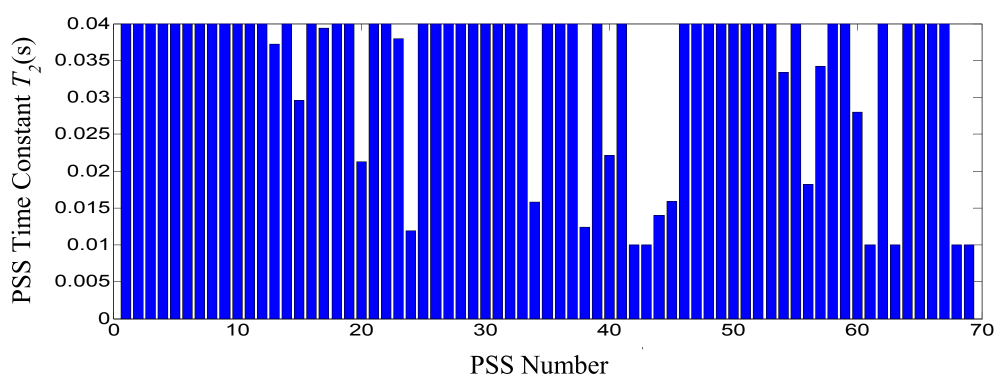

Figure 6-20: Results of PSSs time constants T_2: 69-generator system, Objective 1.

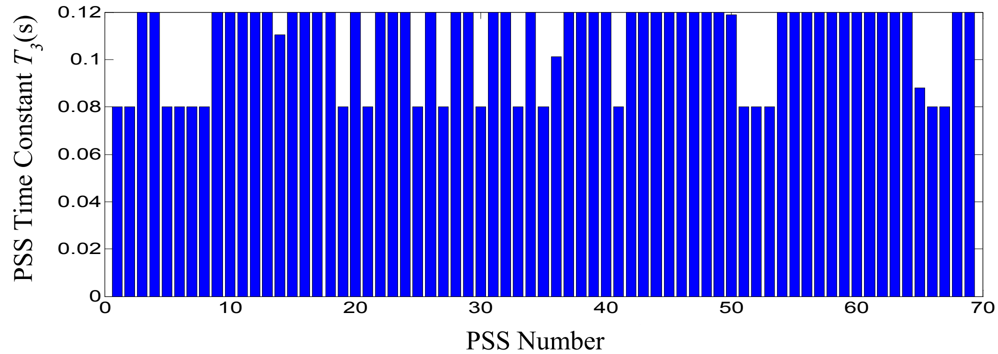

Figure 6-21: Results of PSSs time constants T_3: 69-generator system, Objective 1.

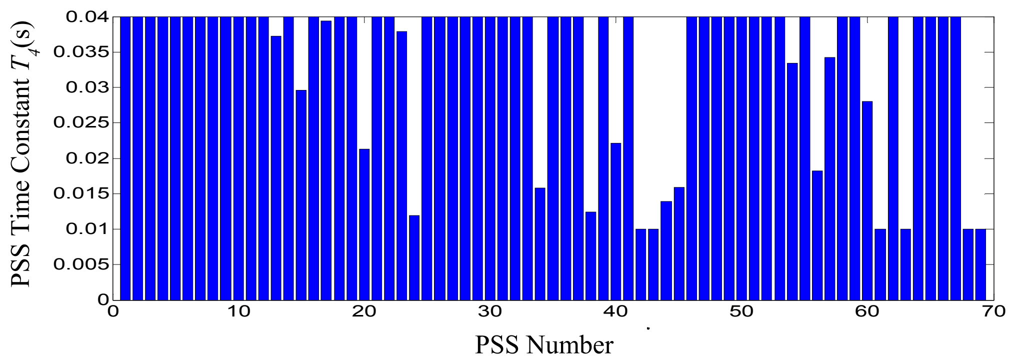

Figure 6-22: Results of PSSs time constants T_4: 69-generator system, Objective 1.

6.3.6 69-Generator System, Objective 2: Maximizing Damping Improvement for the Low Frequency Modes

The study of Section 6.3.3 for the 16-generator system is repeated for the 69-generator system. In the beginning, the first 8 modes are negatively or lightly damped. Therefore the target modes in the objective function of (5-36) are j= 1, 2,…, 8. The weighting functions are W_j=1.

The tuning results are shown in Figure 6-23. Comparison between the x-axis range in Figure 6-16 and Figure 6-23 clearly shows that all 68 eigenvalues have shifted to the left to fulfill (5-36).

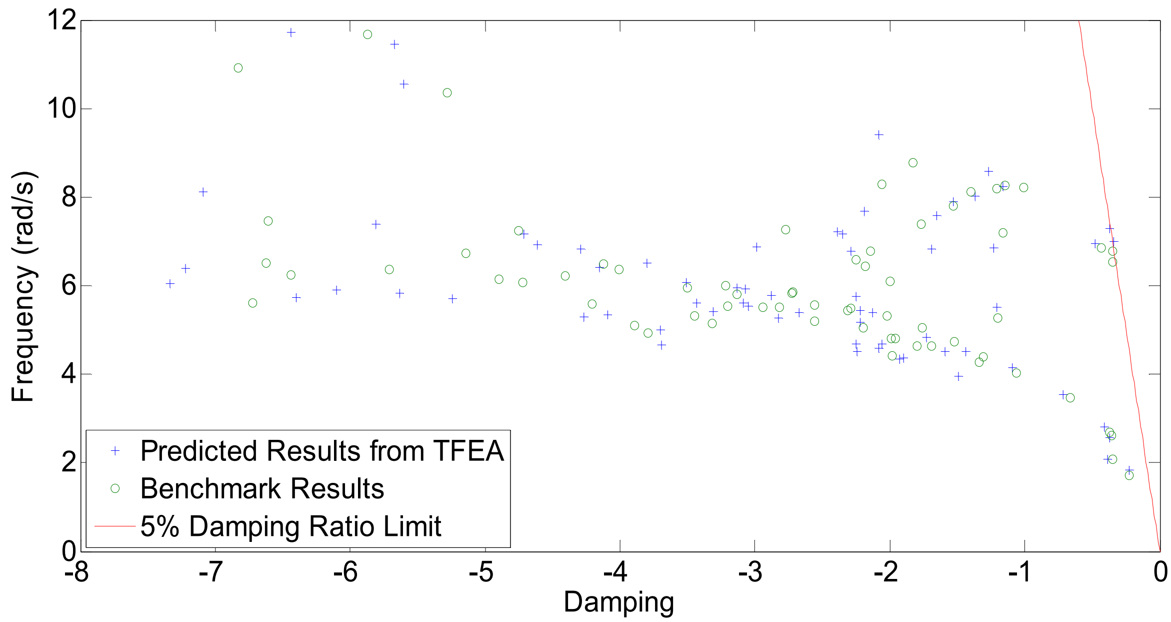

Figure 6-23: Complex plane for the tuning results of Objective 2, 69-generator system.

According to Figure 6-23, the eigenvalues lie on or to the left of the red line representing the 5% constraint of (5-37). On damping prediction by TFEA, 29 modes have less than 5% error, 22 modes have an error between 5-10%. From all the 68 modes, the maximum error does not exceed 15%. Frequency prediction is much better since 43 modes have less than 5% error and the maximum error is limited to 10%. Figure 6-24, which shows the response of generator 44 to perturbation disturbance, confirms that damping has increased compared to Figure 6-17.

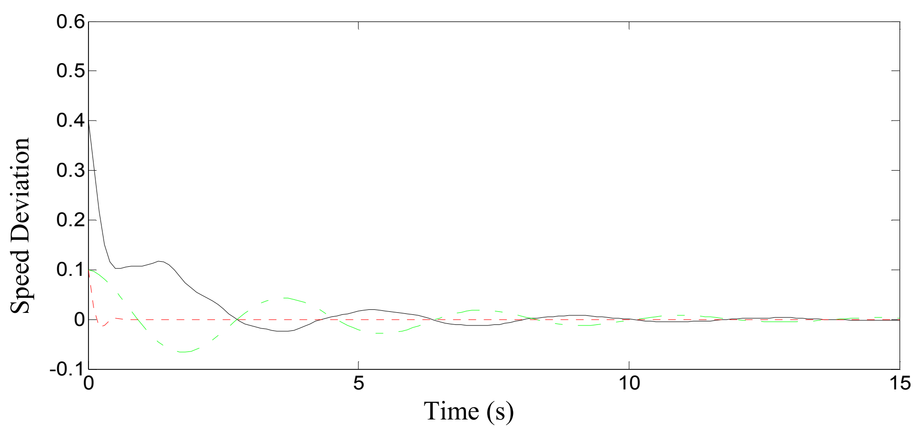

Figure 6-24: Time domain damping of $\Delta\omega_{44}(t)$ after tuning for Objective 2.

The interesting point is that in this case there is no need to do a second iteration because after the first iteration all the 68 modes have a minimum of 5% damping ratio. The sum of the gains is

1222. The average gain is 17.7 compared to the average gain of 5 in Objective 1. The gains of 58 PSSs has reached to the limit of $K_{ST\text{MAX}}$ =20 in (6-8) as shown in Figure 6-25. It can be realized that the extent of the left shift is determined by the gains. The results of the time constants are shown in Figure 6-26 to Figure 6-29.

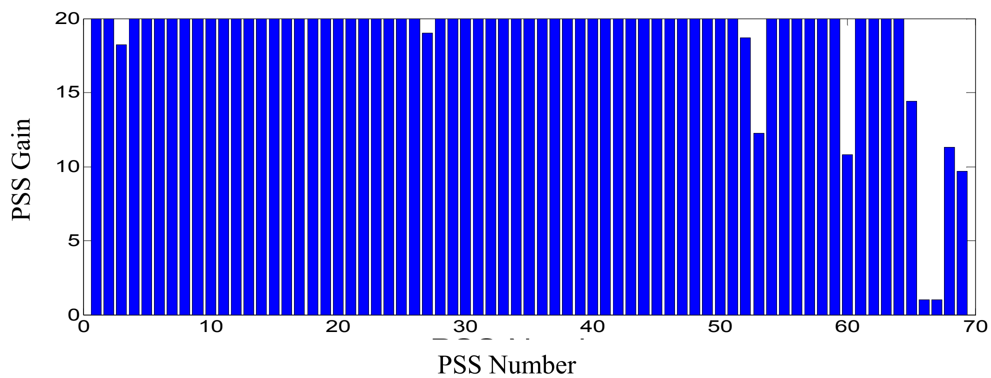

Figure 6-25: Results of PSSs gains: 69-generator system, Objective 2.

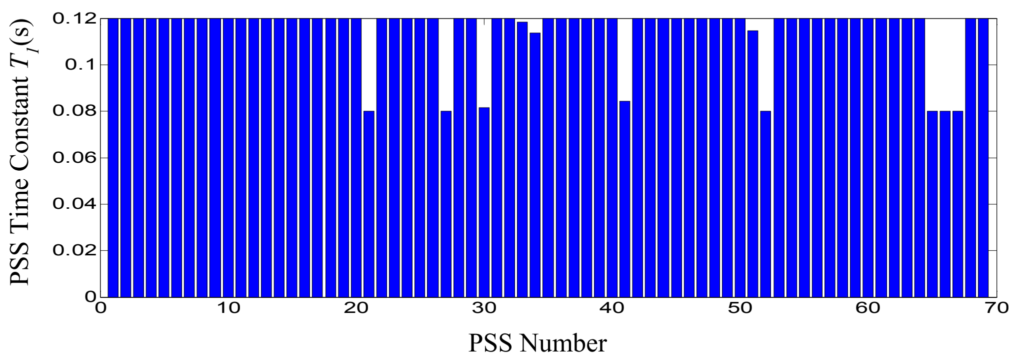

Figure 6-26: Results of PSSs time constants T_1: 69-generator system, Objective 2.

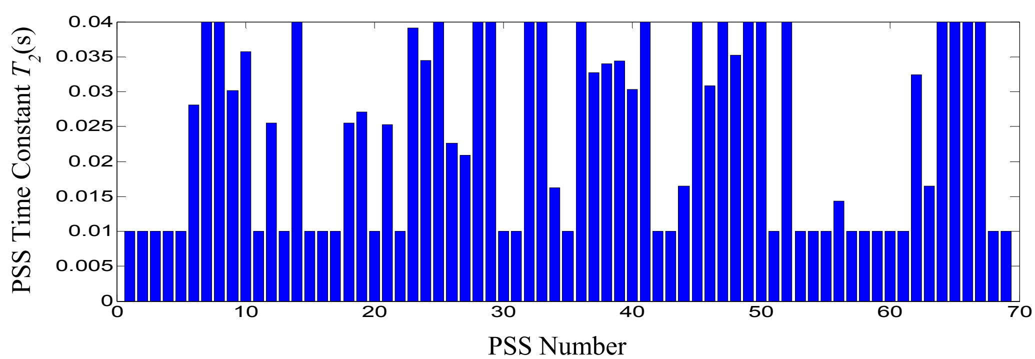

Figure 6-27: Results of PSSs time constants T_2: 69-generator system, Objective 2.

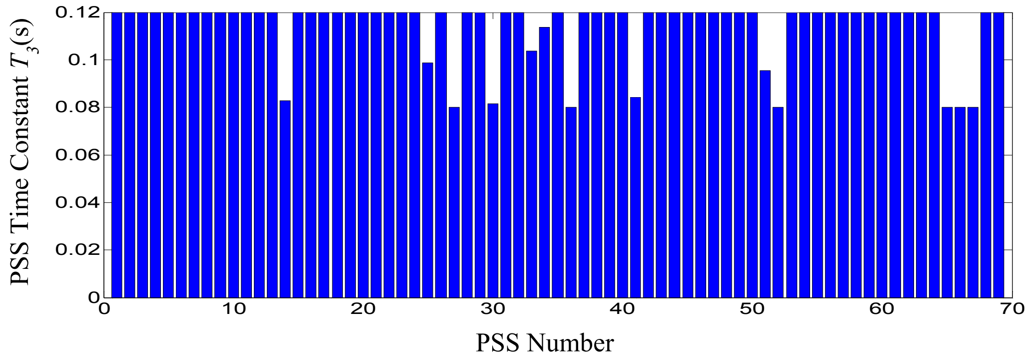

Figure 6-28: Results of PSSs time constants T_3: 69-generator system, Objective 2.

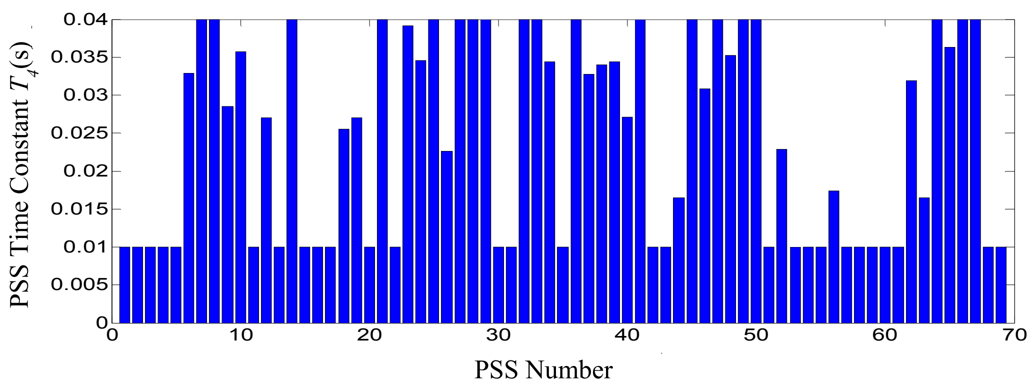

Figure 6-29: Results of PSSs time constants T_4: 69-generator system, Objective 2.

6.3.7 Tuning Robustness for the 69-Generator System

The test is performed to check the robustness of the PSS tuning of Section 6.3.5, for the 69-generator system. An illustrative example based on the 69-generator system is presented here. This system is assumed to be made up of three regions joined by transmission lines as shown in Figure 6-30. Three cases are considered: in Case 1, line 8-1 is disconnected; in Case 2, lines 8-1 and 7-2 are disconnected and in Case 3, lines 8-1, 7-1, 4-15, 5-15 and 6-15 are out of service.

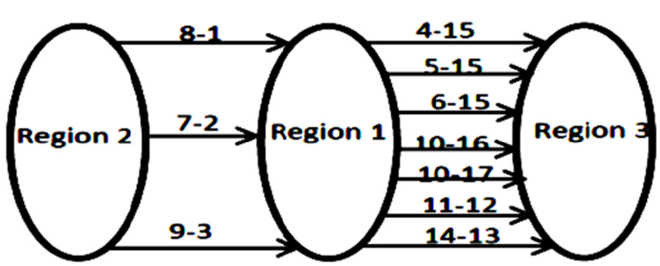

Figure 6-30: Regions connection for the 69-generator system.

The eigenanalysis of the full state matrix is solved after the fault happened in each of the three cases. Some values of the low frequency electromechanical oscillations are listed in Table 6-6. The results of other modes are not shown as they are almost unchanged. Because of topological change, the mode shapes are different from the pre-fault modes. In all the three cases, all the modes are positively damped.

Table 6-6: Eigenanalysis results under different operating conditions, 69-generator system.

Case 1	Mode	$-0.099\pm j1.82$	$-0.28\pm j2.19$	$-0.11\pm j2.89$	$-0.10\pm j2.77$	$-0.22\pm j4.77$
	Damping ratio (%)	5.4	12.7	3.7	3.6	4.6
Case 2	Mode	$-0.13\pm j2.90$	$-0.063\pm j2.1$	$-0.32\pm j2.2$	$-0.5\pm j3.3$	$-0.18\pm j4.7$
	Damping ratio (%)	4.4	3.0	14.3	15.0	3.9
Case 3	Mode	$-0.07\pm j2.14$	$-0.32\pm j2.22$	$-0.12\pm j2.8$	$-0.50\pm j3.39$	$-0.1\pm j4.5$
	Damping ratio (%)	3.2	14.4	4.2	14.7	2.2

6.4 Discussion of the Tuning Results by Optimization

From the results of Figure 6-25, the gains of 58 PSSs reached the limit of $K_{ST\mathrm{MAX}}$=20. In optimization to reach objective function (5-36), the parameters T_1, T_2, T_3 and T_4 seem to migrate to the upper and lower limits set by (6-9)-(6-12). This is illustrated by Figure 6-26 to Figure 6-29. Optimization methods tend to locate their objectives at the parameter limits. But does this tendency yield meaningful tuning? To check on this, the tuned time constants T_1, T_2, T_3 and T_4 of generators 1, 10 and 44 have been selected and listed in Table 6-7.

Table 6-7: Time constants from optimization results of Objective 2.

	$T_1(S)$	$T_2(S)$	$T_3(S)$	$T_4(S)$
Configuration 1 (generator 44)	0.12	0.01	0.12	0.01
Configuration 2 (generator 1)	0.08	0.04	0.08	0.04
Configuration 3 (generator 10)	0.12	0.04	0.12	0.04

Figure 6-31shows a single generator connected to the power system at $\Delta\delta$, the generator angle and at E_t, the stator voltage [11]. In the first instance, the rest of the system is disregarded. This is by holding the generator angle $\Delta\delta$ constant. The objective is to study how the time constants of

Table 6-7 affect the Bode diagrams of $\Delta T_e(s)/\Delta\omega(s)$ of the three generators. The transfer functions of Figure 6-32 to Figure 6-34 begin with the rotor speed deviation $\Delta\omega(s)$ as input, through the PSS, the exciter, the generator electrical dynamics blocks and ends with the electrical torque of the generator $\Delta T_e(s)$ as output. The "generator electrical dynamics" block is taken from [40]. After understanding the role played by individual PSSs to damping, the rest of the system is integrated and Figure 6-36 and Figure 6-37show the differences.

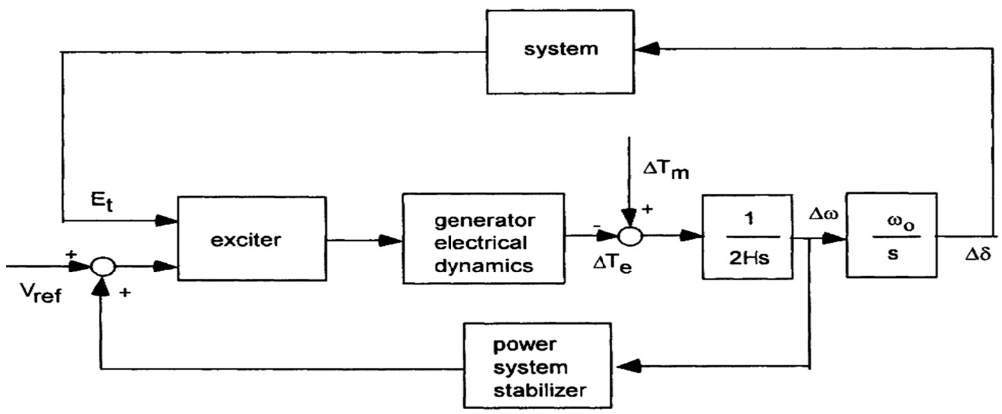

Figure 6-31: Block diagram of generator modeling for dynamic operation [11].

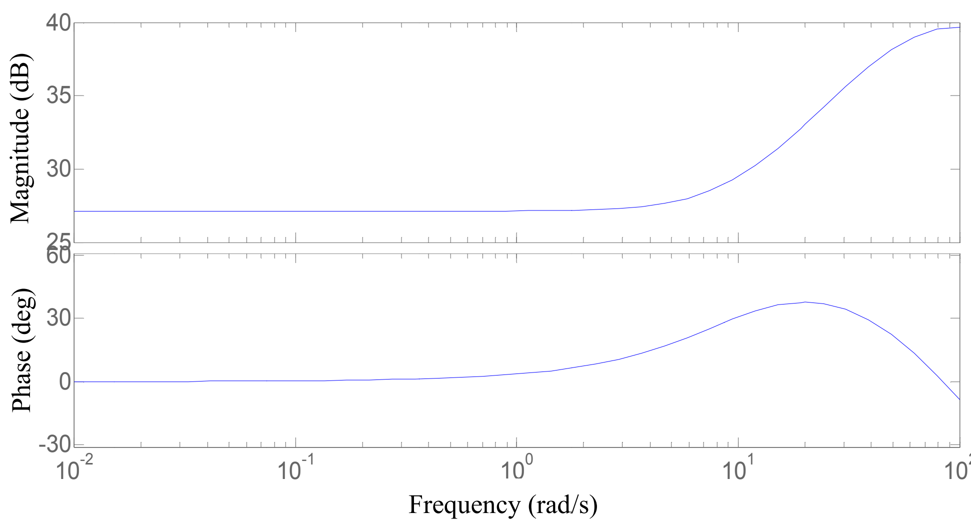

Figure 6-32: Bode diagram of PSS, exciter, generator for Configuration 1.

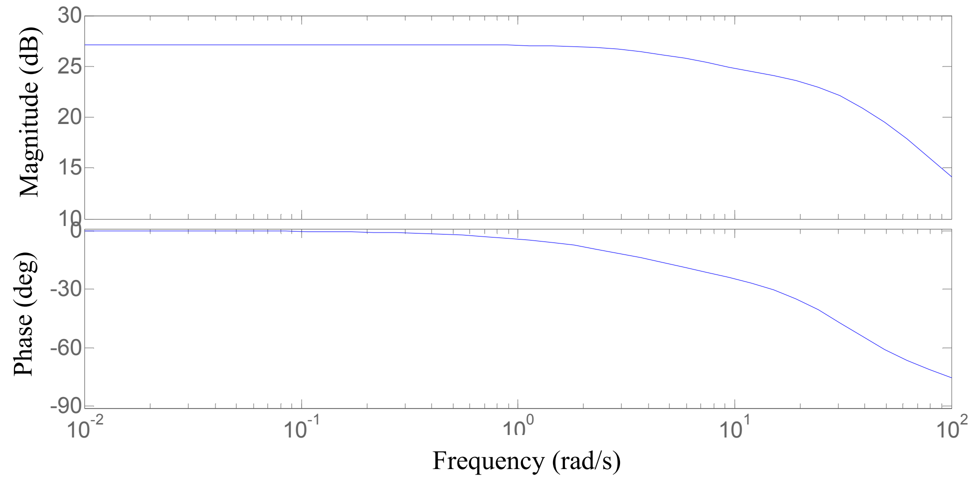

Figure 6-33: Bode diagram of PSS, exciter, generator for Configuration 2.

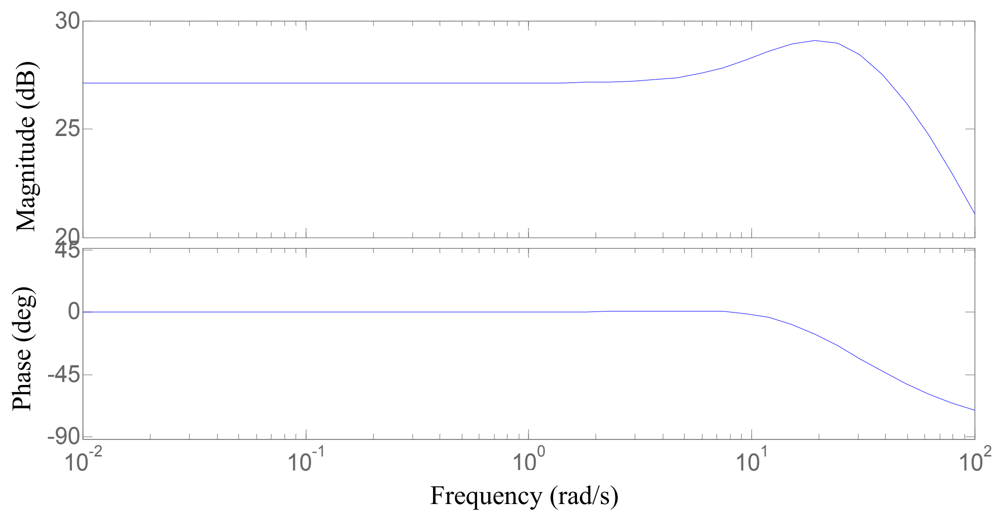

Figure 6-34: Bode diagram of PSS, exciter, generator for Configuration 3.

Although the time constants are chosen by optimization, the Bode diagrams of the three samples show successful phase compensation in the frequency range of interest [2, 11]. This accords with classical design [59] that the choice of the time constants must provide a phase lead in the transfer function of the PSS to compensate for the phase lag in the exciter and generator dynamics. With Bode diagram of Figure 6-34, for a single-generator system of Figure 6-31, the damping torque-vs.-frequency curve takes the form of Figure 6-35.

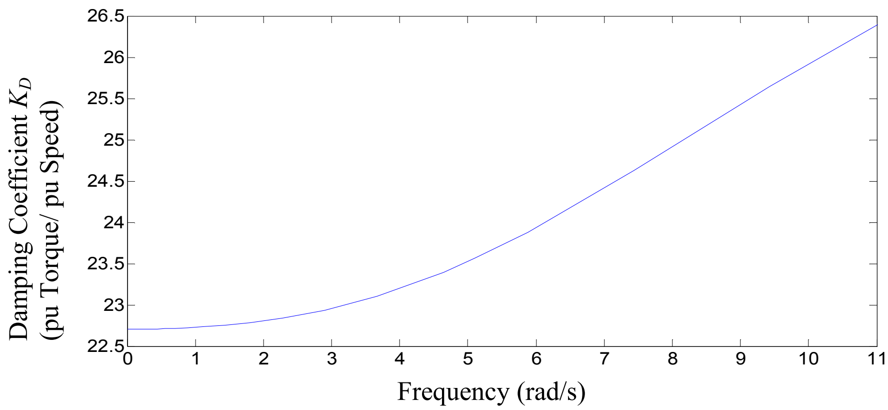

Figure 6-35: Damping torque of a single generator.

The damping torque when the rest of the system is included is more complex. It must take into account the interactions of the other 68 generators of the power system. It is evaluated using the formula from (2-1), which is:

$$\Delta T_{ej}(\omega) = [k_{Dj1}, \ldots, k_{Djj}, \ldots, k_{Djng}][\Delta\omega_1, \ldots, \Delta\omega_j, \ldots, \Delta\omega_{ng}]^T \quad j = 1,\ 2, \ldots,\ ng. \tag{6-13}$$

For a typical generator, such as generator 44 (i.e., j=44 in (6-13)), the damping torque from (6-13) takes the form as shown in Figure 6-36 and Figure 6-37.

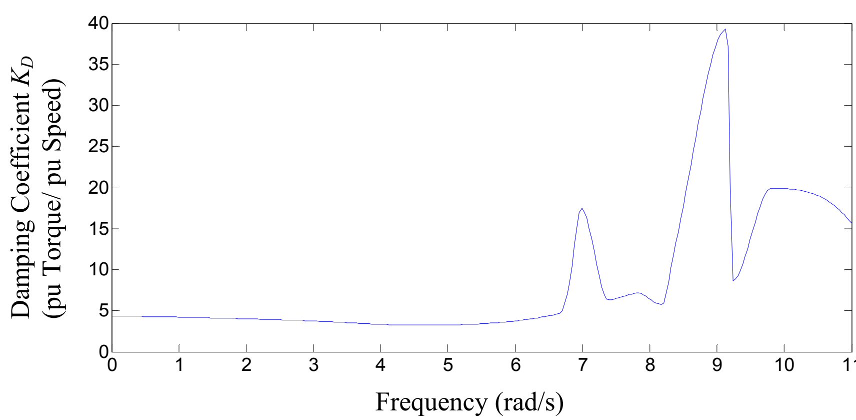

Figure 6-36: Damping torque of generator 44 from Objective 1.

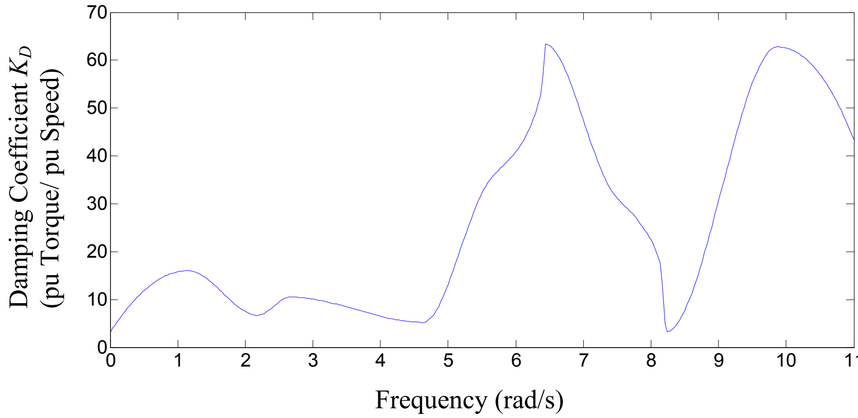

Figure 6-37: Damping torque of generator 44 from Objective 2.

From Figure 6-35 to Figure 6-37, the general trend is that low frequency oscillation has low damping torque. As Objective 2 is optimized to have increased damping in the target modes, Figure 6-37 shows marked increase in damping torque at the low frequency region of the spectrum.

6.5 Computation Time

The computation time for the tuning method is taken by forming (5-26) and by the optimization algorithm. Table 6-8 shows the time components for both test systems. The 3 minutes in Table 6-8 come from forming (5-26) by the TFEA method. The 1.5 minutes are attributed to the optimization algorithm coming from evaluating (5-26) as the PSSs gains and time constants are repeatedly changed by the algorithm to reach the objective function. Table 6-8 shows that the scope for improvement is in organizing the evaluation of (5-26) in a time efficient way.

Table 6-8: CPU time for PSS tuning.

	Forming (5-26) by TFEA	Optimization
16-generator system	3 min	1.5 min
69-generator system	190 min	5 min

6.6 Discussion of Accuracy and Efficiency

Prior to the research of this chapter, reference [76] has been published as a pioneer study in coordinated PSS tuning, and therefore there is interest in making a comparison. As only the two components of eigenvalue sensitivity and optimization package are common with [76], it is hard to compare the efficiency when the TFEA method is the major component of the proposed tuning method. What this thesis has shown is that *any* coordinated PSS tuning can be implemented using the TFEA method. Since TFEA makes PSS tuning computationally efficient, planners are not deterred in using a tuning method even if it requires more iterations to find gains and time constants for which small signal stability is robust.

The tuning method of [76] has the following four major steps.

A- Time constants tuning:

Step 1: The transfer function (time constants) of each PSS is separately designed by the P-Vr method [57, 59].

B- Iterative Gain tuning:

Step 2: Incremental induced torque coefficients (IITC) are obtained [76]. To form the $[IITC(\omega_j)]_{lk,}$ two things are required; participation factors and the transfer function between the reference input of stabilizer l (l= 1, 2,…, ng) and the electrical power output of generator k (k= 1, 2,…,ng) at frequency ω_j *(j= target modes)*.

Step 3: The eigenvalue shifts due to PSSs gains are quantified based on the IITCs of Step 2.

Step 4: An optimization problem is formulated and solved to tune the PSSs gains for a specific damping improvement.

Comparing the method of this thesis with [76], the following conclusions can be made regarding the speed of the method:

- TFEA is fast compared to forming ($ng \times ng \times j$) transfer functions in step 2 of [76].
- The gains and the time constants of the PSSs are obtained simultaneously in the method of this thesis, therefore the tuning is faster.

As to the accuracy, Table 6-9 summarizes the accuracy of the predictions of the tuning results of this thesis and the results of [76]. It should be mentioned that the tuning in [76] has performed on a 29-generator system. According to this table, the accuracy of the predictions of both methods is similar.

Table 6-9: Accuracy comparison between the results of this research and the results of [76].

	Damping	Frequency
Results of Section 6.3.5 and 6.3.6	More than half of the modes have less than 5% error. Maximum error is less than 20%.	Most of the modes have less than 5% error. Maximum error is 10%.
Results of Table 4 in [76]	Most of the modes have less than 10% error. Maximum error is 15%.	Half of the modes have approximately 10% error. Maximum error is approximately 20%.

6.7 Chapter Summary

This chapter has presented the validation test results for the PSS tuning method of Chapter 5. The performance of the tool has been tested in the 16-generator and 69-generator test systems. The test consists of using the reduced matrix from TFEA to tune parameters by optimization. Then the tuned parameters are used to construct the full state matrix whose eigenvalues are the benchmark for comparison. The agreement is strong validation that tuning can be approached from the reduced $[A(\omega_K)]$ matrix of TFEA.

The tests have been performed for PSS gain tuning and simultaneous gain and time constants tuning based on the optimization of objective functions. Design philosophies, operational and strategic planning are evaluated by formulating two objective functions under constraints. Objective 1 consists of minimization the PSSs gains and Objective 2 consists of maximizing the damping of target modes. Tuning of time constants has been achieved using non-linear programming and showed a successful phase compensation for PSS design. Results based on eigenanalysis, transient response and damping torque spectrum have been presented to show that the objectives have been met under constraints. Robustness studies showed that after key transmission lines have been cut, the eigenvalues of degraded system are still on the left side of the complex s-plane.

Chapter Seven

7. Conclusion

7.1 Thesis Summary

7.1.1 New Methodologies for Small Signal Stability Analysis

Power engineers, responsible for the stability of the power grid under their care, apply transient stability analysis, as a matter of course, to ensure that the system returns to stable operating condition after faults are cleared. However, the simulations of transient stability analysis programs are never long enough to assure small signal stability. Small signal stability requires a different research tool. It consists of linearizing the non-linear dynamic equations of power system about the steady-state operating point to obtain a linear [A] matrix. Small signal stability means that all the eigenvalues of [A] lie on the left side of the complex s-plane.

Small signal stability is not widely used because the computations required to evaluate the eigenvalues (typically the QR method) increase roughly by N^3, where N is the dimension of [A]. When the power system has ng generators and each generator has to be modeled by m state variables, $N=m\times ng$. Because power systems have interconnected to take advantage of economy of scale, ng is reaching sizes of 1000 and higher. Including auxiliary equipment such as the exciter and power system stabilizer, each generator has to be modeled by m=11 at least.

This thesis is concerned with making small signal stability analysis practical for large power systems. This is by developing methodologies, such as TFEA. The methodologies are validated in two power system models in which m=11 and ng=16, 69.

7.1.2 TFEA

Transfer Function and Eigenfunction Analysis (TFEA) method, is the centerpiece of the thesis. It reduces computation time by reducing the size of the matrix from ($m \times ng$) in the full state matrix to $2ng$ in the reduced matrix of $[A(\omega_K)]$. Instead of m state-variables, each generator is represented by two mechanical state variables: the perturbation rotor angle and the perturbation rotor speed. This recognizes that eigenvalues closest to the y-axis (lowest damping) are the electromechanical modes. The other (m-2) state variables are embedded in transfer functions, making the reduced state matrix frequency dependent.

7.1.3 Eigenvalue Sensitivity Formula

The second methodology is the eigenvalue sensitivity formula which is exploited in two situations: (i) to improve the accuracy of TFEA; (ii) to relate the eigenvalue shifts to the tuning parameters (gains and time constants), for PSS tuning.

7.1.4 Efficient Improvement of TFEA Accuracy

For ng generators, there are (ng-1) oscillatory modes with angular frequencies ω_n, n= 1, 2,…, (ng-1). If the eigenvalues of $[A(\omega_n)]_{2ng\times 2ng}$ is evaluated at angular frequencies ω_n, the n^{th} mode would be accurately represented. There are two problems here: First, a priori one does not know what value to use for ω_n. Second, (ng-1) eigenvalue evaluations is very expensive.

In the interest of lowering the cost, the eigenvalues and eigenvectors of matrix $[A(\omega_K)]$ are evaluated for one or few representative frequencies ω_K. Using the right and left eigenvectors in the eigenvalue sensitivity formula, improved accuracy is economically obtained by treating (ω_n-ω_K) as a parameter to be corrected.

7.1.5 Curve Fitting Interpolation

It is shown that the cost of forming $[A(\omega_n)]$, used in the eigenvalue correction, can be improved by applying the curve fitting interpolation. The improvement in computation is very significant and there is no effect on accuracy.

7.1.6 Modified Arnoldi Method (MAM)

Although TFEA is a computation time-saver method, $[A(\omega)]$ is a large matrix when ng is large. As MAM is used with confidence in finding a close cluster of eigenvalues of very large matrices, it has been shown that it can predict the selected eigenvalues of $[A(\omega)]$ accurately.

7.1.7 Tuning of PSS Parameters

The eigenvalue sensitivity formula relates perturbation of eigenvalues to perturbation parameters of the reduced state matrix. This opens up the ability to use parameters of all the PSSs of power system to tune the damping of selected modes. The thesis developed the tuning method by optimization under Constraints.

7.1.8 Optimization under Constraints

This thesis shows that software packages such as MATLAB has optimization tools which are available for adoption and adaptation for simultaneous tuning of the PSSs of large power systems. Strategic and operational planning proposals can be evaluated by formulating them as objective functions to be optimized under constraints. Examples, which the optimization method has evaluated, are:

(a) The possibility of increasing the damping of target modes under different conditions such as relaxing the damping of heavily damped modes or maintaining a damping ratio limit.

(b) The possibility of minimizing the PSSs gains while maintaining a damping ratio limit.

The thesis shows that a combination of TFEA, eigenvalues sensitivity, and optimization makes a promising tool for PSS tuning. The feasibility of the method has been validated by examples in 16-generator and 69-generator test systems.

While the objectives of this thesis are mainly to develop tools which can predict and tune the electromechanical modes of large power systems, experience in optimization has uncovered the following:

1. The time constants of the PSS successfully compensate the generator phase lag. This observation comes from detailed analysis of Section 6.4. This comes as a surprise mainly because the time constants are reached by optimization of a power system consisting of 69 generators.

2. The gain of the PSS plays an important role in increasing the damping of the modes.

7.2 Thesis Contributions

With the explanation in Section 7.1 the research contribution is summarized in the following items.

1. Presenting a frequency-dependent method for an efficient eigenanalysis of electromechanical oscillations. The method is called Transfer Function and Eigenfunction Analysis (TFEA) method.
2. The method combines the electrical and mechanical equations of generators and power system network equations. No approximation is considered as all the information of power system elements are embedded as transfer functions.
3. The method uses the eigenvalue sensitivity formula for more accurate eigenanalysis.
4. Selective and limited eigenanalysis performed by applying the Modified Arnoldi Method to the TFEA method.
5. A Coordinated PSS tuning has been analysed by using the three tools of TFEA, eigenvalues sensitivity and optimization algorithms.
6. Numerical tests conducted on three test systems including 4-generator, 16-generator and 69-generator systems. The 69-generator system is considered large enough for educational purposes.

7.3 Future Work

Assuring small signal stability for large power systems is a wide research area for further studies. The advance of fast computational technologies such as parallel computation is hindered by the lack of parallel eigenanalysis methods. Until such a breakthrough comes to pass, some opportunities for further research consist of improving the methodologies developed in this thesis or filling gaps which have not been covered.

7.3.1 Improving the Power System Model in TFEA

The power system and generator models should be improved by:

- Considering different power system elements such as FACTS devices and non-constant current loads.
- Considering the model of turbine/governor for damping the very low frequency modes.

7.3.2 Improving the Efficiency of Accurate Eigenanalysis Methods

Similar to the research of Chapter 4, the TFEA method could be combined with more accurate eigenanalysis methods. The TFEA results could be used as initial guess for the AESOPS and Power Iterations methods to analyse the improvement in convergence and efficiency of the these methods.

7.3.3 Improving the Efficiency of TFEA

The TFEA method can be modified to improve the computation speed up without loss in accuracy by:

- Mathematically proving that the curve fitting interpolation method of Chapter 3 is robust and showing that the synchronizing and damping torque coefficients are continuous functions of frequency.
- Presenting alternative and more effective methods rather than curve fitting interpolation.
- A complete study on the choice of representative frequency.

7.3.4 Improving the Robustness of PSS tuning

More investigation is needed on the robustness of PSS tuning using non-linear programming, specifically for the time constants tuning.

Appendix A: Associated Publications

A.1 Journal Articles

- R. Jalayer, B.T. Ooi, "Estimation of Electromechanical Modes of Power Systems by Transfer Function and Eigenfunction Analysis", *IEEE Transaction on Power Systems*, vol. 28, issue 1, pp. 181-189, Feb 2013.

- R. Jalayer, B.T. Ooi, "Co-ordinated PSS tuning of large power systems by combining Transfer Function-Eigenfunction Analysis (TFEA), Optimization and Eigenvalue Sensitivity" , *IEEE Transaction on Power Systems*, vol. pp, issue 99, pp. 1-9, 2014.

A.2 Conference Proceedings

- R. Jalayer, B.T. Ooi, "Frequency dependant estimation of damping and synchronizing torque coefficients in power systems", in IEEE PES *General Meeting*, San Diego, July 2012.

- R. Jalayer, B.T. Ooi,"Efficient Estimation of Electromechanical Modes by Applying Modified Arnoldi Method (MAM) to Transfer Function and Eigenfunction Analysis (TFEA) Method", in IEEE PES *General Meeting*, Vancouver, July 2013**.**

Appendix B: Computation of the Elements of $A''(s)$ of Section 2.6

From (2-42)-(2-66), for each generator n (n=1, 2,…, ng),

$$\underline{\Delta i}_{kdqn} = A_{kdqn}(s)\underline{\Delta i}_{dqn} + B_{kdqn}(s)\Delta\omega_{rn} \tag{B-1}$$

$$\Delta i_{fdn} = A_{fdn}(s)\underline{\Delta i}_{dqn} + B_{fdn}(s)\Delta\omega_{rn} \tag{B-2}$$

where

$$A_{kdqn}(s) = -\left[g_{33n}^{(1)}\right]^{-1}\left(\left[g_{31n}^{(1)}\right] + \left[g_{32n}^{(1)}\right]A_{fdn}(s)\right) \tag{B-3}$$

$$B_{kdqn}(s) = -\left[g_{33n}^{(1)}\right]^{-1}\left[g_{32n}^{(1)}\right]B_{fdn}(s) \tag{B-4}$$

$$A_{fdn}(s) = \left[g_{22n}^{(2)}\right]^{-1}\left(G_{exc}[A_n(s)]^{-1} - \left[g_{21n}^{(2)}\right]\right) \tag{B-5}$$

$$B_{fdn}(s) = \left[g_{22n}^{(2)}\right]^{-1}\left(G_{pss} - G_{exc}[A_n(s)]^{-1}[B_n(s)]\right) \tag{B-6}$$

Replacing $\underline{\Delta i}_{dqn}$ with $\underline{\Delta i}_{RIn}$ by (2-82), $\underline{\Delta i}_n$ can be found as below,

$$\underline{\Delta i}_n = \begin{bmatrix} \underline{\Delta i}_{dqn} \\ \Delta i_{fdn} \\ \underline{\Delta i}_{kdqn} \end{bmatrix} = \begin{bmatrix} I_{2\times 2} \\ A_{fdn}(s) \\ A_{kdqn}(s) \end{bmatrix}[C(\delta_n)]^T\underline{\Delta i}_{RIn} + \begin{bmatrix} \frac{\omega_0}{s}[C(\delta_n)]\underline{i}_{RI0n} \\ B_{fdn}(s) + A_{fdn}(s)\frac{\omega_0}{s}[C(\delta_n)]\underline{i}_{0RIn} \\ B_{kdqn}(s) + A_{kdqn}(s)\frac{\omega_0}{s}[C(\delta_n)]\underline{i}_{0RIn} \end{bmatrix}\Delta\omega_{rn} \tag{B-7}$$

where Δi_{RIn} can be found in terms of $\underline{\Delta\omega}_r$.

$$\underline{\Delta i}_{RIn} = \left[a_{total}^T(2n-1) \quad a_{total}^T(2n)\right]^T \underline{\Delta\omega}_r \tag{B-8}$$

where $a_{total}(j)$ is the j^{th} row of $[A_{total}]$, and $[A_{total}]$ is defined in (2-105), as

$$[A_{total}(s)]_{2ng\times ng} = \left(\left[I_{2n_g\times 2n_g}\right] - \left[A'_{full}(s)\right][D]\right)^{-1}\left[B'_{full}(s)\right] \tag{B-9}$$

Therefore, $\underline{\Delta i}_n$ would be

$$\underline{\Delta i}_n = \begin{bmatrix} \underline{\Delta i}_{dqn} \\ \Delta i_{fdn} \\ \underline{\Delta i}_{kdqn} \end{bmatrix} = \begin{bmatrix} I_{2\times 2} \\ A_{fdn}(s) \\ A_{kdqn}(s) \end{bmatrix} [C(\delta_n)]^T \left[a^T_{total,(2n-1)} \; a^T_{total,(2n)} \right]^T \underline{\Delta \omega}_r + \begin{bmatrix} \frac{\omega_0}{s}[C(\delta_n)]\underline{i}_{0RIn} \\ B_{fdn}(s) + A_{fdn}(s)\frac{\omega_0}{s}[C(\delta_n)]\underline{i}_{0RIn} \\ B_{kdqn}(s) + A_{kdqn}(s)\frac{\omega_0}{s}[C(\delta_n)]\underline{i}_{0RIn} \end{bmatrix} \Delta \omega_{rn}$$

(B-10)

Back to (2-107), ΔT_{en} is a function of $\underline{\Delta i}_n$, and can be found as,

$$\Delta T_{en} = a_n^{"}(s)\underline{\Delta \omega_r} \qquad \text{(B-11)}$$

where $a_n^{"}(s)$ forms the n^{th} row of $A^{"}(s)$ in (2-110).

Appendix C

C.1 Operating Conditions for 4-Generator System

Table C-1: Operating conditions for 4-generator system.

Generator number	id_0	iq_0	ed_0	eq_0	δ_0 (deg)
1	0.3261	-0.0913	1.0000	0	25.6085
2	0.7685	-0.3468	1.0100	-0.0047	39.0863
3	0.8020	-0.1204	1.0042	0.2290	52.7424
4	0.7935	-0.4545	1.0088	0.0500	38.0890

Table C-2: Exciter and PSS parameters for 4-generator system.

K_A	$T_R(s)$	K_{ST}	$T_w(s)$	$T_1(s)$	$T_2(s)$
400	0.02	10	10	0.08	0.02

C.2 Operating Conditions for 16-Generator System

Table C-3: Operating conditions for 16-generator system.

Generator number	id_0	iq_0	ed_0	eq_0	δ_0 (deg)
1	0.9688	-0.3014	0.9762	0.3729	53.7662
2	0.7244	0.0817	0.8955	0.3981	65.3428
3	0.8396	0.1694	0.8788	0.4404	72.5651
4	0.7234	0.3312	0.8656	0.4947	81.0879
5	0.7213	0.1679	0.8880	0.4832	70.4692
6	0.7688	0.1704	0.8872	0.5615	72.3557
7	0.6769	0.1792	0.8739	0.6052	72.9770
8	0.6065	0.2528	0.9196	0.4639	72.4411
9	0.6799	0.3852	0.8655	0.5492	83.7539
10	0.3978	0.1200	0.9251	0.4054	48.9238
11	0.5831	0.2291	0.9033	0.4291	70.5751
12	0.7237	-0.1126	1.0048	0.1479	48.9594
13	0.2266	-0.0815	1.0110	0	18.8760
14	0.0998	0.1491	0.4696	0.8829	78.6641
15	0.0626	0.0784	0.5600	0.8285	65.6276
16	0.2386	0.2821	0.5006	0.8657	88.9070

Table C-4: Exciter and PSS parameters for 16-generator system.

K_A	$T_R(s)$	K_{ST}	$T_w(s)$	$T_1(s)$	$T_2(s)$
400	0.02	10	10	0.08	0.02

C.3 Operating Conditions for 69-Generator System

Table C-5: Operating conditions for 69-generator system.

Generator number	id_0	iq_0	ed_0	eq_0	δ_0 (deg)	Generator Number	id_0	iq_0	ed_0	eq_0	δ_0 (deg)
1	-0.0328	-0.6558	1.0146	0.0378	-0.5571	35	0.4875	-0.4547	0.9212	-0.3892	14.7170
2	-0.0477	-0.6515	1.0203	0.0221	-1.6645	36	0.3419	-0.5350	0.9623	-0.4201	5.0416
3	-0.0777	-0.6614	1.0000	-0.0453	-4.8479	37	0.2373	-0.6230	0.8858	-0.4641	2.0192
4	-0.2126	-0.6624	0.9125	-0.2928	-17.8546	38	0.6030	-0.2175	1.0081	-0.2556	36.9220
5	-0.3179	-0.6148	0.8556	-0.4424	-27.4055	39	0.4208	-0.5171	0.8962	-0.4436	14.1295
6	0.5086	-0.4054	0.9755	-0.3148	18.4485	40	0.6133	-0.2324	0.9775	-0.2788	36.8655
7	0.5749	-0.2666	1.0374	-0.1749	28.4929	41	0.1241	-0.6483	0.9407	-0.3676	-1.9536
8	0.6127	-0.1620	1.0452	-0.1194	35.1557	42	0.6554	-0.1222	0.9597	-0.2812	44.7247
9	0.6659	-0.0312	0.9670	-0.2547	41.0443	43	0.6121	-0.1689	1.0046	-0.3054	38.4228
10	0.5730	-0.3537	0.9266	-0.3485	22.4751	44	0.5415	-0.3969	0.9450	-0.3049	20.9869
11	0.5878	-0.2504	1.0406	0.0783	39.7346	45	0.4109	-0.5166	0.9514	-0.3390	11.2444
12	0.4588	-0.4625	0.9919	-0.2516	19.7183	46	0.6186	-0.1413	1.0323	0.1960	44.5936
13	-0.2157	-0.6236	0.9548	-0.3302	-19.1409	47	0.6345	0.0018	1.0263	0.2252	52.0901
14	-0.4454	-0.4483	1.0475	-0.1252	-28.0345	48	0.6442	0.0449	1.0037	0.2411	55.4630
15	0.6158	-0.1522	1.0510	-0.0049	38.7069	49	0.6549	-0.0539	1.0110	0.0837	47.5721
16	0.6291	-0.1115	1.0411	0.0708	43.0193	50	0.6298	-0.0770	1.0302	0.2068	47.9158
17	0.5720	-0.2716	1.0503	0.0726	34.7878	51	0.3270	-0.5437	1.0309	-0.2032	10.5697
18	0.5946	0.2177	1.0426	0.1465	61.0278	52	0.6280	-0.0904	1.0448	0.1112	45.2582
19	0.5742	-0.2366	1.0694	0.0936	36.5768	53	0.6402	0.0995	1.0053	0.2196	58.2993
20	0.6089	0.1722	1.0418	0.1569	67.5614	54	0.6275	-0.0966	1.0489	0.0481	42.8016
21	0.6385	0.0209	1.0290	0.1735	56.6588	55	0.5301	-0.3884	0.9844	-0.2452	21.9056
22	-0.0569	0.6899	0.9597	0.0791	4.3821	56	0.6253	-0.1079	1.0507	0	40.9632
23	0.7174	0.0159	0.9290	0.0013	53.4707	57	0.6306	-0.2232	0.9896	-0.1188	41.5765
24	-0.1229	-0.6670	0.9666	-0.1781	-10.4880	58	0.6060	-0.2427	1.0203	-0.0427	40.5954
25	0.6291	-0.0756	1.0496	0.0740	44.9250	59	0.6036	-0.2599	1.0138	0.0369	41.5104
26	0.5746	-0.3279	1.0077	-0.0008	32.4793	60	0.6651	0.0238	0.9955	0.1112	60.2253
27	0.6098	-0.1720	1.0483	-0.0902	36.0003	61	0.4174	-0.5290	0.8930	-0.4257	14.2314
28	0.6139	-0.1223	1.0645	0.0320	40.9638	62	0.6345	0.0070	0.9921	0.3461	61.6370
29	0.6073	-0.1518	1.0649	0.0175	39.1605	63	0.6199	-0.1354	1.0499	0.0414	47.1855
30	0.5454	-0.3190	0.9847	-0.3791	20.5495	64	0.6103	0.2437	0.8364	0.5741	75.5257
31	0.6334	-0.0836	1.0213	0.2142	48.6406	65	-0.5465	-0.3881	0.9379	-0.3308	-38.4256
32	0.5341	-0.3823	0.9486	-0.3610	19.6051	66	-0.6520	0.1390	0.9443	-0.3290	-64.1309
33	0.6141	-0.2419	0.9878	-0.2105	31.5796	67	-0.6571	0.1128	0.9535	-0.3014	-62.1146
34	0.5772	-0.3230	0.9337	-0.3797	22.3096	68	0.6548	-0.1250	0.9924	-0.1230	39.6594
35	0.4875	-0.4547	0.9212	-0.3892	14.7170	69	0.6345	0.0070	0.9921	0.3461	61.6370

Table C-6: Exciter and PSS parameters for 69-generator system.

K_A	$T_R(s)$	K_{ST}	$T_w(s)$	$T_1(s)$	$T_2(s)$
40	0.02	25	10	0.06	0.02

References

[1] P. Kundur and J. Paserba, "Definition and Classification of Power System Stability," *IEEE Trans. Power Sys.,* vol. 19, no. 2, pp. 1387-1401, 2004.

[2] P. Kundur, Power System Stability and Control, New York McGraw-Hill, 1994.

[3] M. Klein, G. Rogers and P. Kundur, "A fundamental study of inter-area oscillations in power systems," *IEEE Trans. Power Sys,* vol. 6, no. 3, pp. 914-921, August 1991.

[4] J. Machowski, J. Bialek and J. Bumby, Power System Dynamics: Stability and Control, Wiley, 2008.

[5] IEEE PES System Oscillations Working Group, "Inter-Area Oscillations in Power Systems," *IEEE PES Special Publication 95 TP 101,* October 1994.

[6] CIGRE Task Force 07- Advisory Group 01- Study Com., "Analysis and control of power system oscillations," December 1996.

[7] IEEE Power System Engineering Committee, Eigenanalysis and frequency domain methods for system dynamic performance, IEEE, 1989, pp. 97-104.

[8] Power System Damping Ad Hoc Task Force of PSDPC, "Damping representation for power system stability studies," *IEEE Trans. Power Sys.,* vol. 14, no. 1, pp. 151-157, 1999.

[9] J. Sanchez-Gasca, V. Vittal, M. Gibbard and A. R. Messina, "Inclusion of higher order terms for small signal (modal) Analysis-Committee report-task force on assessing the need to include higher order terms for small-signal (modal) analysis," *IEEE Trans. Power Sys.,* vol. 20, no. 5, pp. 1886-1904, 2001.

[10] G. Rogers, "Power system structure and oscillations," *IEEE Computer Applications in Power,* vol. 12, no. 2, pp. 14-21, April 1999.

[11] G. Rogers, Power System Oscillations, Springer, December 1999.

[12] P. Kundur and P. Dandeno, "Practical Application of Eigenvalue Techniques in the Analysis of Power System Dynamic Stability Problem," in *Proc. Fifth Power System Computation Conference*, Cambridge, England, September 1975.

[13] G. Geist, G. W. Howell and D. S. Watkins, "The BR eigenvalue Algorithm," *SIAM Journal of Matrix Analysis and Applications,* vol. 20, no. 4, pp. 1083-1098, 1999.

[14] J. Ma , Z. Yang Dong and . P. Zhang, "Comparison of BR and QR eigenvalue algorithms for power system small signal stability analysis," *IEEE Trans. Power Sys.,* vol. 21, no. 4, pp. 1848 - 1855, November 2006.

[15] W. Arnoldi, "The principle of minimized iterations in the solution of the matrix eigenvalue problem," *Quarterly of Applied Mathematics,* vol. 17, no. 9, pp. 17-29, 1951.

[16] L. Wang and A. Semlyen, "Application of sparse eigenvalue techniques to the small signal stability analysis of large power systems," *IEEE Trans. Power Sys.,* vol. 5, no. 2, pp. 635-642, May 1990.

[17] N. Uchida and T. Nagao, "A new eigen-analysis method of steady-state stability studies for large power systems: S matrix method," *IEEE Trans. Power Sys,* vol. 3, no. 2, pp. 706-714, May 1998.

[18] G. H. Golub and C. Van Loan, Matrix Computations, Baltimore and London: The Johns Hopkins University Press, 1996.

[19] R. Byerly, R. Bennon and D. Sherman, "Eigenvalue analysis of synchronizing power flow oscillations in large electric power systems," *IEEE Trans. Power App. Sys,* Vols. PAS-101, pp. 235-243, January 1982.

[20] I. Perez-Arriaga, G. Verghese and F. Schweppe, "Selective modal analysis with applications to electric power systems, Part I:Heuristic introduction, Part II: The dynamic stability problem," *IEEE, Trans. Power App. Sys.,* pp. 3117-3134, 1982.

[21] G. Angelidis and A. Semlyen, "Improved methodologies for the calculation of critical eigenvalues in small signal stability," *IEEE Trans. Power Sys.,* vol. 11, no. 3, pp. 1209-1217, 1996.

[22] D. Wong , G. Rogers , B. Porretta and P. Kundur, "Eigenvalue analysis of very large power systems," *IEEE Trans. Power Sys.,* vol. 3, no. 2, pp. 472 - 480, May 1988.

[23] A. Semlyen and L. Wang, "Sequential computation of the complete eigensystem for the study zone in small signal stability analysis of large Power systems," *IEEE Trans. Power Sys.,* Vols. PWRS-3, no. 2, pp. 715-725, May 1988.

[24] F. Bauer, "On modern matrix iteration processes of bernoulli and graeffe type," *Journal of the ACM,* vol. 5, no. 3, pp. 246-257, July 1958.

[25] N. Martins, "Efficient Eigenvalue and Frequency Response Methods Applied to Power System Small-Signal Stability Studies," *IEEE Trans. Power Sys.,* Vols. PWRS-1, no. 1, pp. 217-224, February 1986.

[26] Y. Hua, Y. Xiang, T. Chen, K. Abed-Meriam and Y. Miao, "A new look at the power method for fast subspace tracking," *Digital Signal Processing,* vol. 9, no. 4, pp. 297-314, October 1999.

[27] K. Abed-Meraim, A. Chkeif and Y. Hua, "Fast orthonormal PAST algorithm," *IEEE Signal Procsessing Letters,* vol. 7, no. 3, pp. 60-62, March 2000.

[28] J. Watkinson, The Algebraic Eigenvalue Problem, Clarendon Press, Oxford 1965.

[29] J. Rommes, "Methods for eigenvalue problems with applications in model order reduction," Ph.D. dissertation, Utrecht, The Netherlands, 2007.

[30] J. Rommes, N. Martins and F. Freitas, "Computing rightmost eigenvalues for small-signal stability assessment of large-scale power systems," *IEEE Trans. Power Sys,* vol. 25, no. 2, pp. 929-938, May 2010.

[31] G. Angelidis and A. Semlyen, "Efficient calculation of critical eigenvalue clusters in the small signal stability analysis of large power systems," *IEEE Trans. Power Sys.,* vol. 10, no. 1, pp. 427 - 432, February 1995.

[32] W. J. Stewart and A. Jennings, "A Simultaneous Iteration Algorithm for Real Matrices," *ACM Trans. on Mathematica Software,* vol. 7, no. 2, pp. 184-198, June 1981.

[33] M. Clint and A. Jennings, "A Simultaneous Iteration Method for the unsymmetric eigenvalue problem," *IMA Journal of Applied Mathematics,* vol. 8, no. 1, pp. 111-121, 1971.

[34] Y. Saad, Numencal Methods for Large Eigenvalue Problems: Theory andAlgorithms, New York: John Wiley & Sons, 1992.

[35] D. Watkins, The Matrix Eigenvalue Problem: GR and Krylov Subspace Methods, Society for Industrial Mathematics, 2007.

[36] Z. Er-Zhuan, N. Yi-Xin , S. S. Chen and B. Zhang, "Modified selective modal analysis method and its application in the analysis of power system dynamics," *IEEE Trans. Power Sys.,* vol. 6, no. 3, pp. 1189 - 1195, 1991.

[37] L. Rouco and I. Perez-Arriaga, "Multi-area analysis of small signal stability in large electric

power systems by SMA," *IEEE Trans. Power Sys.,* vol. 8, no. 3, pp. 1257 - 1265, 1993.

[38] D. Lam, H. Yee and B. Campbell, "An efficient improvement of the AESOPS algorithm for power system eigenvalue calculation," *IEEE Trans. Power Sys.,* vol. 9, no. 4, pp. 1880 - 1885, November 1994.

[39] P. Sauer, C. Rajagopalan and M. Pai, "An explanation and generalization of the AESOPS and PEALS algorithms," *IEEE Trans. Power Sys.,* vol. 6, no. 1, pp. 293 - 299, February 1991.

[40] P. Kundur, G. Rogers, D. Wong, L. Wang and M. G. Lauby, "A comprehensive computer program for small signal stability analysis of power systems," *IEEE Trans. Power Sys.,* vol. 5, no. 4, pp. 1076-1083, November 1990.

[41] B. Ooi and M. Nishimoto, "Analytical structures for eigensystem study of power flow oscillations in large power systems," *IEEE Trans. Power Sys.,* vol. 3, no. 4, pp. 1609-1615, November 1988.

[42] D. Bleecker and G. Csordas, Basic Partial Differential Equations, Chapman & Hall, 1995.

[43] J. Van. Ness, J. Boyle and F. Imad, "Sensitivity of large multiple-loop control systems," *IEEE Trans. Automatic Control,* Vols. AC-10, pp. 308-315, July 1995.

[44] K. Wang, C. Chung, C. Tse and K. Tsan, "Multimachine Eigenvalue Sensitivities of Power System Parameters," *IEEE Trans. Power Sys.,* vol. 15, no. 2, pp. 741-747, 2000.

[45] M. Adibi, "Power Systems Test Case Archive, IEEE Test Systems Task Force," 1993. [Online]. Available: http://www.ee.washington.edu/research/pstca/pf300/pg_tca300bus.htm.

[46] H. Saadat, Power System Analysis, PSA Publishing, 2010.

[47] G. Rogers, J. Chow and L. Vanfretti, "Power System Toolbox Webpage," [Online]. Available: http://www.ecse.rpi.edu/pst/PST.html.

[48] N. G. Hingorani and L. Gyugyi, Understanding FACTS: Concepts and Technology of Flexible AC Transmission Systems, Wiley-IEEE press.

[49] C. Grigg, "The IEEE Reliability Test System-1996. A report prepared by the Reliability Test System Task Force of the Application of Probability Methods Subcommittee," *IEEE Trans. Power Sys.,* vol. 14, no. 3, pp. 1010-1020, 1999.

[50] E. A. Faulkner, Introduction to the Theory of Linear Systems, Chapman & Hall, 1969.

[51] T. H. Cormen, Introduction to Algorithms, MIT Press, 2001.

[52] K. Morison, L. Wang and P. Kundur, "Power system security assessment," *IEEE Power and Energy Magazine,* vol. 2, no. 5, pp. 30-39, 2004.

[53] D. Sorensen, "Implicit application of polynomial filters in a k-step arnoldi method," *SIAM Journal of Matrix Analysis and Applications,* vol. 13, no. 1, pp. 357-385, 1992.

[54] R. B. Lehoucq and D. C. Sorensen, "deflation techniques for an implicitly restarted Arnoldi iteration," *SIAM Journal of Matrix Analysis and Applications,* vol. 17, no. 4, pp. 789-821, 1996.

[55] R. Richard , B. Lehoucq, D. Danny and . C. Sorensen, Arpack User's Guide: Solution of Large-Scale Eigenvalue Problems With Implicityly Restorted Arnoldi Methods, SIAM, 1998.

[56] Z. Bai, K. Meerbergen and Y. Su, "Arnoldi Methods for Structure-Preserving Dimension Reduction of Second-Order Dynamical Systems," in *Dimension Reduction of Large-Scale Systems, Lecture Notes in Computational Science and Engineering*, Springer, 2005, pp. 173-189.

[57] F. de Mello and C. Cocncordia, "Concepts of synchronous machine stability as affected by excitation control," *IEEE Trans. Power App. and sys.,* vol. PAS 88, no. 4, pp. 316-329, 1969.

[58] M. Gibbard, "Co-ordinated design of multimachine power system stabilisers based on damping torque concepts," *Generation, Transmission and Distribution, IEE Proceedings,* vol. 135, no. 4, pp. 276-284, 1988.

[59] E. Larsen and D. Swann, "Applying Power System Stabilizers Part I,II and III," *IEEE Trans. Power App. and Sys.,* vol. PAS 100, no. 6, pp. 3017-3046, 1981.

[60] P. Kundur, M. Klein , G. Rogers and M. Zywno, "Application of power system stabilizers for enhancement of overall system stability," *IEEE Trans. Power Sys.,* vol. 4, no. 2, pp. 614 - 626, 1989.

[61] M. Gibbard and . D. Vowles, "Reconciliation of methods of compensation for PSSs in multimachine systems," *IEEE Trans. Power Sys.,* vol. 19, no. 1, pp. 463 - 472, 2004.

[62] N. Martins, S. Corsi, G. Andersson, M. Gibbard, J. Sanchez-Gasca, A. Silva and G. Taranto, "Impact of Interactions Among Power System Controllers," Status Report of CIGRE TF 38.02.16, 2000.

[63] F. Pagola , I. Perez-Arriaga and G. Verghese, "On sensitivities, residues and participations: applications to oscillatory stability analysis and control," *IEEE Trans. Power Sys.,* vol. 4, no. 1, pp. 278 - 285, 1989.

[64] J. Zhang, C. Chung and Y. Han, "A Novel Modal Decomposition Control and Its Application to PSS Design for Damping Interarea Oscillations in Power Systems," *IEEE Trans. Power Sys.,* vol. 27, no. 4, pp. 2015 - 2025, 2012.

[65] M. J. Gibbard, "Robust design of fixed-parameter power system stabilisers over a wide range of operating conditions," *IEEE Trans. Power Sys.,* vol. 6, no. 2, pp. 794 - 800, 1991.

[66] M. J. Gibbard, D. Vowels and P. Pourbeik, "Interactions Between, and Effectiveness of, Power System Stabilizers and FACTS Device Stabilizers in Multimachine Systems," *IEEE Trans. Power Sys.,* vol. 15, no. 2, pp. 748-755, 2000.

[67] H. Gooi, E. Hill, M. Mobarak, D. Thorne and T. Lee, "Coordinated multi-machine stabilizer settings without eigenvalue drift," *IEEE Trans. Power App. and sys.,* Vols. PAS-100, no. 8, pp. 3879 - 3887, 1981.

[68] S. Lefebvre, "Tuning of Stabilizers in Multimachine Power Systems," *IEEE Trans Power App. and Sys.,* Vols. PAS-102, no. 2, pp. 290 - 299, 1983.

[69] V. N. Degtyarev and B. J. Cory, "Determination of stabiliser settings in multimachine power systems," *IEE Proceedings Generation, Transmission and Distribution,* vol. 133, no. 6, pp. 308 - 313, 1986.

[70] F. de Mello, P. Nolan, T. Laskowski and J. Undrill, "Coordinated application of stabilizers in multimachine power systems," *IEEE Trans. Power App. and Sys.,* Vols. PAS-99, no. 3, pp. 892 - 901, 1980.

[71] A. Doi and S. Abe, "Coordinated synthesis of power system stabilizers in multimachine power systems," *IEEE Tans. Power App. and Sys.,* vol. PAS103, no. 6, pp. 1473 - 1479, 1984.

[72] B. C. Pal, N. Martins and J. C. R. Ferraz, "Robust and coordinated tuning of power system stabiliser gains using sequential linear programming," *IET Proceedings, Generation, Transmission & Distribution,* vol. 4, no. 8, pp. 893-904, 2010.

[73] V. Arcidiacono, E. Ferrari, R. Marconato and J. Ghal, "Evaluation and improvement of electromechanical oscillation damping by means of eigenvalue-eigenvector analysis. practical results in the central Peru power system," *IEEE Trasn. Power App. and Sys.,* Vols.

PAS-99, no. 2, pp. 769 - 778, 1980.

[74] E.-Z. Zhou , O. Malik and G. Hope, "Design of stabilizer for a multimachine power system based on the sensitivity of PSS effect," *IEEE Trans. Energy Conversion,* vol. 7, no. 3, pp. 606 - 613, 1992.

[75] V. Maslennikov and S. Ustinov, "Method and software for coordinated tuning of power system regulators," *IEEE Trans. Power Sys.,* vol. 12, no. 4, pp. 1419-1424, 1997.

[76] P. Pourbeik and M. J. Gibbard, "Simultaneous coordination of power system stabilizers and FACTS device stabilizers in a multimachine power system for enhancing dynamic performance," *IEEE Trans. Power Sys.,* vol. 13, no. 2, pp. 473 - 479, 1998.

[77] N. Martins and L. Lima, "Determination of suitable locations for power system stabilizers and static VAR compensators for damping electromechanical oscillations in large scale power systems," *IEEE Trans. Power Sys.,* vol. 5, no. 4, pp. 1455 - 1469, 1990.

[78] J. da Cruz and L. Cera Zanetta Jr., "Stabilizer design for multimachine power systems using mathematical programming," *International Journal of Electrical Power & Energy Systems,* vol. 19, no. 8, p. 519–523, 1997.

[79] A. Andreoiu and K. Bhattacharya, "Robust tuning of power system stabilisers using a Lyapunov method based genetic algorithm," *IEE Proceedings - Generation, Transmission and Distribution,* vol. 149, no. 5, pp. 585-592, 2002.

[80] W. Qiu, V. Vittal and M. Khammash, "Decentralized power system stabilizer design using linear parameter varying approach," *IEEE Trans. Power Sys.,* vol. 19, no. 4, pp. 1951 - 1960, 2004.

[81] G. Chen , O. Malik, G. Hope and Y. Qin, "An adaptive power system stabilizer based on the self-optimizing pole shifting control strategy," *IEEE Trans. Energy Conversion,* vol. 8, no. 4, pp. 639-645, 1993.

[82] S. Cheng, S. J., O. Malik and G. Hope, "Damping of multi-modal oscillations in power systems using a dual-rate adaptive stabilizer," *IEEE Trans. Power Sys.,* vol. 3, no. 1, pp. 101-108, 1988.

[83] P. Shamsollahi and O. Malik, "Application of neural adaptive power system stabilizer in a multi-machine power system," *IEEE Trans. Power Conversion,* vol. 14, no. 3, pp. 731-736, 1999.

[84] Y. Zhang, O. Malik and G. Chen, "Artificial neural network power system stabilizers in

multi-machine power system environment," *IEEE Trans. Power Conversion,* vol. 10, no. 1, pp. 147-155, 1995.

[85] A. Hasanovic, A. Feliachi, A. Hasanovic and N. Bhat, "Practical robust PSS design through identification of low-order transfer functions," *IEEE Trans. Power Sys.,* vol. 19, no. 3, pp. 1492 - 1500, 2004.

[86] A. Hasanovic and A. Feliachi, "Low order transfer function identification and robust PSS control design," in *IEEE PES General Meeting*, Toronto, 2003.

[87] P. Pourbeik and M. J. Gibbard, "Damping and synchronizing torques induced on generators by FACTS stabilizers in multimachine power systems," *IEEE Trans. Power Sys.,* vol. 11, no. 4, pp. 1920 - 1925, 1996.

[88] I. Kamwa, R. Grondin, D. Asber and J. P. Gingras, "Active-power stabilizers for multi-machine power systems: challenges and prospects," *IEEE Trans. Power Sys.,* vol. 18, no. 4, pp. 1352-1358, 1998.

[89] I. Kamwa, R. Grondin and Y. Hebert, "Wide-area measurement based stabilizing control of large power systems -- a decentralized/hierarchical approach," *IEEE Trans. Power Sys.,* vol. 16, no. 1, pp. 136-153, 2001.

[90] H. Golestani Far, H. Banakar, P. Li, C. Luo and B. Ooi, "Damping Inter-Area Oscillations by Multiple Modal Selectivity Method," in *IEEE PES*, 2009.

[91] S. Attaway, MATLAB: A Practical Introduction to Programming and Problem Solving, Elsevier Science, 2013.

[92] A. Gilat and V. Subramaniam, Numerical Methods for Engineers and Scientists, John Wiley & Sons, 2014.

[93] J. Nocedal and S. Wright, Numerical Optimization, Springer, 2006.

[94] I. Kamwa, R. Grondin and G. Trudel, "IEEE PSS2B versus PSS4B: the limits of performance of modern power system stabilizers," *IEEE Trans. Power Sys.,* vol. 20, no. 2, pp. 903 - 915, 2005.

[95] Energy Development and Power Generation Committee, "421.5-2005 - IEEE Recommended Practice for Excitation System Models for Power System Stability Studies," The Institute of Electrical and Electronics Engineers, Inc., New York, 2005.

[96] K. Schittkowski, "NLQPL: A FORTRAN-Subroutine Solving Constrained Nonlinear

Programming Problems," *Annals of Operations Research,* vol. 5, no. 1, pp. 485-500, 1985.

[97] R. Fletcher and M. J. D. Powell, "A Rapidly convergent descent method for minimization," *Computer Journal,* vol. 6, no. 2, pp. 163-168, 1963.

[98] D. Goldfarb, "A Family of Variable Metric Updates Derived by Variational Means," *Mathematics of Computing,* vol. 24, no. 109, pp. 23-26, 1970.